



US Army Corps
of Engineers

AD-A225 384



2

REPAIR, EVALUATION, MAINTENANCE, AND
REHABILITATION RESEARCH PROGRAM

TECHNICAL REPORT REMR-GT-14

FILE COPY

SURFACE ROUGHNESS CHARACTERIZATION
OF ROCK MASSES USING THE FRACTAL
DIMENSION AND THE VARIOGRAM

by

James R. Carr

Geotechnical Laboratory

DEPARTMENT OF THE ARMY

Waterways Experiment Station, Corps of Engineers
3909 Halls Ferry Road, Vicksburg, Mississippi 39180-6199

DTIC
ELECTE
AUG 15 1990
S D
Co D



March 1990

Final Report

Approved For Public Release; Distribution Unlimited

Prepared for DEPARTMENT OF THE ARMY
US Army Corps of Engineers
Washington, DC 20314-1000

Under Civil Works Work Unit No. 32306

The following two letters used as part of the number designating technical reports of research published under the Repair, Evaluation, Maintenance, and Rehabilitation (REMR) Research Program identify the problem area under which the report was prepared:

	<u>Problem Area</u>		<u>Problem Area</u>
CS	Concrete and Steel Structures	EM	Electrical and Mechanical
GT	Geotechnical	EI	Environmental Impacts
HY	Hydraulics	OM	Operations Management
CO	Coastal		

Destroy this report when no longer needed. Do not return it to the originator.

The findings in this report are not to be construed as an official Department of the Army position unless so designated by other authorized documents.

The contents of this report are not to be used for advertising, publication, or promotional purposes. Citation of trade names does not constitute an official endorsement or approval of the use of such commercial products.

COVER PHOTOS:

TOP — Wedge failure in rock - Old Notch 2.

MIDDLE — Wedge failure in rock - Backus Creek Notch.

BOTTOM — Left abutment - Libby, Montana - DS+122 Failure Wedge

Unclassified

SECURITY CLASSIFICATION OF THIS PAGE

REPORT DOCUMENTATION PAGE				Form Approved OMB No. 0704-0188	
1a. REPORT SECURITY CLASSIFICATION Unclassified		1b. RESTRICTIVE MARKINGS			
2a. SECURITY CLASSIFICATION AUTHORITY		3. DISTRIBUTION/AVAILABILITY OF REPORT Approved for public release; distribution unlimited.			
2b. DECLASSIFICATION/DOWNGRADING SCHEDULE					
4. PERFORMING ORGANIZATION REPORT NUMBER(S) Technical Report REMR-GT-14		5. MONITORING ORGANIZATION REPORT NUMBER(S)			
6a. NAME OF PERFORMING ORGANIZATION USAEWES Geotechnical Laboratory		6b. OFFICE SYMBOL (if applicable)	7a. NAME OF MONITORING ORGANIZATION		
6c. ADDRESS (City, State, and ZIP Code) 3909 Halls Ferry Road Vicksburg, MS 39180-6199		7b. ADDRESS (City, State, and ZIP Code)			
8a. NAME OF FUNDING/SPONSORING ORGANIZATION US Army Corps of Engineers		8b. OFFICE SYMBOL (if applicable)	9. PROCUREMENT INSTRUMENT IDENTIFICATION NUMBER		
8c. ADDRESS (City, State, and ZIP Code) Washington, DC 20314-1000		10. SOURCE OF FUNDING NUMBERS			
		PROGRAM ELEMENT NO.	PROJECT NO.	TASK NO.	WORK UNIT ACCESSION NO. 32306
11. TITLE (Include Security Classification) Surface Roughness Characterization of Rock Masses Using the Fractal Dimension and the Variogram					
12. PERSONAL AUTHOR(S) Carr, James R.					
13a. TYPE OF REPORT Final report		13b. TIME COVERED FROM 6/10/85 TO 7/15/86		14. DATE OF REPORT (Year, Month, Day) March 1990	15. PAGE COUNT 157
16. SUPPLEMENTARY NOTATION (See reverse).					
17. COSATI CODES			18. SUBJECT TERMS (Continue on reverse if necessary and identify by block number)		
FIELD	GROUP	SUB-GROUP	Rock mass	Variogram	
			Discontinuities	Rock shear strength	
			Fractal dimension	Roughness	(Continued)
19. ABSTRACT (Continue on reverse if necessary and identify by block number)					
<p>A branch of mathematical topology, called fractal dimension analysis and the variogram construction from the theory of regionalized variables were described and applied to natural geologic rock surface descriptive data. The purposes of application were to determine the techniques applicabilities to characterization of the rock surface roughness and the semi-empirical prediction of the surface shear strengths.</p> <p>Both the fractal dimensions and variograms were determined from data obtained on the DS + 122 slide surface at Libby Dam, MT. The data used were a fine-scale photogrammetric contour map of the joint surface and string line profiles measured on the joint surface. The fractal dimensions were found to exactly reflect the qualitative roughness of the surface and found to be directly proportional to the roughness in a numerical comparison. The variograms of the natural surface data demonstrate that roughness elevations are spatially</p> <p style="text-align: right;">(Continued)</p>					
20. DISTRIBUTION/AVAILABILITY OF ABSTRACT <input type="checkbox"/> UNCLASSIFIED/UNLIMITED <input type="checkbox"/> SAME AS RPT <input type="checkbox"/> DTIC USERS			21. ABSTRACT SECURITY CLASSIFICATION Unclassified		
22a. NAME OF RESPONSIBLE INDIVIDUAL		22b. TELEPHONE (Include Area Code)		22c. OFFICE SYMBOL	

Unclassified

SECURITY CLASSIFICATION OF THIS PAGE

16. SUPPLEMENTARY NOTATION (Continued).

This is a report of the Repair, Evaluation, Maintenance, and Rehabilitation (REMR) Research Program. Report is available from National Technical Information Service, 5285 Port Royal Road, Springfield, VA 22161.

18. SUBJECT TERMS (Continued).

Topology
Surface characterization

19. ABSTRACT (Continued).

correlated and have a finite spatial continuity. The variogram is also useful for examining asperity magnitude differences across the joint surface. The variogram demonstrated more descriptive ambiguity than did the fractal dimension.

Fractal dimensions of roughness profiles of small rock specimens were calculated and compared to the Joint Roughness Coefficient (JRC) used in the empirical rock shear strength criterion. A least squares relationship:

$$JRC = -1022.55 + (1023.92) D$$

with D as the fractal dimension was determined. Thus the JRC component of the empirical shear strength component can be directly obtained from surface profile data.

Unclassified

SECURITY CLASSIFICATION OF THIS PAGE

PREFACE

The work described in this report was authorized by Headquarters, US Army Corps of Engineers (HQUSACE), as part of the Geotechnical-Rock Problem Area of the Repair, Evaluation, Maintenance, and Rehabilitation (REMR) Research Program. The work was performed under Work Unit 32306, "Stability of Large Concrete Structures on Rock," for which Mr. James B. Warriner was Principal Investigator. Mr. Lewis Gustafson (CECW-EG) was the REMR Technical Monitor for this work.

Mr. Jesse A. Pfeiffer, Jr. (CERD-C) was the REMR Coordinator at the Directorate of Research and Development, HQUSACE; Mr. James E. Crews (CECW-OM) and Dr. Tony C. Liu (CECW-ED) served as the REMR Overview Committee; Mr. William F. McCleese (CEWES-SC-A), US Army Engineer Waterways Experiment Station (WES) was the REMR Program Manager. Mr. Jerry S. Huie was the Problem Area Leader.

The work was performed at the University of Missouri-Rolla and this report was prepared by Dr. James R. Carr, Department of Geological Sciences under an Intergovernmental Personnel Act Agreement and under the general supervision of Dr. William F. Marcuson III, Chief, Geotechnical Laboratory and the direct supervision of Dr. Don C. Banks, Chief, Soil and Rock Mechanics Division.

Commander and Director of WES was COL Larry B. Fulton, EN. Technical Director was Dr. Robert W. Whalin.

Accession For	
NTIS CRA&I	<input checked="" type="checkbox"/>
DTIC TAB	<input type="checkbox"/>
Unannounced	<input type="checkbox"/>
Justification	
By	
Distribution/	
Availability Codes	
Dist	Availability
A-1	Special



CONTENTS

	<u>Page</u>
PREFACE.....	1
CONVERSION FACTORS, NON-SI TO SI (METRIC)	
UNITS OF MEASUREMENT.....	4
LIST OF TABLES.....	5
LIST OF FIGURES.....	5
PART I: INTRODUCTION.....	8
General Description of the DS + 122 Rock Slide.....	8
Fractal Dimensions and Variograms.....	9
PART II: FRACTAL DIMENSION OF JOINT SURFACES.....	10
Fractal Dimension.....	10
Cross-Section Segmentation of the DS + 122 Joint Surface.....	11
Fractal Dimension of Selected Cross Sections.....	15
Results of the Fractal Dimension Calculations.....	16
Control Calculation: Fractal Dimension of the Australian Coast.....	25
PART III: VARIOGRAM ANALYSIS OF THE DS + 122 JOINT SURFACE.....	28
Variogram.....	28
Variograms of Selected Cross Sections.....	28
Results of the Variogram Analysis.....	40
Potential Application of the Variogram: Kriging.....	40
PART IV: COMPARISON OF THE USE OF THE FRACTAL DIMENSION AND THE VARIOGRAM TO ACCEPTED ROCK SURFACE ROUGHNESS EVALUATION TECHNIQUES.....	42
PART V: APPLICATION OF THE FRACTAL DIMENSION AND VARIOGRAM TO STRING LINE DATA FOR ROCK SURFACES NEAR LIBBY DAM, MONTANA.....	49
Fractal Dimension of String Line Cross Sections.....	49
Computer Calculation of the Fractal Dimension.....	57
Variogram Analysis of String Line Cross Sections.....	59
PART VI: REGRESSION: RELATIONSHIP BETWEEN THE FRACTAL DIMENSION AND JOINT ROUGHNESS COEFFICIENT.....	68
Regression Analysis.....	70
Regression Analysis for Estimation of the Joint Roughness Coefficient.....	72
PART VII: CONCLUSION.....	79
Implication of Results.....	79
Problems Encountered in this Research.....	79
Solutions to Problems.....	80
Research Contribution.....	80
REFERENCES.....	82
BIBLIOGRAPHY.....	84

	<u>Page</u>
APPENDIX A: CONCEPT OF THE FRACTAL DIMENSION.....	A1
Introduction.....	A1
Fractal Dimension.....	A1
Example Calculations.....	A12
Mandelbrot Set.....	A12
APPENDIX B: THEORY OF REGIONALIZED VARIABLES, A GEOSTATISTICAL TECHNIQUE.....	B1
Introduction.....	B1
Variogram.....	B1
Linear Estimation of Regionalized Variables: Kriging.....	B2
Intrinsic Hypothesis.....	B5
Example Calculations.....	B6
APPENDIX C: FRACTAL DIMENSION CALCULATIONS.....	C1
APPENDIX D: NUMERICAL VARIOGRAM RESULTS.....	D1
APPENDIX E. FORTRAN PROGRAM FOR THE CALCULATION OF THE FRACTAL DIMENSION.....	E1
APPENDIX F: VARIOGRAMS FOR STRING LINE CROSS SECTIONS.....	F1

CONVERSION FACTORS, NON-SI TO SI (METRIC)
UNITS OF MEASUREMENT

Non-SI units of measurement used in this report can be converted to SI
(metric) unit as follows:

<u>Multiply</u>	<u>By</u>	<u>To Obtain</u>
feet	0.3048	metres

LIST OF TABLES

<u>No.</u>		<u>Page</u>
1	Fractal Dimension Calculations (Method 2).....	15
2	Fractal Dimension Summary.....	23
3	Fractal Dimension Calculation, Australian Coast.....	27
4	Properties of Stationary Variograms.....	40
5	List of Rock Surfaces Associated with String Line Data.....	50
6	Fractal Dimension Calculation for String Line Cross Sections.....	56
7	Computer Calculation of String Line Fractal Dimensions.....	59
8	Variogram Results for String Line Cross Sections.....	60
9	Joint Roughness Coefficient (JRC) for String Line Cross Sections.....	70
10	Application of Regression Equations for Estimation of JRC.....	75
11	Fractal Dimension Calculations for Profiles of Figure 41.....	77
12	Predicted JRC Values for Profiles of Figure 41.....	78
A1	Fractal Dimension Calculation, West Coast of Great Britain.....	A15
A2	Fractal Dimension Calculation, Southern California Coast.....	A15
B1	Computation of a Variogram for the Data of Figure B1.....	B8
B2	Example Kriging Computation.....	B12
C1	Fractal Dimension Summary (Method 1 Calculation).....	C2
C2	Fractal Dimension Summary (Method 2 Calculation).....	C3
D1	Variogram Results for Cross Section BG.....	D2
D2	Variogram Results for Cross Section AF.....	D3
D3	Variogram Results for Cross Section AL.....	D4
D4	Variogram Results for Cross Section AS'.....	D5
D5	Variogram Results for Cross Section BA.....	D6
D6	Variogram Results for Cross Section BB.....	D7
D7	Variogram Results, Cross Section from Patton and Deere (1970).....	D8
D8	Variogram Results for Cross Section BG (Filtered).....	D9

LIST OF FIGURES

<u>No.</u>		<u>Page</u>
1	DS + 122 joint surface showing cross section locations.....	12
2	Cross sections AS', AL, AE, AD for fractal dimension calculations.....	13
3	Cross sections BF, BA for fractal dimension.....	14
4	$\log_{10}(N)$ versus $\log_{10}(y)$ plot for cross section AD.....	17
5	$\log_{10}(N)$ versus $\log_{10}(y)$ plot for cross section AE.....	18
6	$\log_{10}(N)$ versus $\log_{10}(y)$ plot for cross section AL.....	19
7	$\log_{10}(N)$ versus $\log_{10}(y)$ plot for cross section AS'.....	20
8	$\log_{10}(N)$ versus $\log_{10}(y)$ plot for cross section BA.....	21
9	$\log_{10}(N)$ versus $\log_{10}(y)$ plot for cross section BF.....	22
10	Fractal dimension summary for the DS + 122 joint surface.....	24
11	Outline of the coast of Australia.....	26
12	$\log_{10}(N)$ versus $\log_{10}(y)$ plot for the Australian coast.....	27
13	Cross sections AL, AF, BG analyzed using the variogram.....	30

LIST OF FIGURES (Continued)

<u>No.</u>		<u>Page</u>
14	Cross sections BB, AS', BA analyzed using the variogram.....	31
15	Variogram for cross section BG, an example of non-stationary behavior in the variogram.....	32
16	Variogram for cross section AF. Variogram is stationary, but at h = 400 cm , it becomes non-stationary.....	33
17	Variogram for cross section AL, an example of a stationary variogram.....	34
18	Variogram for cross section AS', an example of stationary behavior.....	35
19	Variogram for cross section BA, an example of stationary behavior.....	36
20	Variogram for cross section BB, an example of a non-stationary variogram.....	37
21	Diagram of the procedure used to remove the influence of the plane of inclination from cross-sectional data.....	38
22	Variogram for cross section BG subsequent to the removal of the inclination.....	39
23	Cross section from Patton and Deere (1970).....	42
24	Cross section from Patton and Deere (1970), plotted at an enlarged scale and without inclination.....	44
25	Variogram for the section of Patton and Deere (1970).....	45
26	Variogram for cross section AL, presented here to emphasize its periodic behavior.....	46
27	Variogram for cross section AS', presented here to emphasize its subtle periodic behavior.....	47
28	Cross sections AL and AS', plotted for comparison with the variograms of Figures 26 and 27.....	48
29	Plot of string line cross sections: Backus Notch No. 1 (bedding); Backus Creek Notch No. 1 (bedding); and DS + 122 (C joint).....	51
30	Plot of string line cross sections: Island Notch (joint); DS + 122 (minor joint); and DS + 122 (joint No. 2).....	52
31	Plot of string line cross sections: 914R.b (joint); Dunn Creek Notch (joint); and 930 (joint).....	53
32	Plot of string line cross sections: Island Notch (joint/bedding plane intersection); Island Notch (bedding); and Wolf Creek Jct. (joint).....	54
33	Plot of string line cross sections: Dunn Creek Notch (bedding); Old Notch No. 1 (joint); and Backus Notch No. 1 (joint).....	55
34	Algorithm for fractal dimension calculation program.....	58
35	Artificial string line cross section formed using random elevation values.....	62
36	Variogram for string line cross section shown in Figure 35.....	63
37	Three filtered results developed from the string line cross section shown in Figure 35; filter sizes are shown.....	64
38	Variogram for the 3X1 filtered string line cross section.....	65
39	Variogram for the 7X1 filtered string line cross section.....	66
40	Variogram for the 15X1 filtered string line cross section.....	67
41	JRC profiles (Barton and Choubey 1977).....	68
42	Example case of two linearly correlated variables.....	71
43	Two regression plots: JRC versus fractal dimension and JRC versus variogram nugget.....	73

LIST OF FIGURES (Concluded)

<u>No.</u>		<u>Page</u>
44	Plot of JRC versus fractal dimension for the profiles shown in Figure 41.....	77
A1	Trace of the Amazon River system, Brazil.....	A3
A2	Schematic representation of the unbounded increase in length as the ruler measure, y , decreases.....	A4
A3	Amazon River trace, showing the measurement of its length using 160 km step sizes (y).....	A5
A4	Amazon River trace, showing the measurement of its length using 80 km step sizes (y).....	A6
A5	Amazon River trace, showing the measurement of its length using 25 km step sizes (y).....	A7
A6	$\text{Log}_{10}(N)$ versus $\text{Log}_{10}(y)$ plot for the Amazon River.....	A9
A7	Linear idealization of the Amazon drainage system.....	A10
A8	$\text{Log}_{10}(N)$ versus $\text{Log}_{10}(y)$ plot for the linear Amazon.....	A11
A9	Outline of the coast of Great Britain.....	A13
A10	Outline of the coast of Southern California.....	A14
A11	$\text{Log}_{10}(N)$ versus $\text{Log}_{10}(y)$ plot for western coast of Great Britain.....	A16
A12	$\text{Log}_{10}(N)$ versus $\text{Log}_{10}(y)$ plot for the southern California coast.....	A17
A13	Mandelbrot set.....	A19
A14	IBM compatible BASIC language program used to create the Mandelbrot set of Figure A13.....	A20
B1	Example of a spherical variogram showing the nugget, range, sill and shape.....	B3
B2	Example arrangement of sample locations and values.....	B7
B3	Variogram for the data of Figure B2.....	B10
F1	Variogram for the Backus Notch No. 1 bedding surface.....	F2
F2	Variogram for the Backus Creek Notch No. 1 bedding surface.....	F3
F3	Variogram for the DS + 122, C joint surface.....	F4
F4	Variogram for the Island Notch joint surface.....	F5
F5	Variogram for the DS + 122 minor joint surface.....	F6
F6	Variogram for the DS + 122 joint No. 2 surface.....	F7
F7	Variogram for the 914 Rib joint surface.....	F8
F8	Variogram for the Dunn Creek Notch joint surface.....	F9
F9	Variogram for the 930 joint surface.....	F10
F10	Variogram for the Island Notch joint/bedding plane intersection...	F11
F11	Variogram for the Island Notch bedding surface.....	F12
F12	Variogram for the Wolf Creek Jct. joint surface.....	F13
F13	Variogram for the Dunn Creek Notch bedding surface.....	F14
F14	Variogram for the Old Notch No. 1 joint surface.....	F15
F15	Variogram for the Backus Notch No. 1 joint surface.....	F16

SURFACE ROUGHNESS CHARACTERIZATION OF ROCK MASSES
USING THE FRACTAL DIMENSION AND THE VARIOGRAM

PART I: INTRODUCTION

1. This report summarizes the first known attempt to describe the roughness of rock surfaces using the concepts of the fractal dimension and the variogram. For this investigation, joint surfaces adjacent to Libby Dam, MT, were used. One joint surface was part of a rock slide designated as the DS + 122 slide. The objective of this study was to examine the utility of the fractal dimension and the variogram for the classification of surface roughness of rock masses.

General Description of the DS + 122 Rock Slide

2. The DS + 122 rock slide occurred at Libby Dam, MT, on January 31, 1971 (Hamel 1974). This slide consisted of a rock wedge which slid toward the dam abutment. The volume of this rock wedge was approximately $46,000 \text{ m}^3$. The DS + 122 wedge was formed and bounded by the intersection of a bedding plane and a fracture (joint). From a qualitative viewpoint, the surface of the bedding plane was quite smooth whereas the joint surface had a rougher texture (Banks and Strohm 1974). This report presents a quantitative description of the roughness of the joint surface.

3. This description involved the characterization of the spatial variation in the roughness across the planar surface of this joint. In analyses of the sliding stability of rock masses, asperities along a potential slip surface are a key consideration (Patton 1966; Patton and Deere 1970; Hoek and Bray 1974; and Goodman 1976). This report does not describe the characteristics of the asperities along the DS + 122 joint surface. A quantitative description of the roughness of this slide surface derived from a field survey is presented. From this description, it is hoped that a method for deriving properties of slip surface asperities can be developed.

Fractal Dimensions and Variograms

4. A quantitative assessment of the roughness of the DS + 122 slide surface was completed using the concept of the fractal dimension. This concept describes the degree of variation a natural surface has from its topological facsimile. Topology is a branch of mathematics devoted to the study of geometrical configurations. For example, the topological model of a joint in a rock is a plane. In reality, a joint is not a perfect plane, but has surface irregularities which impart a greater surface area to the joint when compared to its topological model. The fractal dimension describes the degree of variation a curve, a surface, or a volume has from its topological ideal.

5. For example, a coastline is modeled topologically as a line or a semi-circle. The topological dimension is therefore one (a one dimensional feature). A coastline is rarely linear or circular, however, and is often highly irregular. This irregularity gives the coastline a greater length compared with its topological model. Hence, the fractal dimension of such an irregular coastline is greater than one. A fractal is a curve, a surface, or a volume whose dimension exceeds its topological dimension. The more irregular or rough a surface is, the greater will be its fractal dimension.

6. Once the irregularity of a surface has been described by the fractal dimension, the spatial variation of the surface irregularities, or asperities, can be described using variograms. The variogram describes the spatial continuity and relationship inherent to a type of regionally distributed natural data. The variogram can be used to show the spatial behavior of the asperities whether these irregularities are of a local extent with little spatial continuity or are continuous with a more regular spatial variation. Furthermore, the variogram can be used to evaluate the different magnitudes of asperity sizes which are present on a rock surface. The resolution of these asperities is important. Goodman (1976) has shown, for example, that asperities increase the friction angle of a joint by an amount equal to the mean or predominate asperity angle. Hence, any investigation of the sliding stability of a joint (or, in general, any rock surface) must be concerned with the characteristics of the asperities along the surface.

PART II: FRACTAL DIMENSION OF JOINT SURFACES

Fractal Dimension

7. A detailed description of fractals and the fractal dimension is provided in Appendix A. In summary, a fractal is a line, a surface, or a volume whose Hausdorff-Besicovitch dimension (i.e., fractal dimension, see Appendix A) exceeds its topological dimension. In Appendix A, the coastline of Great Britain is used as an example. The topological dimension of this coast is 1 (a line or a semi-circle). The length of this coast can be measured by selecting a particular segment length, y , then counting the number, N , of these y -length segments which are needed to approximate the total length, L , of the coastline. This length is computed as

$$L = Ny \quad (1)$$

But, as we are realizing when we measure with increasing resolution, we encounter an increasing number of microvariabilities, thus equation (1) should be expressed as

$$L \approx Ny \quad (1a)$$

This is a phenomenon that has no real mathematical proof and is conceptually shown in Appendix A.

8. It is an interesting phenomenon that as y decreases, L increases without bound (for the actual coast, not for its mapped representation; a map has a certain resolution limit and increments of y below that limit yield the same measure of length, L , hence with a map, L does have a limit). Despite this fact, if we plot $\log_{10}(N)$ versus $\log_{10}(y)$, a straight line is obtained. The negative of the slope of this line is the Hausdorff-Besicovitch dimension, D . This dimension is the fractal dimension (Mandelbrot 1982).

9. The fractal dimension can be incorporated into equation (1) to become

$$L = Ny^D \quad (2)$$

If, throughout the plot of $\log_{10}(N)$ versus $\log_{10}(y)$, D is found to be greater than the topological dimension, a fractal is defined. In Appendix A, for instance, the fractal dimension of the west coast of Great Britain is shown to be 1.25. This is greater than the topological dimension, 1 ; hence, the west coast of Great Britain is a fractal.

10. For the analysis of the surface roughness of the joint bounding the DS + 122 slide, the concept of the fractal dimension is intuitively useful. The more irregular a surface is, the larger will be its fractal dimension. The DS + 122 joint surface, however, is planar with a topological dimension of two ($D_T = 2$). To measure the fractal dimension of this surface, equation (2) is rewritten to become

$$A = Na^D \quad (3)$$

where A is the total area of the surface and a is some small, regular area analogous to y in equation (2). From equation (3), D is found by plotting $\log_{10}(N)$ versus $\log_{10}(a)$. For two dimensional surfaces, a fractal surface is defined if D exceeds 2.

Cross-Section Segmentation of the DS + 122 Joint Surface

11. For the elevation of the DS + 122 slide surface, the solution for D using equation (3) is difficult to obtain. As an alternative, cross sections were plotted along discrete sections of the joint surface. These cross sections were plotted using a contour plot derived from ground-based photogrammetry. The map scale was 1:40 and the contour interval was 2 cm. In total, thirty cross sections were analyzed. Of these, twenty were orthogonal to the direction of shear failure, and ten were parallel to the direction of shear failure. The locations of these thirty cross sections are shown in Figure 1.

12. Selected cross sections are plotted in Figures 2 and 3. By analyzing cross sections, the two-dimensional analysis offered by equation (3) was transformed to thirty one-dimensional analyses using equation (20). Topologically, the trace of each cross section is a line. A particular cross section was determined to be a fractal if its fractal dimension was greater than 1. Once calculated for each cross section, the fractal dimension served as an

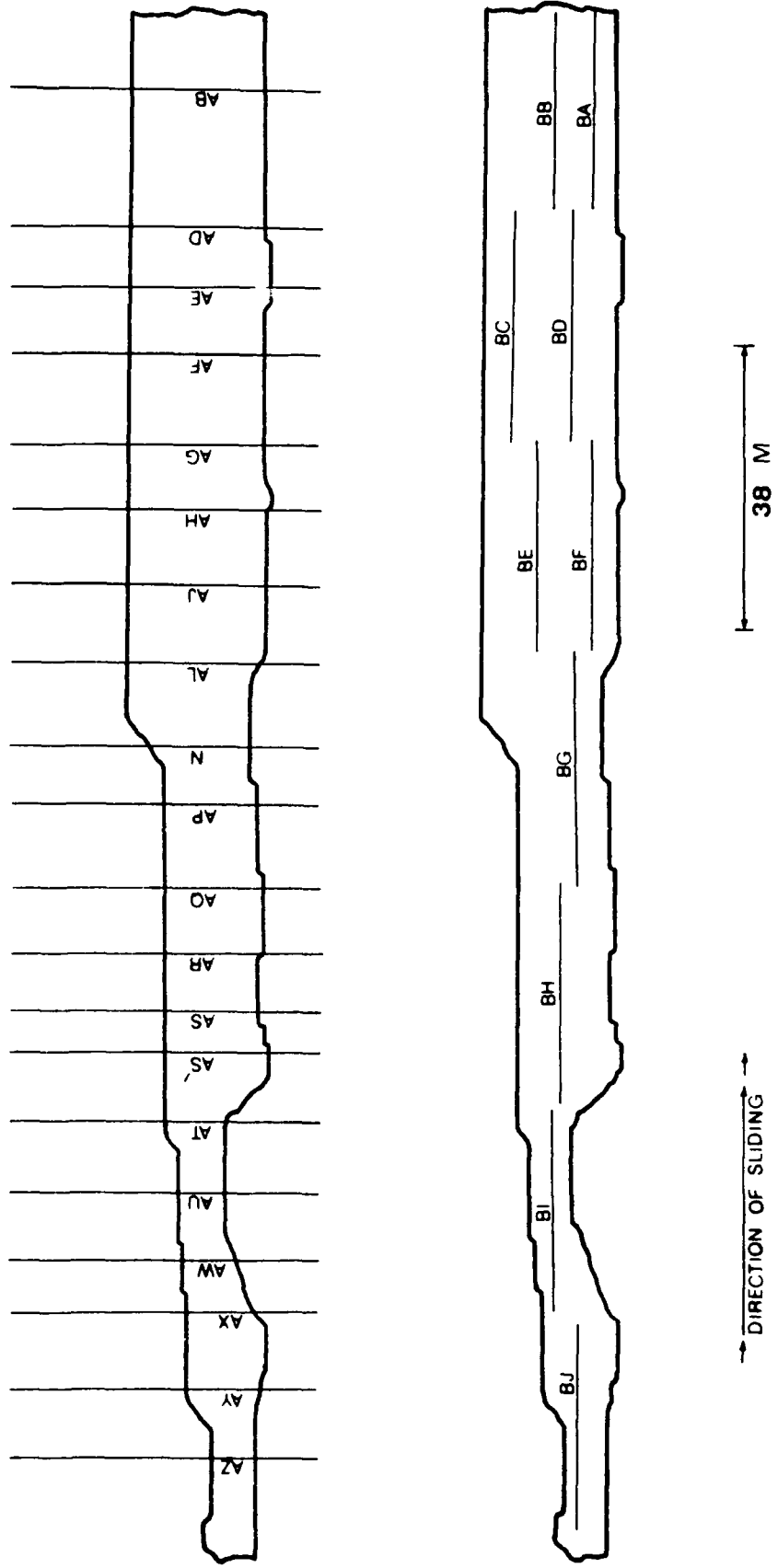


Figure 1. DS + 122 joint surface showing cross-section locations

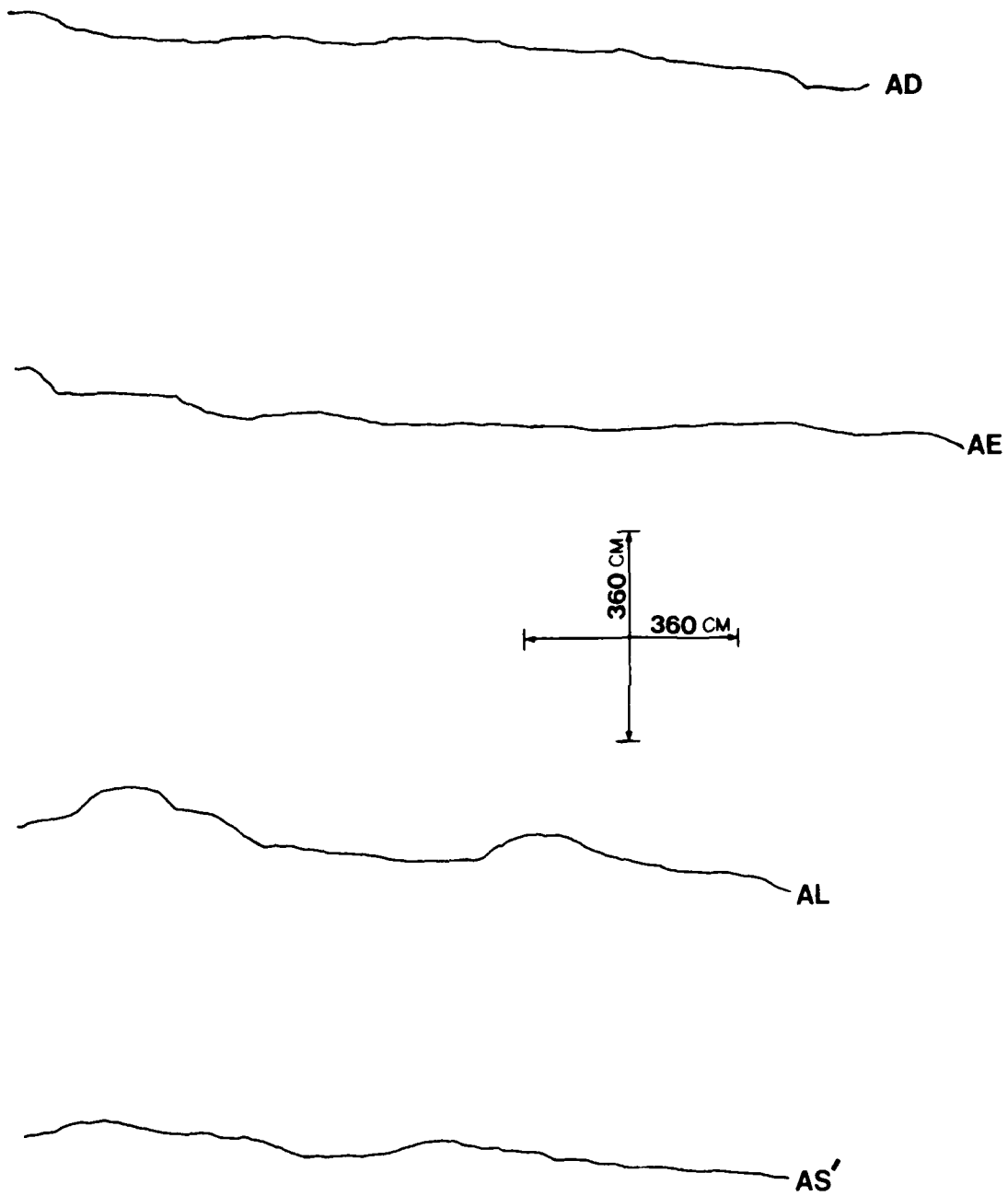


Figure 2. Cross Sections AS', AL, AE, AD for fractal dimension calculations

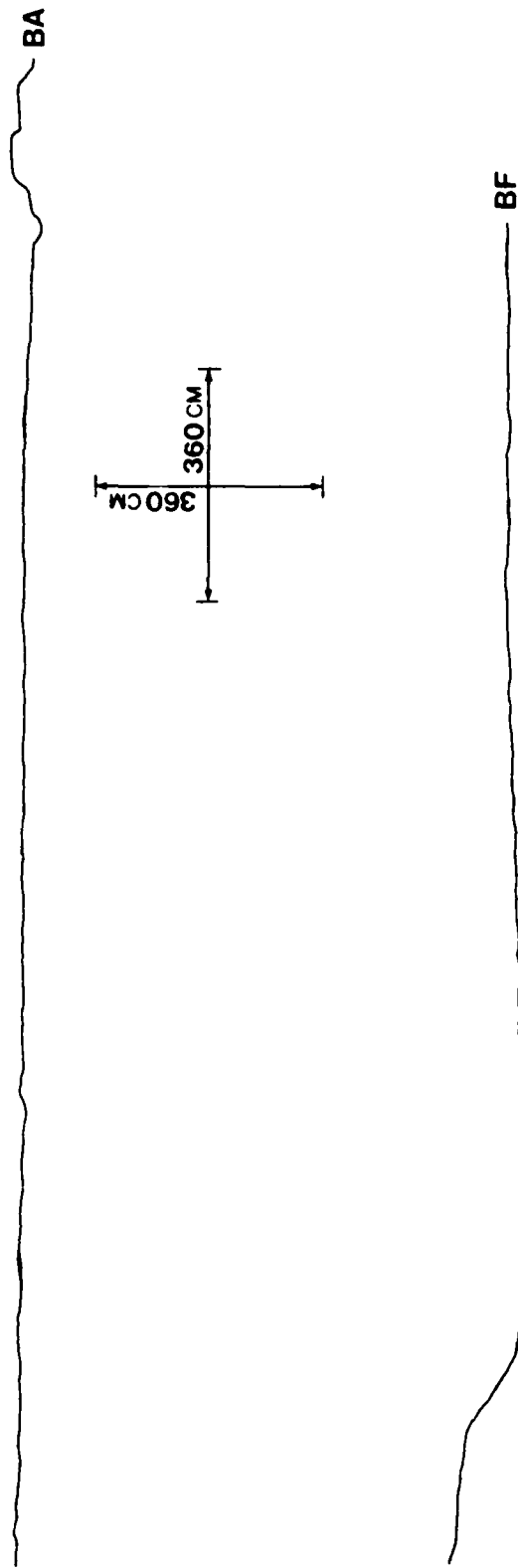


Figure 3. Cross sections BF, BA for fractal dimension calculations

indicator of surface roughness. Because each cross section represented a unique spatial location along the DS + 122 slide, the analysis of thirty cross sections described the spatial variation in the surface roughness along the slide.

Fractal Dimension of Selected Cross Sections

13. A fractal dimension was computed for each of the thirty cross sections plotted in Figure 1. To minimize the length of this report, Table 1 presents calculations only for those cross sections shown in Figures 2 and 3. Calculations of fractal dimensions for other cross sections and presented in Appendix C.

Table 1
Fractal Dimension Calculations (Method 2)

Cross Section	Number of Segment Increments, N			-slope = D*
	y = 305 cm	y = 100 cm	y = 20 cm	
AD	4.056	12.400	62.500	1.0038
AE	3.810	11.680	58.900	1.0050
AL	3.900	9.240	60.968	1.0091
AS'	4.118	12.610	63.700	1.0052
BA	7.793	23.770	118.843	1.0000
BF	6.832	20.940	105.330	1.0040

* Slope = $(\log_{10}(N_{20}) - \log_{10}(N_{305})) / (\log_{10}(20) - \log_{10}(305))$.

14. For each cross section, several consistently smaller segment lengths, y, were selected for the calculation of the fractal dimension. Usually, three different lengths were chosen: 305 cm, 100 cm, and 20 cm. This was an arbitrary choice and seemed to work well for this application. In no way do these lengths conform to a special property of these cross sections. For the calculation of the fractal dimension, measurable lengths, y, must be selected by arbitrary decision. For this study, the lengths 200 cm, 50 cm, and 5 cm could have been chosen and would have yielded similar results.

15. For each cross section, the fractal dimension, D, was evaluated quantitatively using a pair of segment lengths, y. In addition, $\log_{10}(N)$

versus $\log_{10}(y)$ plots were developed for each cross section for graphical analysis. These plots are shown in Figures 4 through 9 with visually best fit lines. The negative of the slope of each plot is the fractal dimension. The fractal dimension for each cross section was determined by comparing the $\log_{10}(N)$ versus $\log_{10}(y)$ graphical results to the quantitative calculation results.

Results of the Fractal Dimension Calculations

16. The results of the fractal dimension calculations for all thirty cross sections are presented in Table 2. To make these results more meaningful, Figure 10 shows the fractal dimension for each cross section plotted on the map of the DS + 122 joint surface. This figure demonstrates the spatial variation in the fractal dimension across the DS + 122 joint surface.

17. Figure 10 shows the DS + 122 joint surface between cross sections AB through AF to be rather smooth. The joint surface becomes rougher toward the AZ cross section. The direction parallel to sliding has a roughness which increases from cross sections BA and BL to cross sections BI and BJ. The direction of shear failure along this surface was from cross sections AZ, BI, BJ toward cross sections AB, BA, BB.

18. It is important to evaluate the method used to calculate the fractal dimension for each cross section. As we reviewed previously, the calculation of the fractal dimension begins by selecting a segment length, y . Then, beginning from one end of an irregular line, the number of steps, N , is counted to reach the opposite end. Here a dilemma is reached. In counting the number of steps, N , what happens if a small section of the irregular line remains at the end and this remainder is smaller than the length, y ? It is necessary to add the remainder, normalized by y , to the number of steps, N ; i.e., $N = N + \text{remainder}/y$ (Mandelbrot 1985). Table 2 shows that this remainder is considerably important for calculations. The method 1 calculation does not consider the remainder whereas the method 2 calculation does include the remainder. Hereafter, in this study, only the method 2 calculation is used to determine the fractal dimension of rock surfaces.

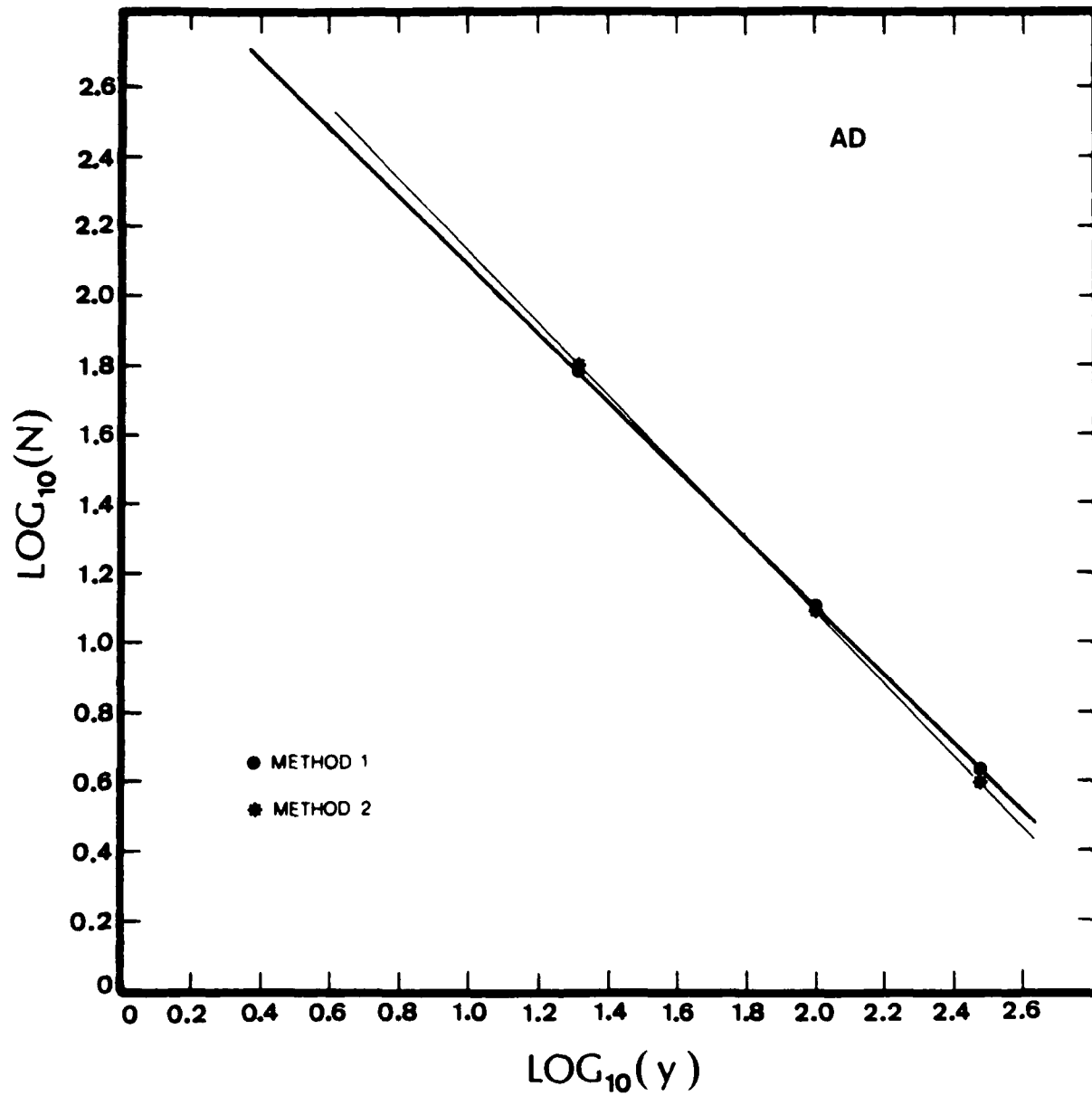


Figure 4. $\text{Log}_{10}(N)$ versus $\text{log}_{10}(y)$ plot for cross section AD

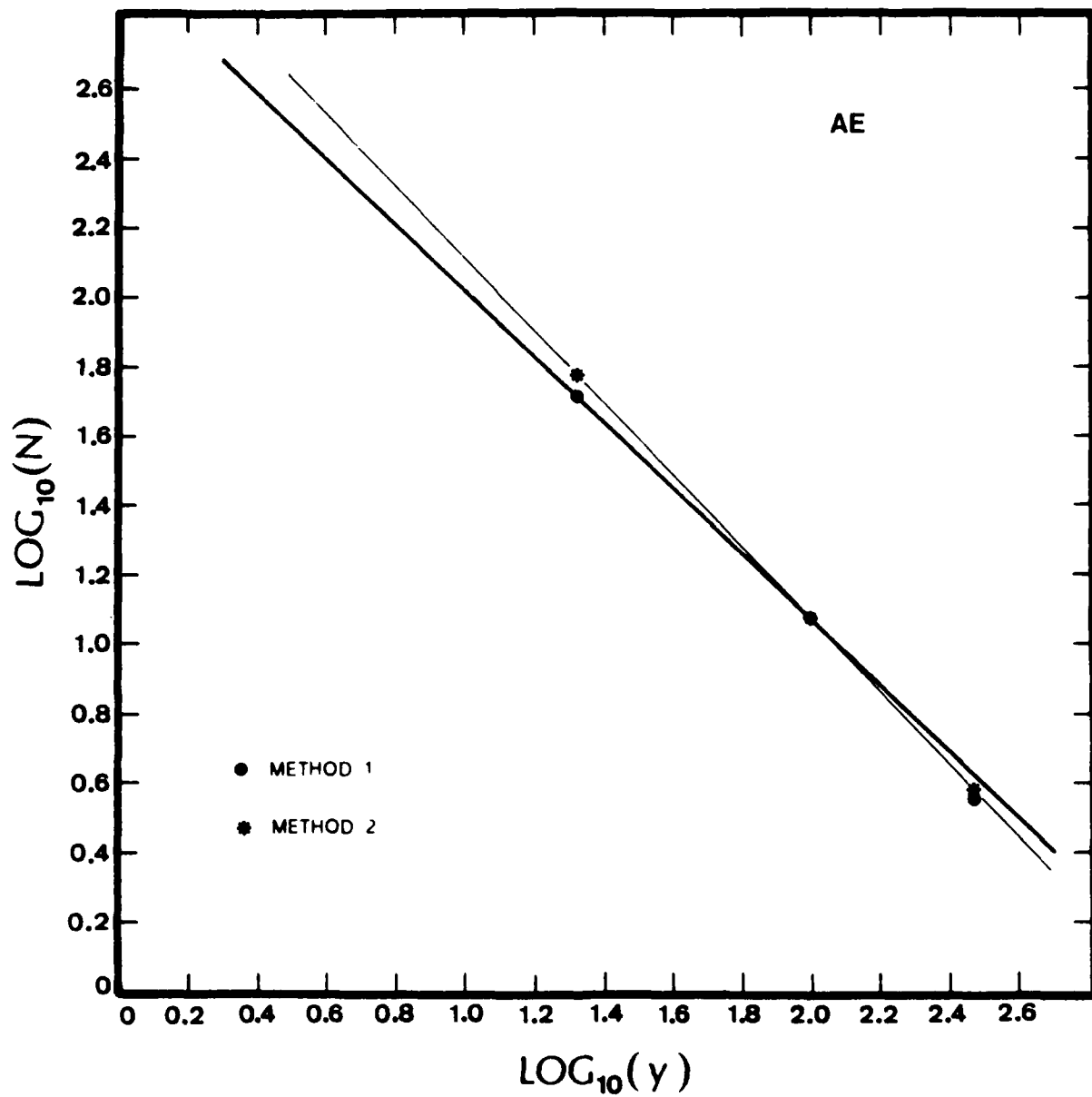


Figure 5. $\text{Log}_{10}(N)$ versus $\text{log}_{10}(y)$ plot for cross section AE

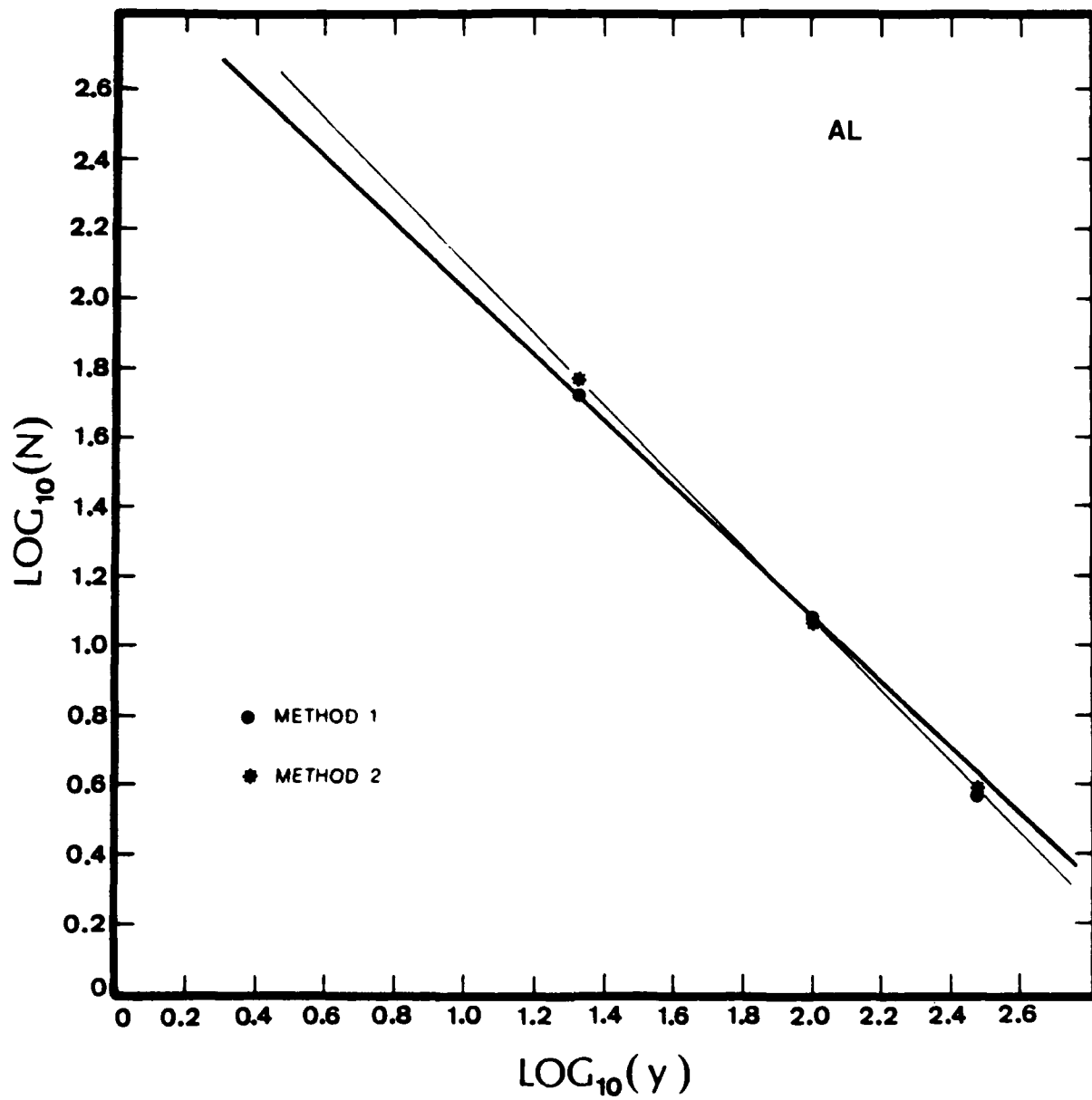


Figure 6. $\log_{10}(N)$ versus $\log_{10}(y)$ plot for cross section AL

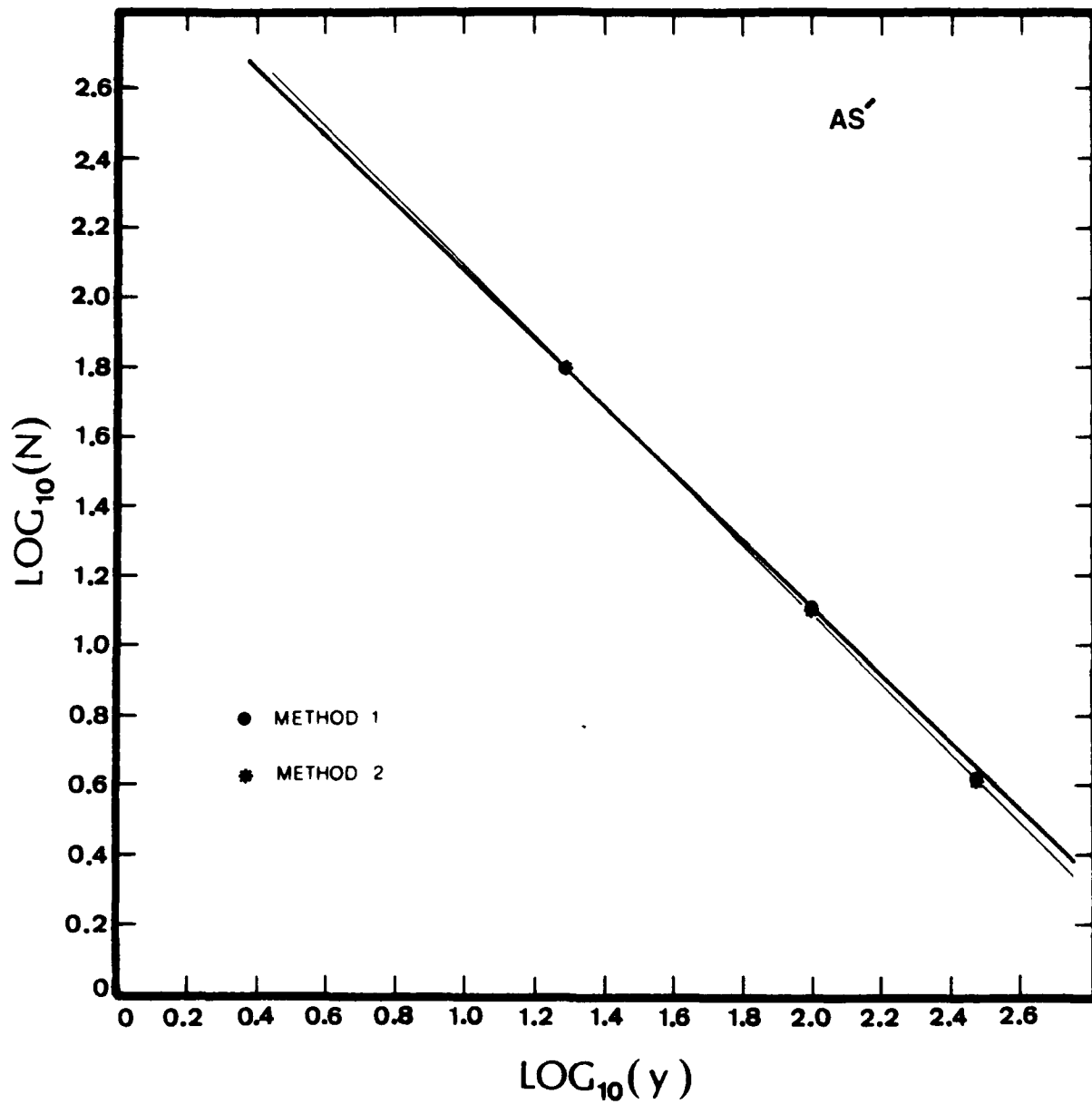


Figure 7. $\text{Log}_{10}(N)$ versus $\text{log}_{10}(y)$ plot for cross section AS'

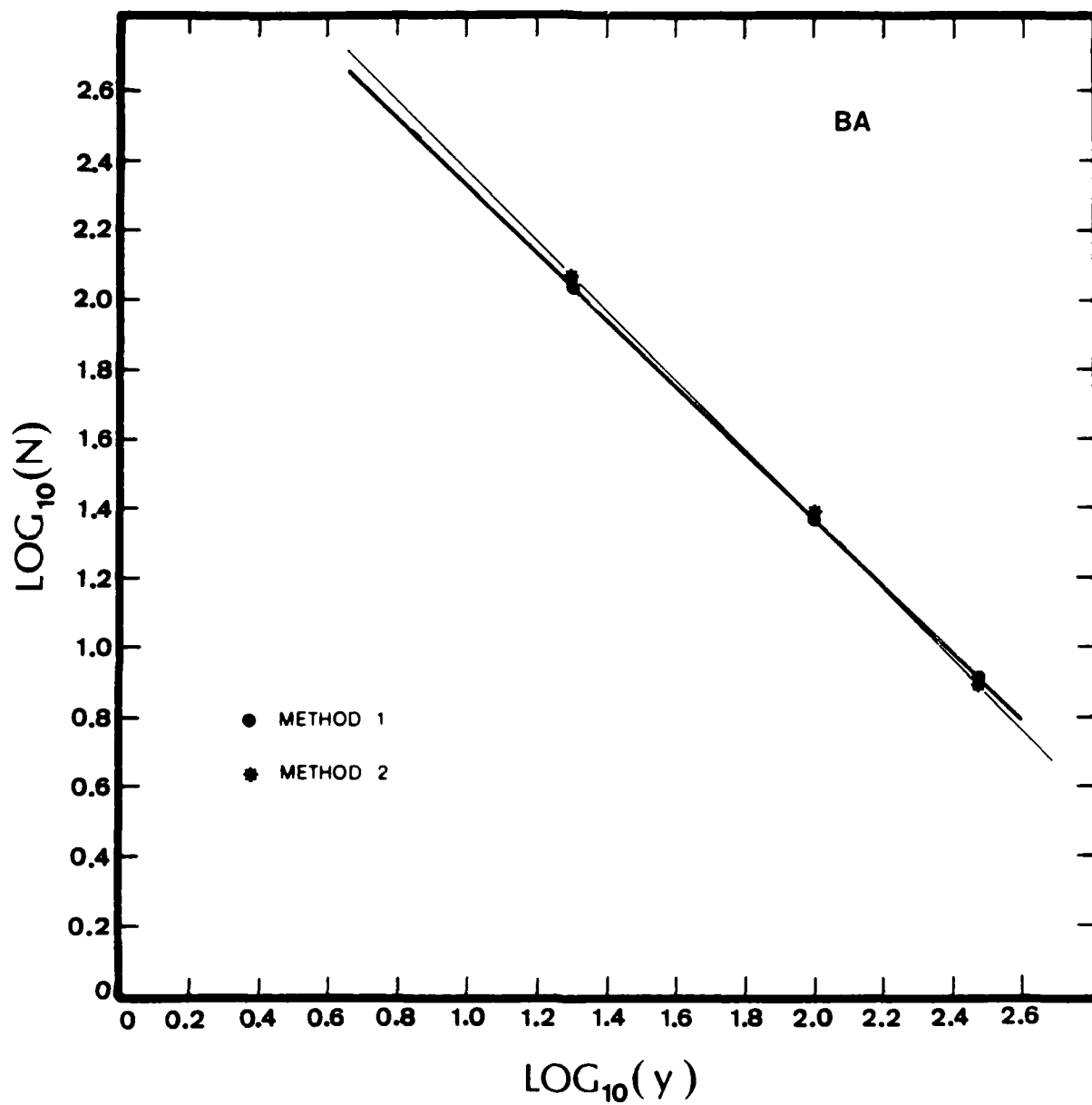


Figure 8. $\text{Log}_{10}(N)$ versus $\text{log}_{10}(y)$ plot for cross section BA

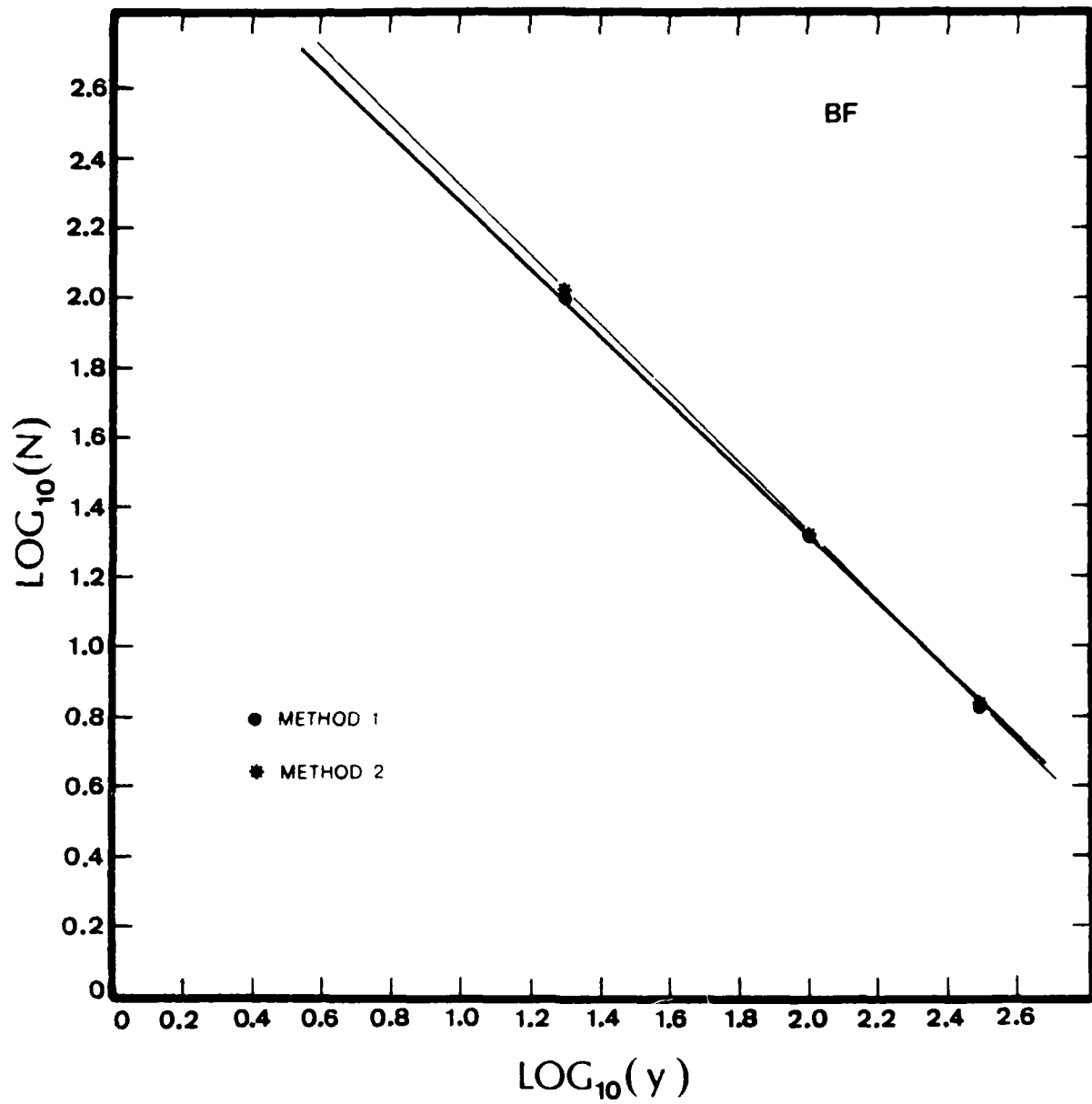


Figure 9. $\text{Log}_{10}(N)$ versus $\text{log}_{10}(y)$ plot for cross section BF

Table 2
Fractal Dimension Summary

Cross Section	Fractal Dimension	
	Method 1*	Method 2**
AB	1.020	1.0027
AD	1.007	1.0038
AE	1.060	1.0050
AF	1.007	1.0000
AG	1.020	1.0072
AH	1.030	1.0119
AJ	1.020	1.0060
AL	1.070	1.0100
AN	1.010	1.0012
AP	1.010	1.0009
AQ	1.030	1.0061
AR	1.020	1.0107
AS	1.030	1.0100
AS'	1.030	1.0052
AT	1.050	1.0200
AU	1.010	1.0040
AW	1.010	1.0268
AX	1.050	1.0189
AY	1.070	1.0100
AZ	1.110	1.0030
BA	1.040	1.0000
BB	1.003	1.0000
BC	1.007	1.0000
BD	1.003	1.0000
BE	1.040	1.0000
BF	1.040	1.0040
BG	1.030	1.0000
BH	1.020	1.0020
BI	1.010	1.0030
BJ	1.040	1.0050

* For method 1, only whole numbers are used for N .
 ** For method 2, the fractional remainder is added to N .

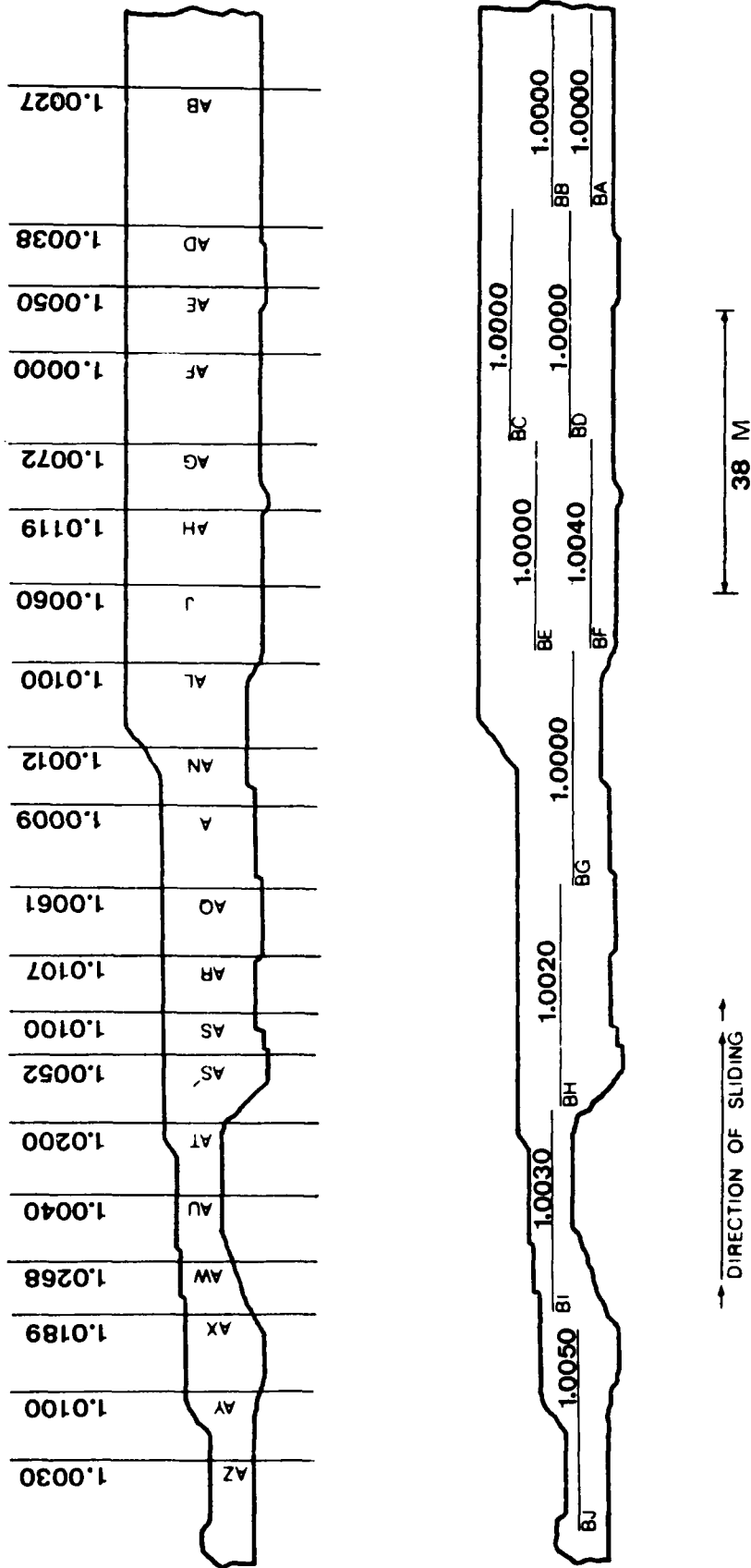


Figure 10. Fractal dimension summary for the DS + 122 joint surface

Control Calculation: Fractal Dimension of the
Australian Coast

19. A control calculation was sought to verify the fractal dimension calculation procedure. In a previous study, Mandelbrot (1967) reviewed the fractal dimension of coastlines. He found the fractal dimension of coastlines varied from a maximum of 1.25, for the west coast of Great Britain, to a minimum of 1.02, for the South African coast. For the Australian coast, Mandelbrot found the fractal dimension to be 1.13. This work is a standard reference because Mandelbrot was the first to demonstrate the fractal dimension of coastlines; moreover, he developed the concept of the fractal dimension.

20. Mandelbrot's results give interesting examples which can be used for control calculations. For this purpose, the coastline of Australia was chosen. The outline of this continent is shown in Figure 11. Using the segment lengths, y , shown in Table 3, the fractal dimension was found to be 1.11 using the method 2 technique; this fractal dimension was determined from the plot shown in Figure 12. This result is close to the value reported by Mandelbrot. Mandelbrot used the method 2 calculation for his research (Mandelbrot 1985). There is no proof that has been presented which supports the use of the method 2 technique. Its use is justified by the realization that the exclusion of the remainder can introduce considerable error in the calculation especially if the segment length, y , is large with respect to the line being measured.

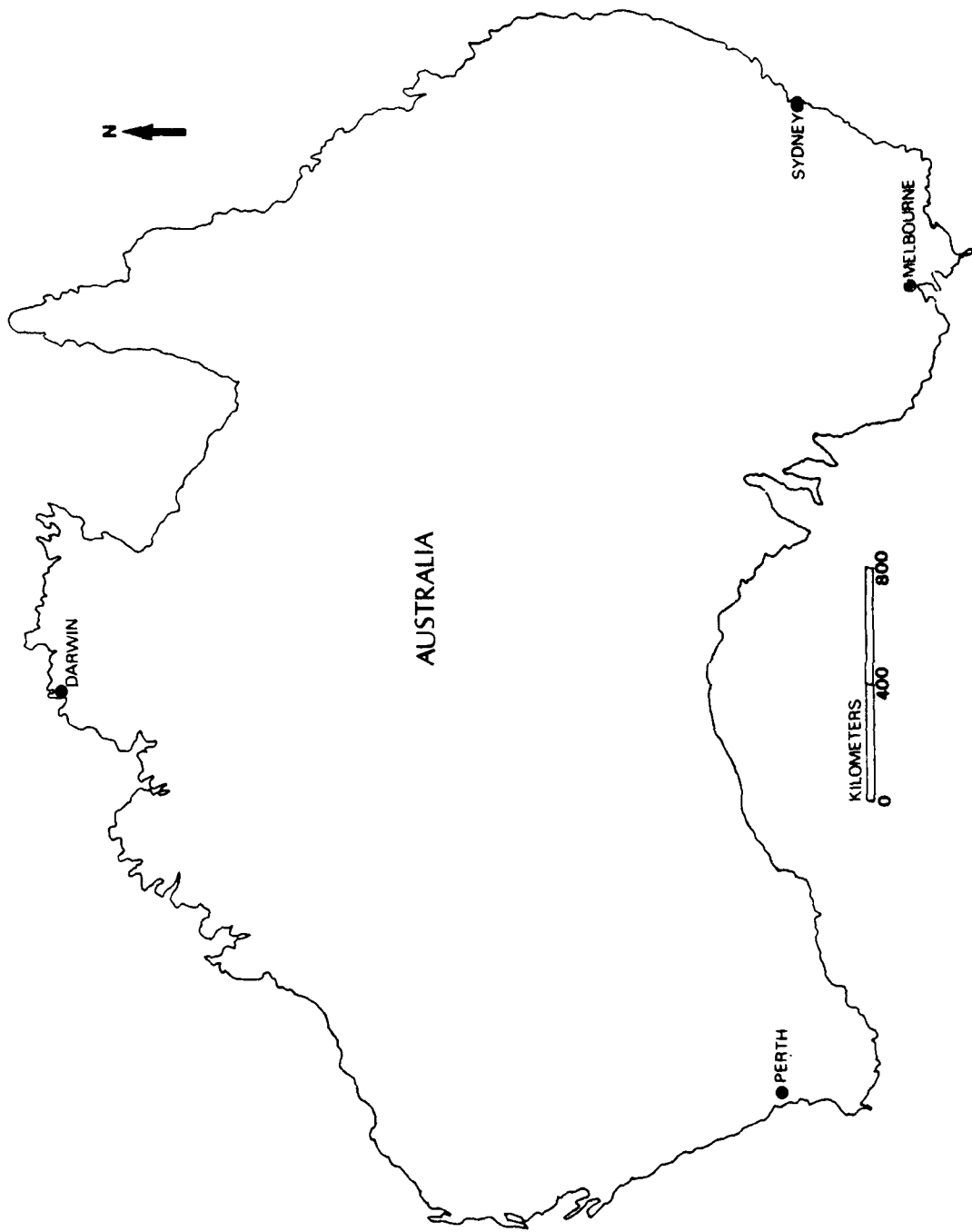


Figure 11. Outline of the coast of Australia

Table 3
Fractal Dimension* Calculation, Australian Coast

Ruler length y (km)	$\log_{10}(y)$	Segment Counts, N	$\log_{10}(N)$
500	2.700	24.442	1.3881
300	2.477	43.868	1.6421
100	2.000	154.471	2.1889

* Fractal dimension is 1.11.

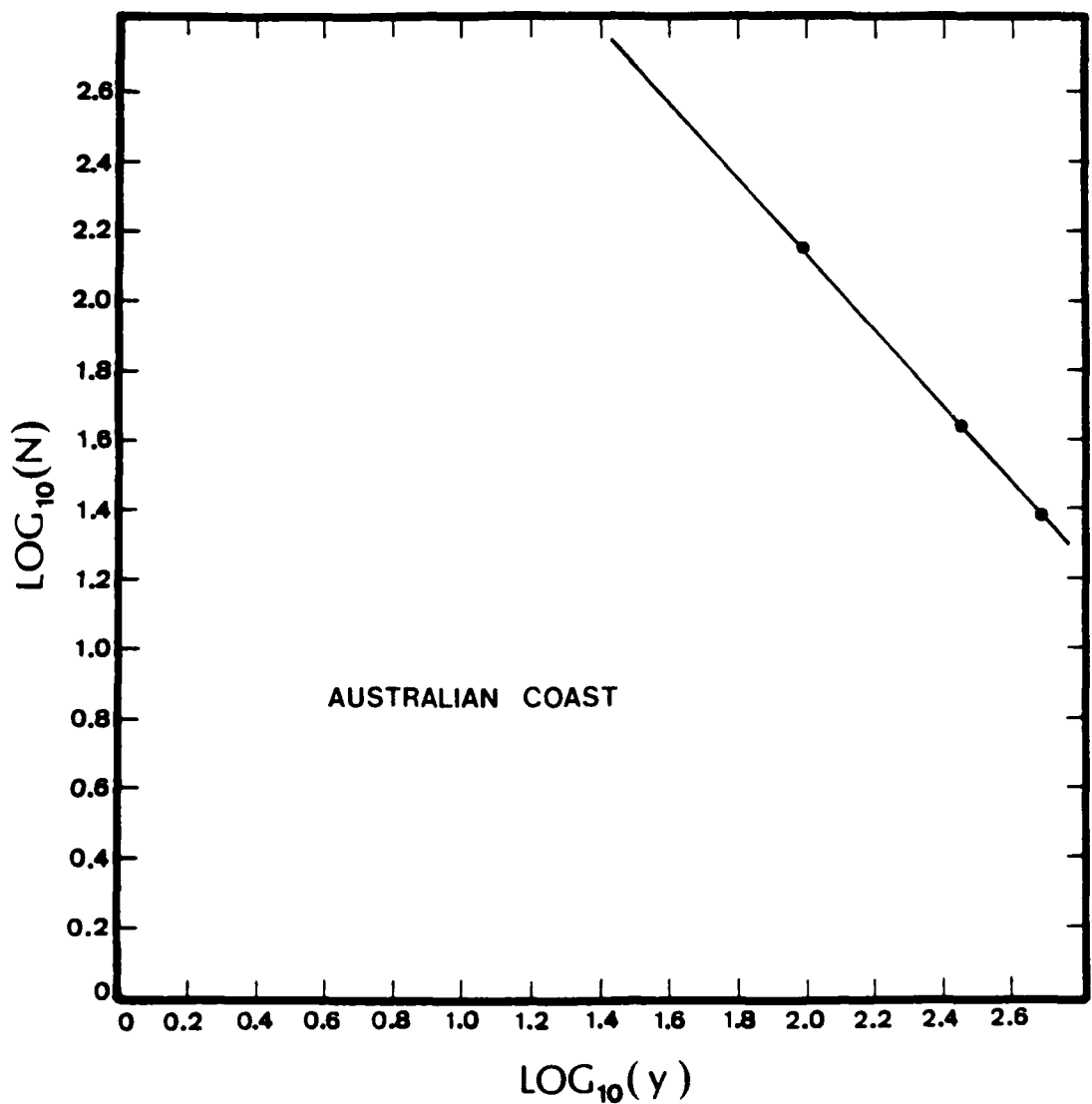


Figure 12. $\log_{10}(N)$ versus $\log_{10}(y)$ plot for the Australian coast

Variogram

21. In brief overview, the variogram is a mathematical function which describes the spatial similarity between the value of a geological phenomenon at one location and the value at a different location. The variogram is described in detail in Appendix B. This function is an important concept in modern geostatistics and has the form:

$$2 \gamma(h) = 1/N \sum \left[Z(x_i) - Z(x_i + h) \right]^2 \quad (4)$$

where Z is a vector containing the data which represents the spatial phenomenon under study, N is the number of pairs of these data separated by a distance, h , and γ is the variogram function. By describing the spatial similarity, the variogram also captures spatial continuity; that is, the variogram shows how rapidly the similarity between two data locations decreases with increasing distance separating them.

22. For rock mechanics applications, the variogram function, along with geostatistics, has received some use. These applications have been for the analysis of the spatial variation in rock mass features, particularly fracture density and orientation (LaPointe 1980). Early work with this type of analysis has been extended to the simulation of rock mass properties (Miller and Borgman 1985). The variogram has also been used to describe the spatial variation in rock mass features adjacent to and involved in ground subsidence over abandoned mines (Van Besien 1985). Hence, the variogram is known technique in the field of rock mechanics.

Variograms of Selected Cross Sections

23. Variogram analysis was used for this study to describe the spatial correlation and continuity of joint surface asperities. The objectives of this application were to: (a) simply evaluate the utility of the variogram function for this type of analysis; (b) investigate the spatial correlation and continuity of rock mass asperities; and (c) determine the correlation, if any, between the variogram and the fractal dimension.

24. Selected cross sections are chosen and presented for this application. These are shown in Figures 13 and 14. The variograms for these cross sections are presented in Figures 15 through 20. The actual variogram results used to develop these figures are presented in Appendix D. The variograms of Figures 15 through 20 are representative of the types of results observed for variograms in this study.

25. Many of the cross sections of the DS + 122 joint surface were associated with variograms showing a behavior attributable to the data being non-stationary (see Appendix B for an explanation of the Intrinsic Hypothesis). This type of behavior results when a change in data values occurs in a regular fashion over a particular direction, such as elevation values which increase as one travels upslope. Cross sections which yielded such variograms did show a distinct inclination. Non-stationary variograms are parabolic and concave upward in shape. Figure 15 shows a variogram of this type for cross section BG. In Figure 13, this cross section is seen to be inclined.

26. For this study, and non-stationary variogram in general, one procedure to make the data more amenable to geostatistical analysis is to filter the non-stationary component from the data. If the data are denoted as $Z(x)$, two components comprise these data, $S(x)$ and $N(x)$, such that

$$Z(x) = S(x) + N(x) \quad (5)$$

where $S(x)$ is the stationary component and $N(x)$ is the non-stationary component. For this study, $S(x)$ is the elevation value due to surface asperities and $N(x)$ is the elevation value due to the inclination of the cross section.

27. For an enhanced analysis, $N(x)$ was filtered from the cross section data, such as cross section BG, to yield

$$S(x) = Z(x) - N(x) \quad (5a)$$

The procedure used to remove $N(x)$ is shown in Figure 21. The angle of inclination was calculated, and the elevation of the plane defined by this angle was removed from each of the cross section elevation values. This resulted in filtered cross sections. A variogram computed for cross section BG, after filtering, is shown in Figure 22.

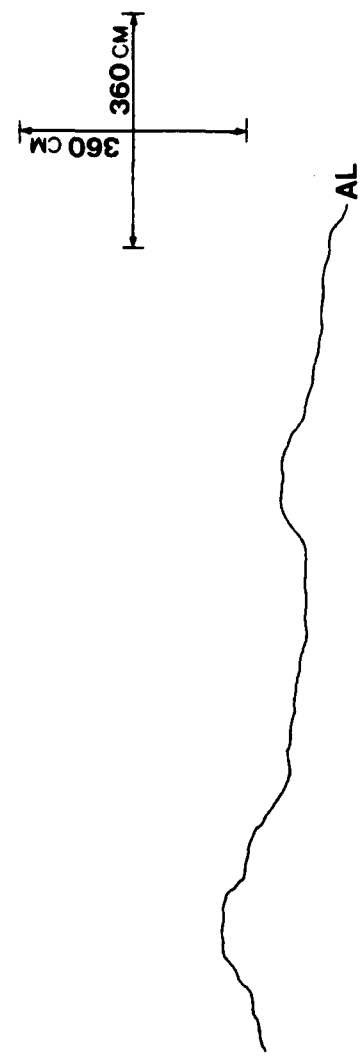
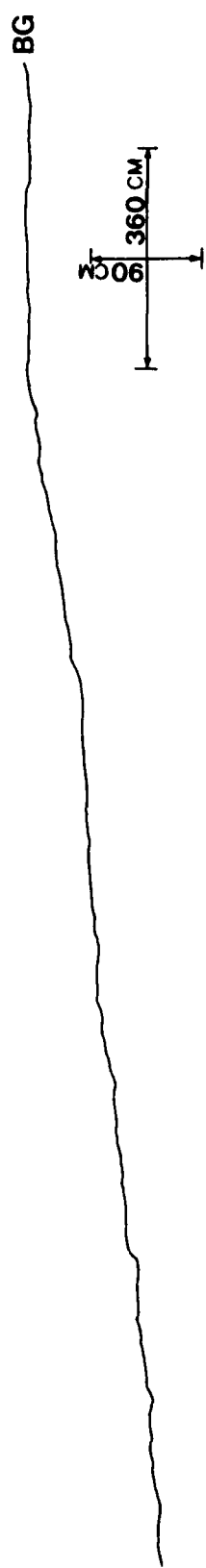


Figure 13. Cross sections AL, AF, BG analyzed using the variogram

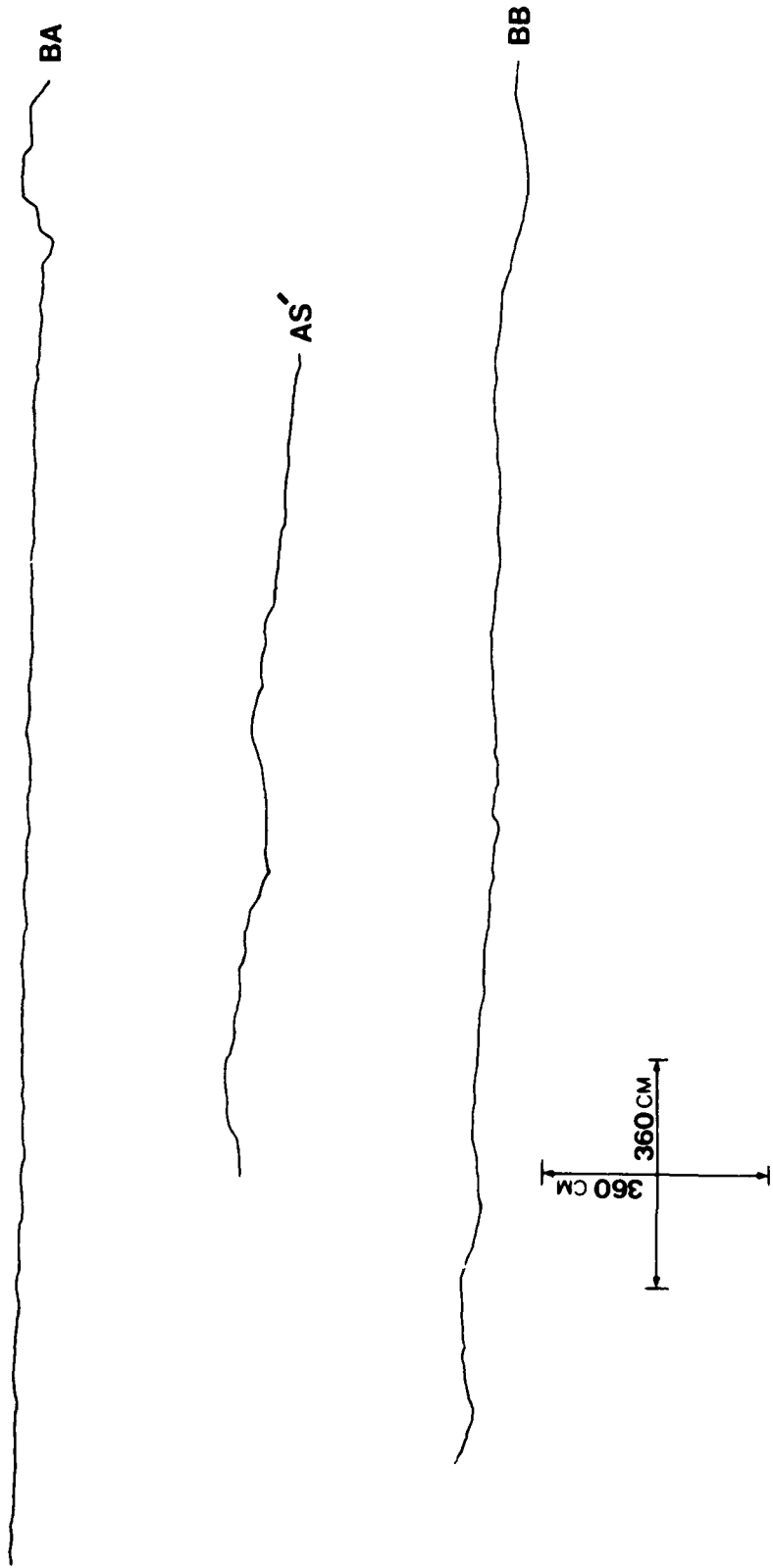


Figure 14. Cross sections BB, AS', BA analyzed using the variogram

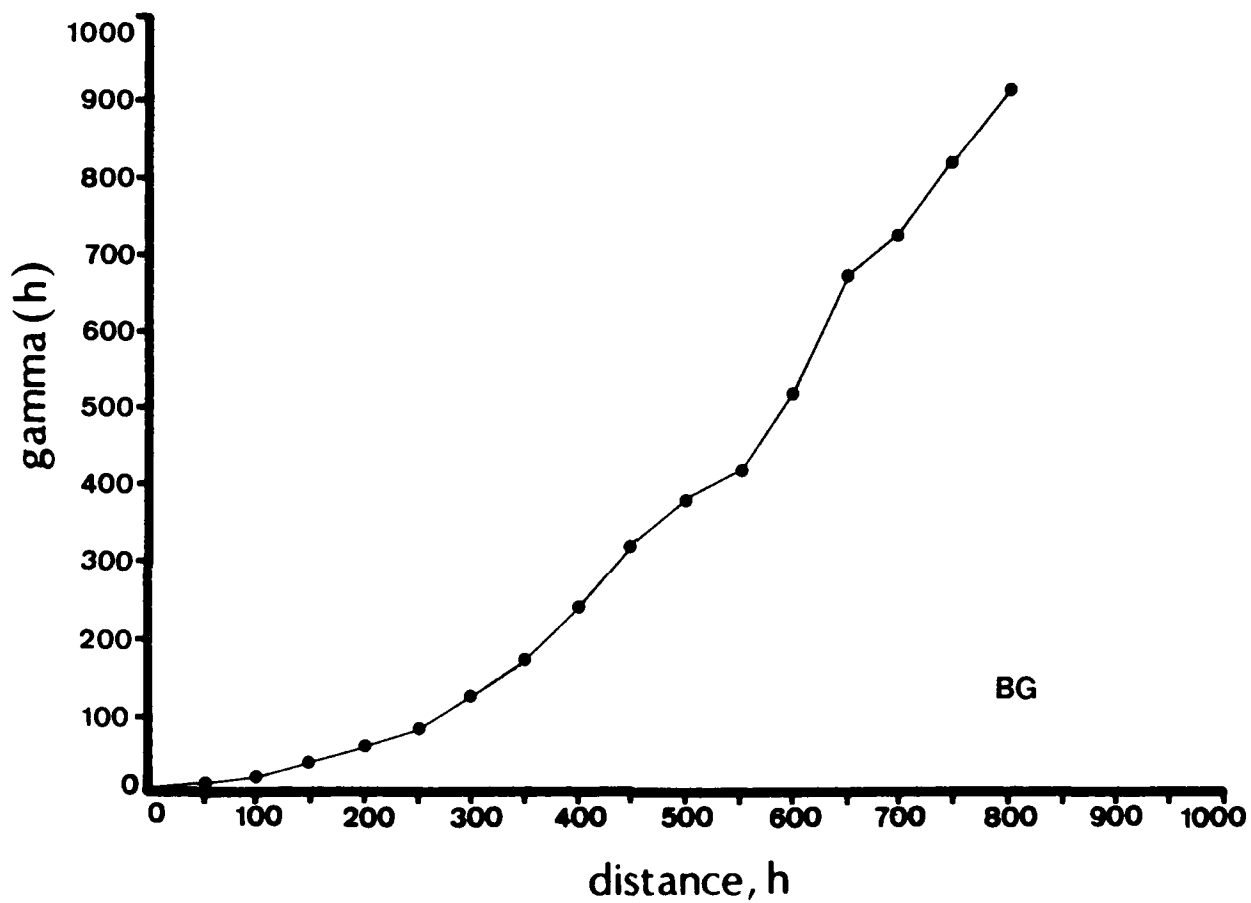


Figure 15. Variogram for cross section BG, an example of non-stationary behavior in the variogram

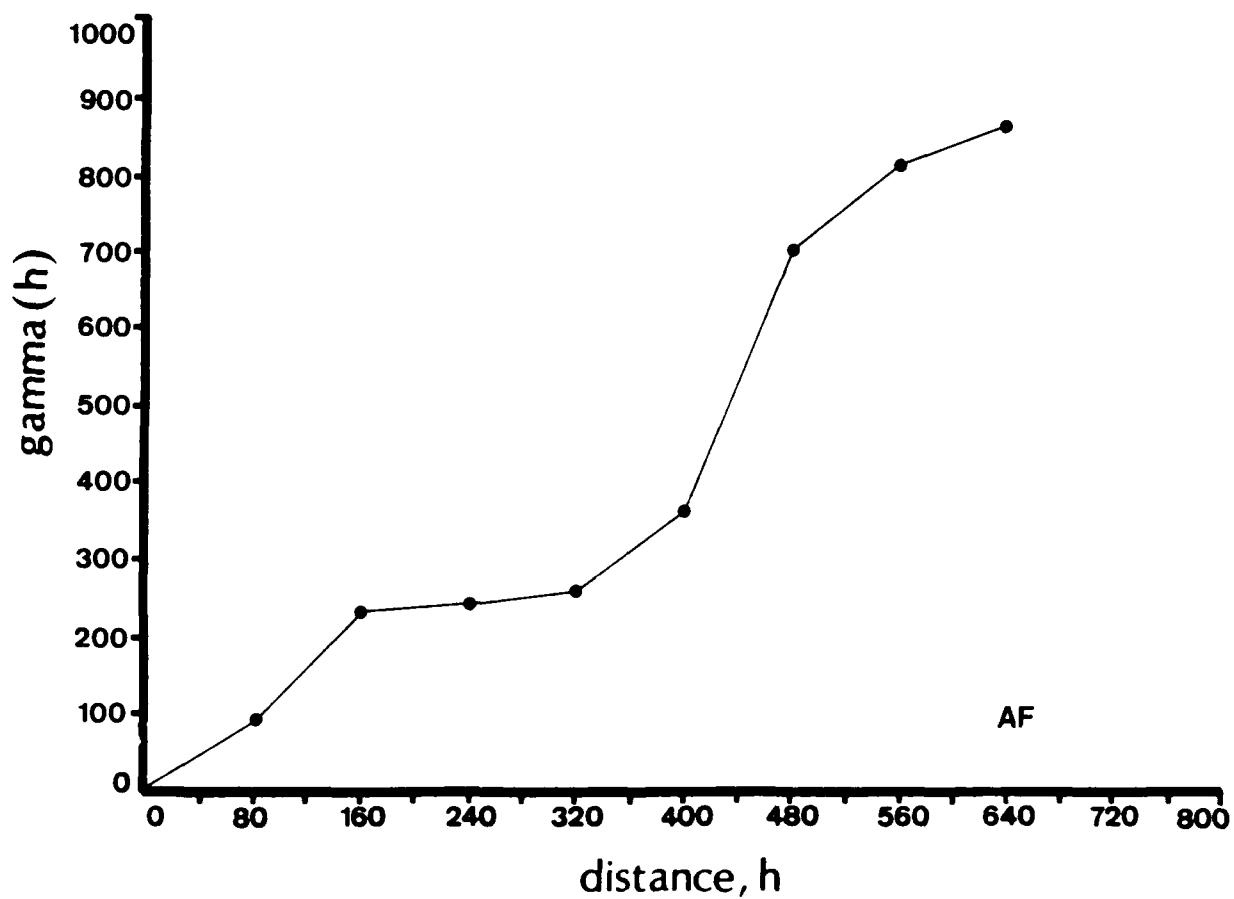


Figure 16. Variogram for cross section AF. Variogram is stationary, but at $h = 400$ cm, it becomes non-stationary

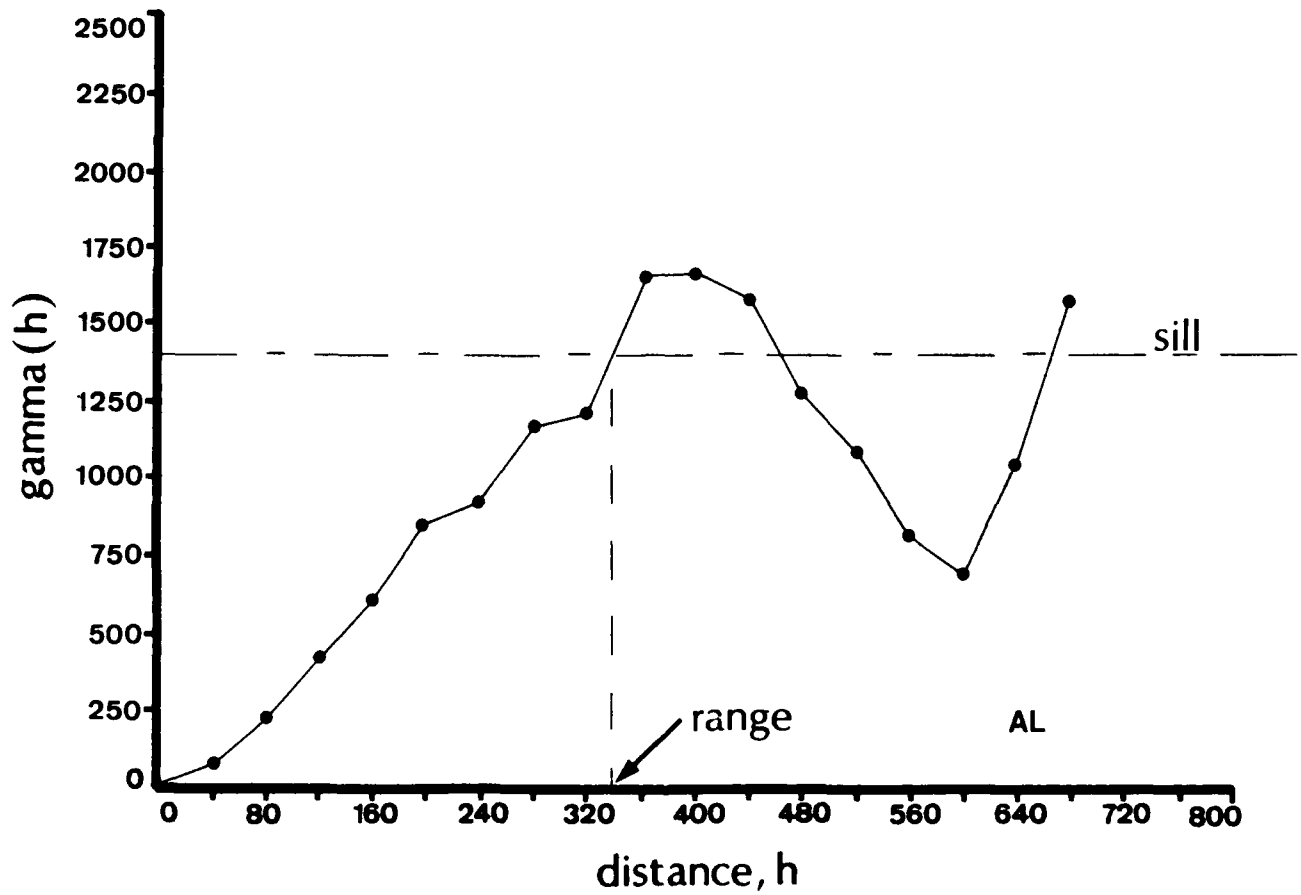


Figure 17. Variogram for cross section AL, an example of stationary variogram

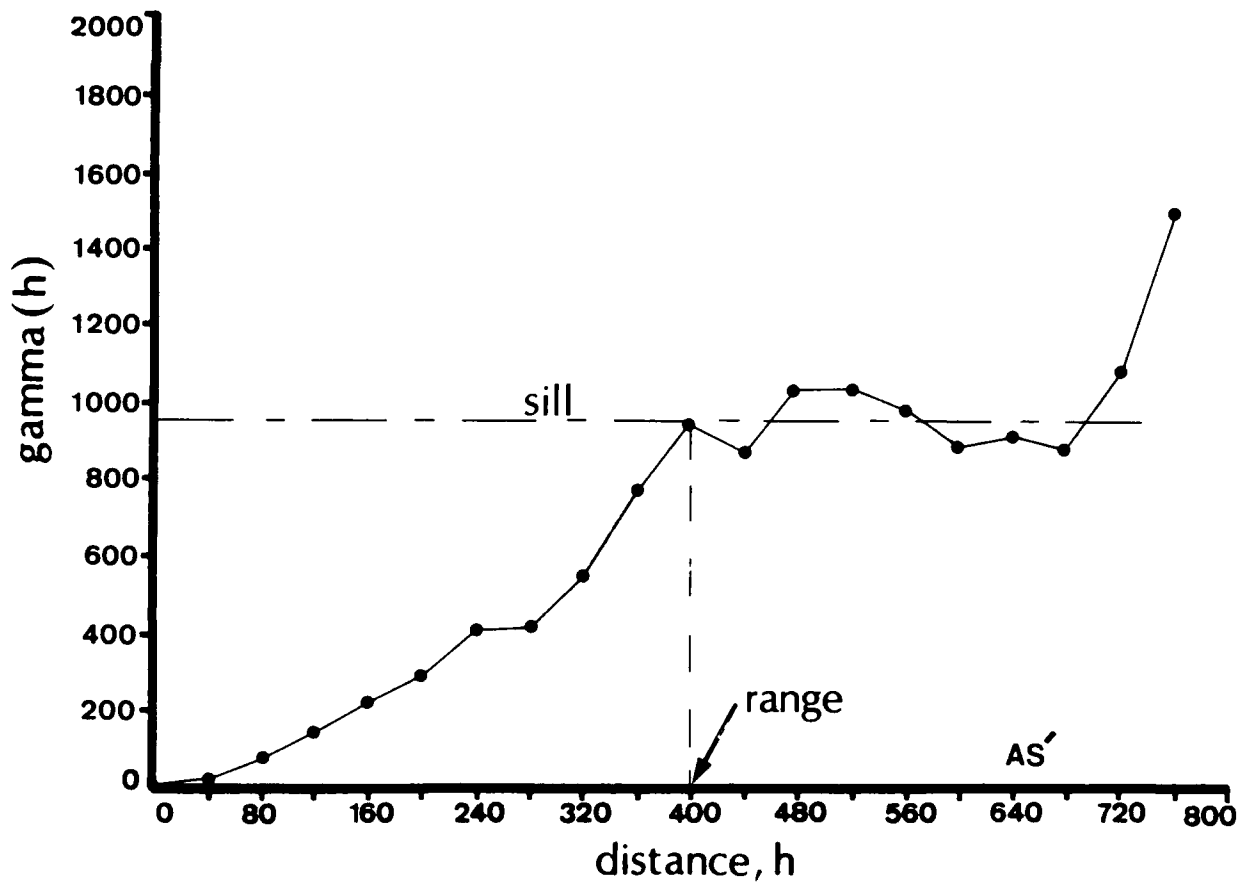


Figure 18. Variogram for cross section AS', an example of stationary behavior

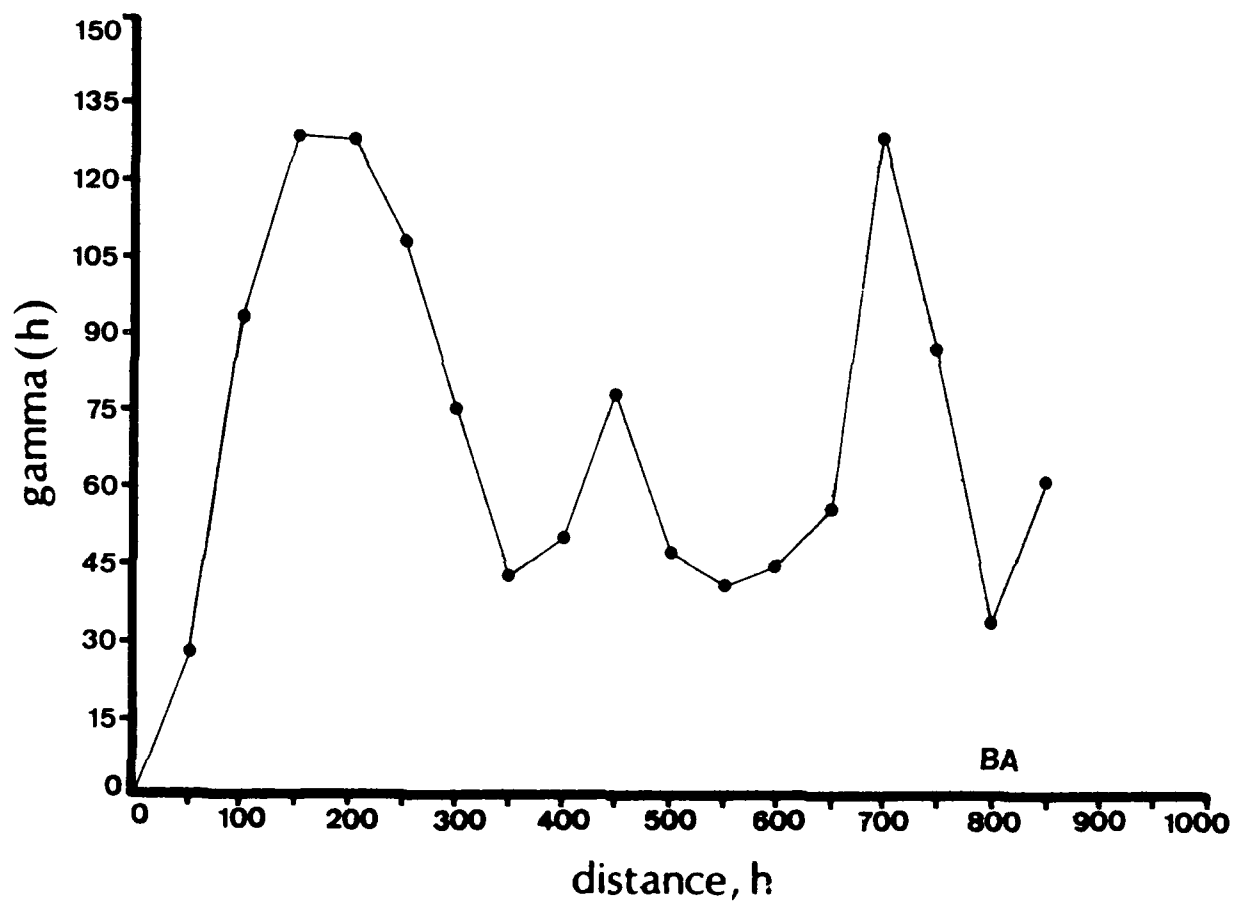


Figure 19. Variogram for cross section BA, an example of stationary behavior

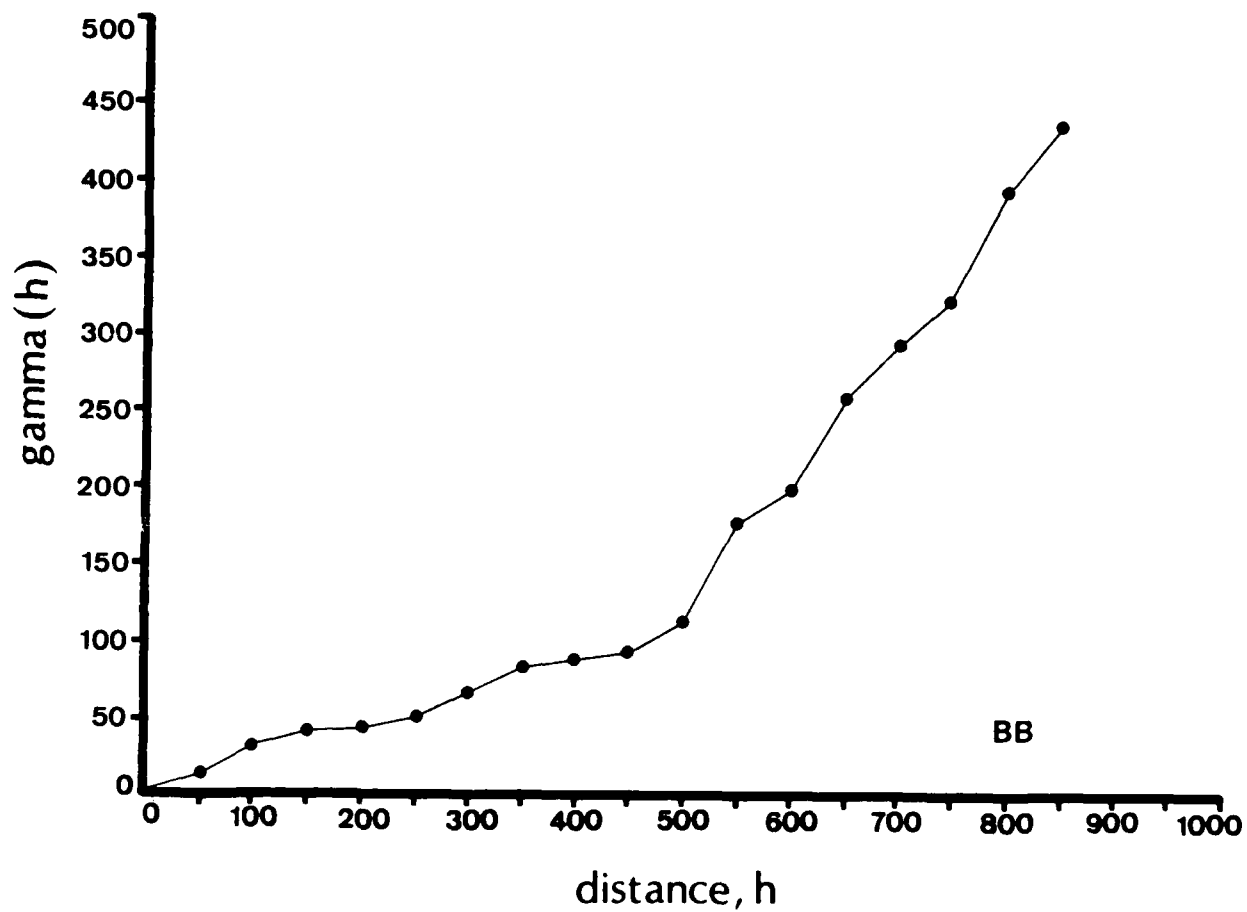
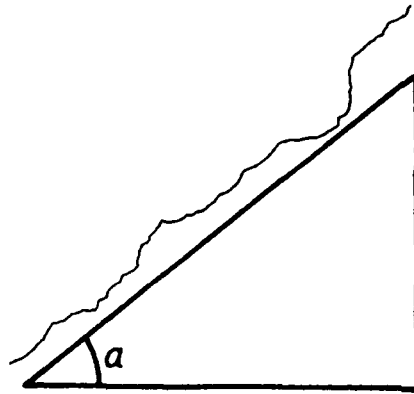
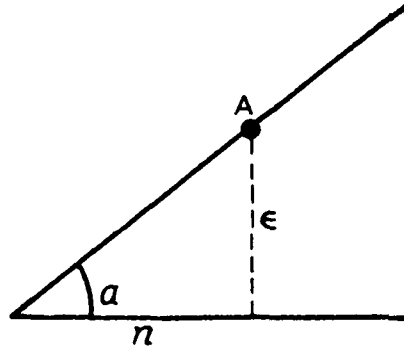


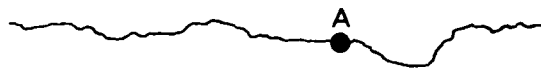
Figure 20. Variogram for cross section BB, an example of a non-stationary variogram



JOINT SURFACE INCLINED
AT AN ANGLE OF a



ELEVATION (ϵ) AT (A) DUE
TO INCLINATION EQUALS
 $n \tan(a)$



REVISED CROSS SECTION
NEW ELEVATION AT (A) =
OLD ELEVATION - ϵ

Figure 21. Diagram of the procedure used to remove the influence of the plane of inclination from cross-sectional data

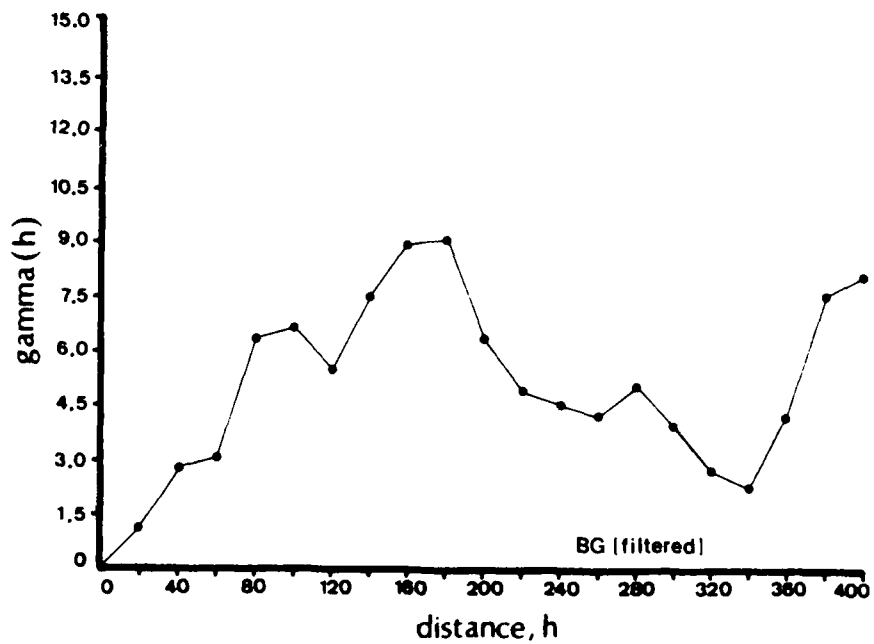
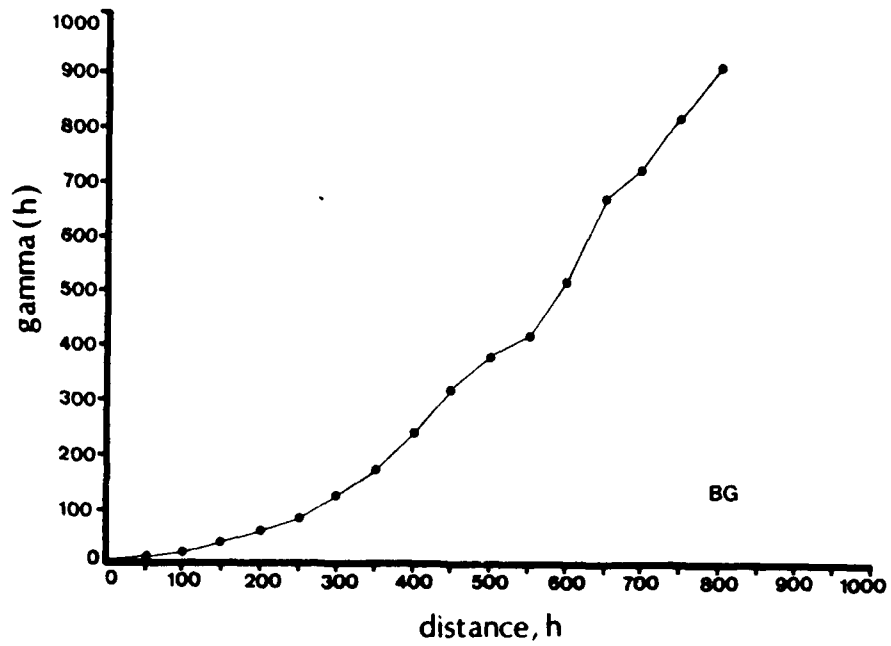


Figure 22. Variogram for cross section BG subsequent to the removal of the inclination

Results of the Variogram Analysis

28. Stationary variograms (Figures 17, 18, 19, and 22) show that asperity undulations along a joint surface are spatially correlated. Table 4 lists the properties of these four variograms. The sill, a more or less constant value the variogram attains at a certain separation distance, of each variogram is slightly larger than the variance of the elevation values along each cross section. The range, that separation distance at which the variogram attains the sill, of each variogram shows the spatial continuity of asperity values; there is not spatial correlation for separation distances greater than the range. The nugget value, the intercept of the variogram with the ordinant axis, shows the level of noise (random variations) present in the elevation data; for each cross section, the nugget value is small as expected for this type of precisely measured data. Finally, each variogram is compared to the fractal dimension for a particular cross section. There appears, on the basis of at least these four variograms, to be little correlation between the variograms and the fractal dimension. The fractal dimension offers a unique method for the description of surface roughness. The variogram, while yielding no clear information on surface roughness, analyzes other features of a joint surface, particularly the spatial distribution of asperities.

Table 4
Properties of Stationary Variograms

<u>Cross Section</u>	<u>Nugget</u>	<u>Sill</u>	<u>Range (cm)</u>	<u>Fractal Dimension</u>
AL	0.0	1400.00	300.00	1.0100
AS'	0.0	650.00	330.00	1.0052
BA	0.0	130.00	150.00	1.0000
BG (filtered)	0.0	6.00	80.00	1.0000

Potential Application of the Variogram: Kriging

29. One value result of this study was the demonstration that variograms can be developed for elevation data measured along a joint surface. Because these data are shown to be spatially correlated, this correlation can be used to estimate elevation values at locations where such values were not

measured. This estimation process is achieved using the geostatistical estimator known as kriging. This technique is described in Appendix B.

30. For geostatistical analyses, such as were reviewed in this study, kriging is useful in mapping available data. For the cross sections used for this study, kriging could be used to develop greater detail in these plots. For example, kriging could be used to estimate an elevation value between two measured locations. This estimate would be based on the two known elevation measurements and the variogram. In this manner, the spatial correlation and continuity shown by the asperities could be used to better define each asperity (i.e., to fill in data between measurement points).

31. More importantly, this study relied on a plotted contour map of the DS + 122 joint surface as a source of data. Elevation values of such detail, already mapped, are rare. More often, elevation values are typically measured across a joint surface at irregular locations with a rather sparse sampling interval. The results of this study imply that a variogram could be developed for this type of sparse data. Kriging could be used to estimate elevation values at intersections of a regular grid superimposed over the joint surface. In this manner, kriging could be useful in developing the type of contour map which served as the data base for this study without the need for photogrammetrically mapping the entire surface.

32. Kriging is often used for gridding purposes (i.e., the interpolation of data at intersections of a regular grid; Olea 1974). This is done especially in preparation for data contouring; an algorithm for contouring usually requires a regular grid of data. A rock joint is a two dimensional surface and can be represented by a two dimensional grid. This report, however, examines one dimensional profiles along certain directions across a joint surface. Kriging might be used in a broader investigation to form a two dimensional digital grid of a joint surface. Such a grid could then be used to calculate a fractal dimension for the entire surface, rather than for discrete profiles. This might lead to a significant contribution to the procedures used for the analysis of sliding stability of rock masses.

PART IV: COMPARISON OF THE USE OF THE FRACTAL DIMENSION
AND THE VARIOGRAM TO ACCEPTED ROCK SURFACE
ROUGHNESS EVALUATION TECHNIQUES

33. It is emphasized that the use of the fractal dimension and the variogram supplements, but does not replace, classic surface roughness evaluation techniques. It has been noted in the past that different types of joint and fault surfaces display quite different surface roughness patterns (Patton 1966). It was further observed that the surface roughness varies with direction across a rock surface (Patton and Deere 1970). These orientation differences are especially important for sliding stability analyses.

34. Surface roughness is caused by irregularities, also called asperities. There are usually several orders of magnitudes of surface asperities, from microscopic pits to megascopic folds (Piteau 1970). For the analysis of sliding stability, it is often assumed that small magnitude asperities bear the initial shear load, but quickly shear. Subsequent to this, the megascopic asperities bear the load and control the sliding stability (Hoek and Bray 1974).

35. The different magnitudes of asperities are easily recognized in Figure 23, which is reproduced from Patton and Deere (1970). This figure shows an actual cross section along a bedding plane and is analogous to the

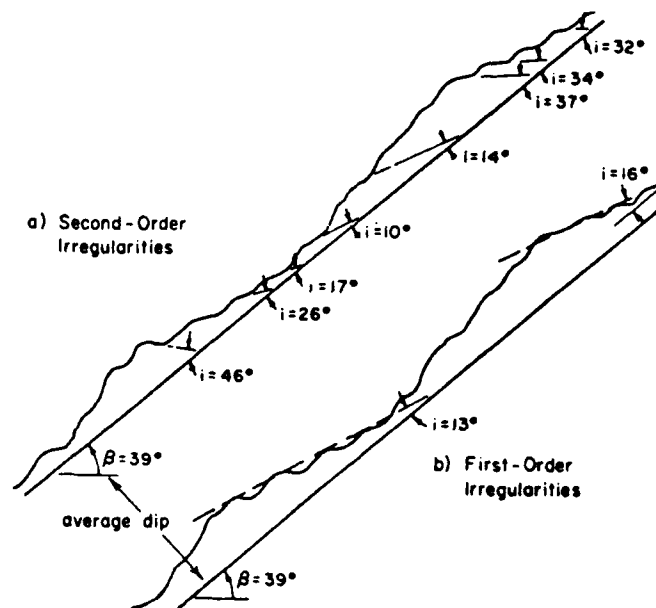


Figure 23. Cross section from Patton and Deere (1970)

cross sections plotted for the DS + 122 joint surface. The fractal dimension of the cross section of Figure 23 is 1.01.

36. It is evident from this example that the fractal dimension does not clearly identify the different orders of asperity magnitudes. The fact that there are different magnitudes of asperities, however, does follow the concept of self-similarity (Mandelbrot 1982). Each of the small asperities is self-similar to the next larger size of asperity, and so on. It is hypothesized that the more magnitudes of asperity sizes a joint surface has, the larger will be its fractal dimension. In this sense, the fractal dimension might serve as an indicator of the presence of different magnitudes of asperities.

37. The variogram is more valuable for the analysis of asperity magnitudes. The cross section of Figure 23 is replotted in Figure 24 to remove the inclination and increase the scale. Assigned for this study to be consistent with the horizontal scale, an elevation scale is shown. This scale was not originally provided by Patton and Deere (1970), but can be assumed to be correct based on the inclination values noted in Figure 23. A variogram was developed for this cross section and is plotted in Figure 25.

38. Of particular interest to this study, the variogram of Figure 25 shows a periodic behavior. The variogram increases initially away from the origin, attains a plateau (the sill), then decreases, but subsequently increases to a second plateau. The distance, h , between the origin and the point at which the variogram begins its second increase is approximately 100 cm.

39. In Figure 24, there is a 100 cm distance between the peaks of the megascopic asperities. The variogram of Figure 25 is interpreted to represent the spatial correlation between the small asperities (the first increase and plateau) and the spatial correlation between the larger and more widely spaced asperities (the second increase and plateau). This is a valuable application of the variogram because it appears from this example that the variogram can help to describe the various magnitudes of asperities.

40. For the cross sections of the DS + 122 joint surface, several variograms displayed the type of behavior shown by the variogram of Figure 25. Two of these variograms are again plotted in Figures 26 and 27; the cross sections are plotted in Figure 28. For cross section A1, the variogram identifies a second, larger asperity group with an average spacing of 600 cm. For

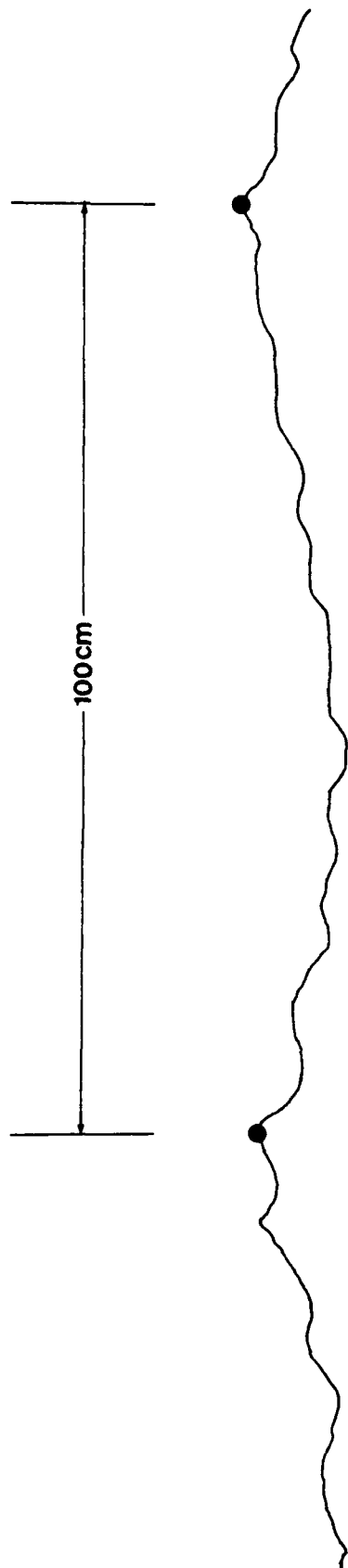


Figure 24. Cross section from Patton and Deere (1970), plotted at an enlarged scale and without inclination

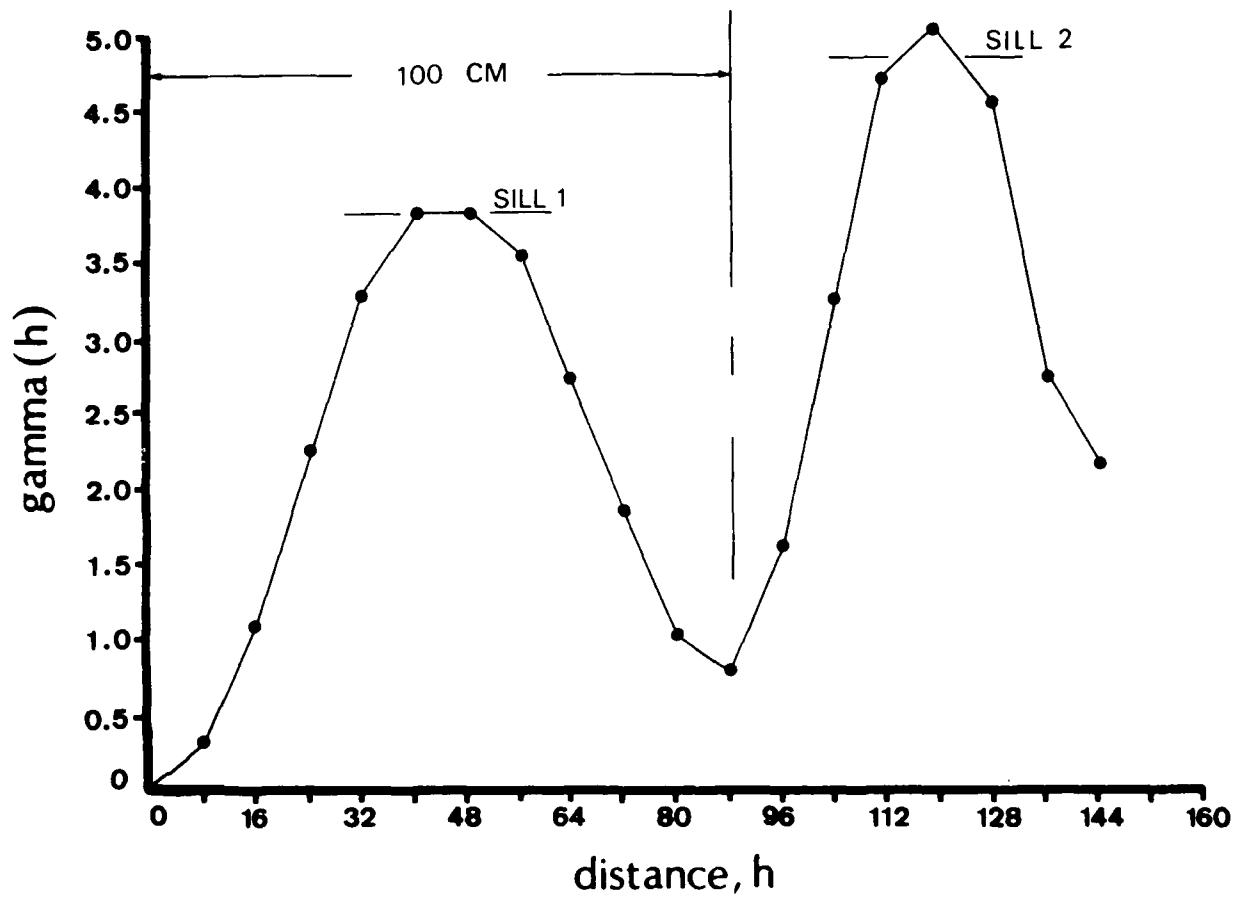


Figure 25. Variogram for the cross section of Patton and Deere (1970). Note the periodic (bimodal) behavior

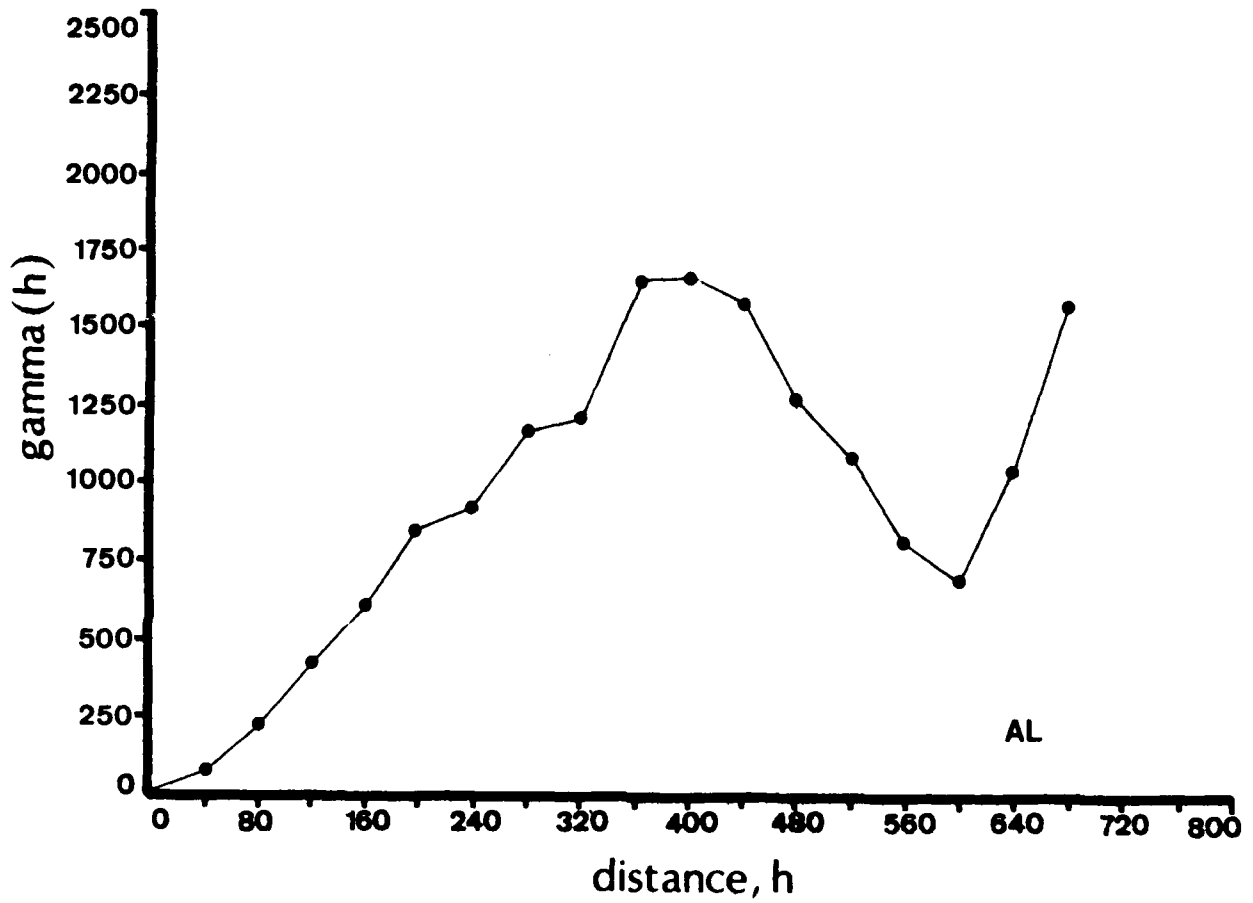


Figure 26. Variogram for cross section AL, presented here to emphasize its periodic behavior

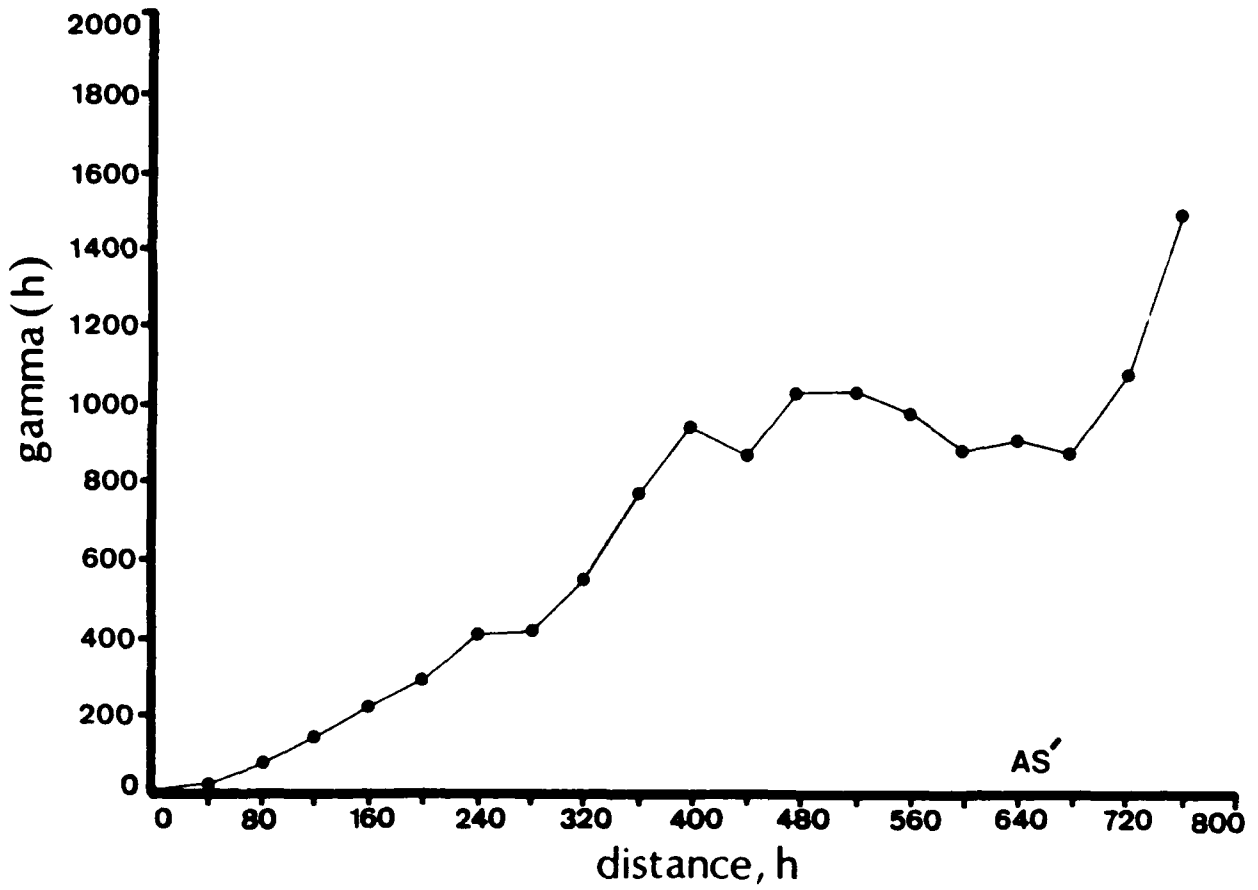


Figure 27. Variogram for cross section AS', presented here to emphasize its subtle periodic behavior

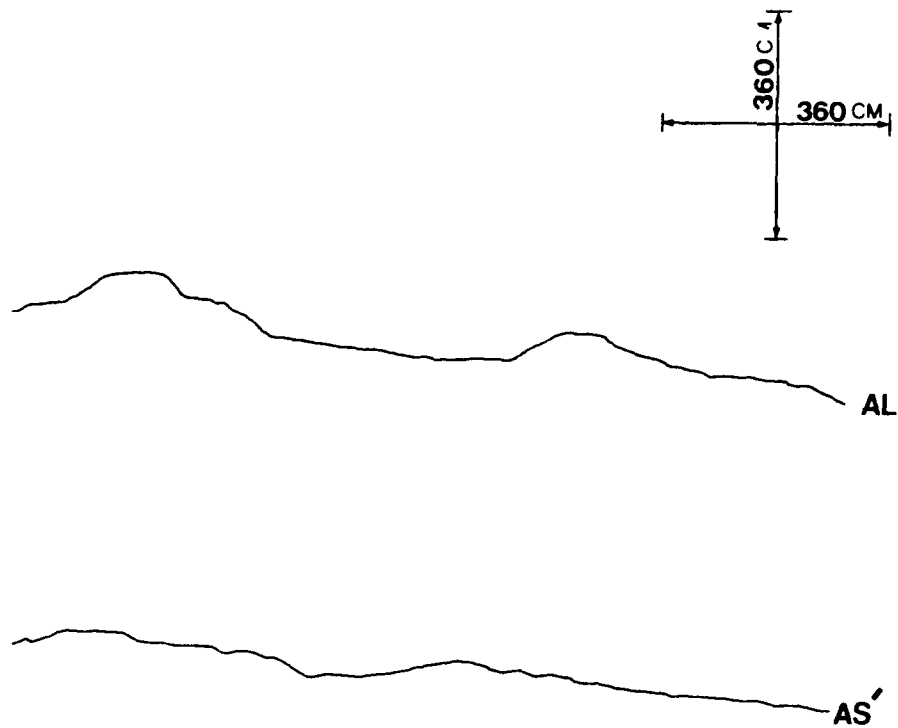


Figure 28. Cross sections AL and AS', plotted for comparison with the variograms of Figures 26 and 27

cross section AS', the spacing of the larger asperities is found from the variogram to be 680 cm.

41. Directional characteristics of surface roughness, as noted by Patton and Deere (1970), can be evaluated using the fractal dimension or the variogram. Cross sections along the DS + 122 joint surface had specific orientations. Hence, each computed fractal dimension and variogram indicated a specific directional characteristic. The combination of fractal dimension and variogram is ideally suited for the description of joint properties. The qualitative descriptions offered by Patton (1966), Patton and Deere (1970), and Piteau (1970) can be quantitatively described by the fractal dimension and the variogram.

PART V: APPLICATION OF THE FRACTAL DIMENSION AND VARIOGRAM
TO STRING LINE DATA FOR ROCK SURFACES NEAR
LIBBY DAM, MT

42. Previous sections of this report reviewed the application of the fractal dimension and variogram to the analysis of the DS + 122 slide surface adjacent to Libby Dam, MT. Subsequent to this slide, ground-based reconnaissance was made of older joint and bedding plane surfaces in proximity to the DS + 122 slide. During the reconnaissance, string line measurements were made of several rock surfaces. This process involved the placement of a string approximately parallel to and above the rock surface. Elevations were measured from the string line to the rock surface at 0.5 ft* intervals. The rock surfaces for which string line data were collected are listed in Table 5. These data are plotted in Figures 29 through 33.

43. These string line data provided a different means for evaluating the fractal dimension and spatial continuity of rock surfaces. The data used previously to describe the fractal dimension of the DS + 122 slide were derived from a highly detailed contour map of the rock surface plotted at 2 cm contour intervals. At times, this contour map was difficult to read. Moreover, the map was plotted from stereo photo pairs, and the true data resolution is estimated by observations during this study to be 20 cm. Hence, the string line data may be a higher resolution data source and possibly more reliable than the data obtained from the contour map.

Fractal Dimension of String Line Cross Sections

44. Fractal dimensions were calculated for the rock surfaces listed in Table 5. The procedure used was the one reviewed for the DS + 122 cross section using the technique whereby the fractional remainder is added to the number of counts, N , for each segment length, y . The results are listed in Table 6.

45. For this application, $\log_{10}(N)$ versus $\log_{10}(y)$ plots were not drawn to determine the fractal dimension. Instead, a least squares regression

* A table of factors for converting non-SI units of measurement to SI (metric) units is presented on page 4.

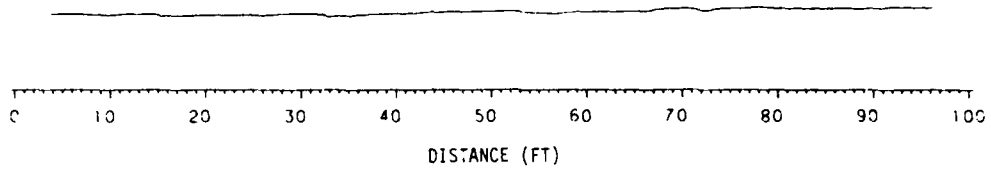
Table 5

List of Rock Surfaces Associated with String Line Data

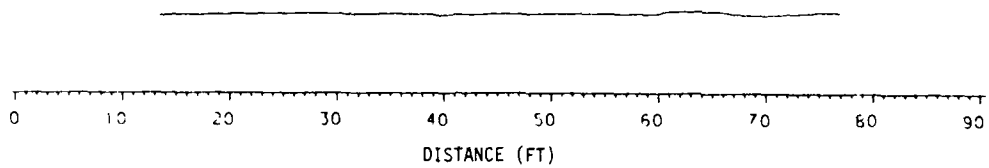
<u>Rock Surface (Names from Nearest Topographic Feature)</u>	<u>Type of Feature</u>
1. Backus Notch No. 1	Bedding plane
2. Backus Creek Notch No. 1	Bedding plane
3. DS + 122, C	Joint
4. Island Notch	Joint
5. DS + 122 (minor)	Joint
6. DS + 122, No. 2	Joint
7. 914 Rib*	Joint
8. Dunn Creek Notch	Joint
9. 930 joint	Joint
10. Island Notch	Joint/bedding plane intersection
11. Island Notch	Bedding plane
12. Wolf Creek Jct.	Joint
13. Dunn Creek Notch	Bedding plane
14. Old Notch No. 1	Joint
15. Backus Notch No. 1	Joint

* Note: The 914 Rib joint, the 930 joint and the Old Notch No. 1 joint are prehistoric slide scars. The DS + 122 C, DS + 122 minor and DS + 122 No. 2 profiles are in situ traces of joints exposed on the primary DS + 122 bedding surface and are members of the same set as the failed joint. The remainder of the surfaces are natural surfaces exposed during construction of the highway and the Burlington Northern railroad relocations.

BACKUS NOTCH (BEDDING)



BACKUS CREEK NOTCH #1 (BEDDING)



DS+122 (C JOINT)

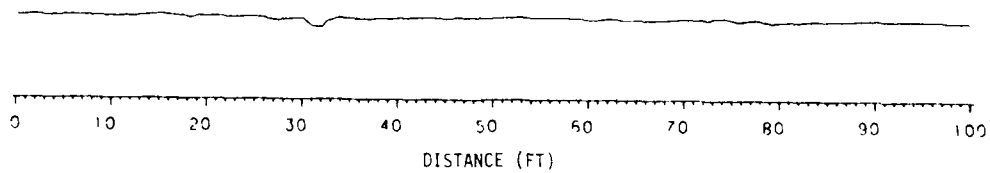
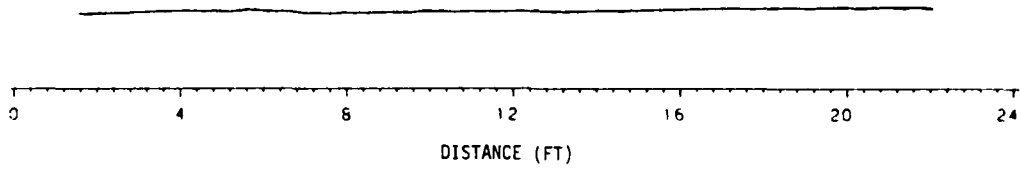
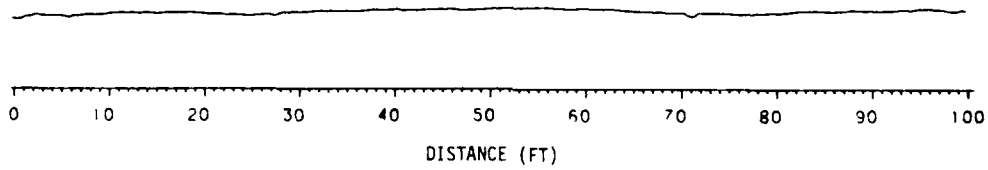


Figure 29. Plot of string line cross sections: Backus Notch No. 1 (bedding); Backus Creek Notch No. 1 (bedding); and DS + 122 (C joint)

ISLAND NOTCH (JOINT)



DS+122 (MINOR JOINT)



DS+122 (JOINT #2)

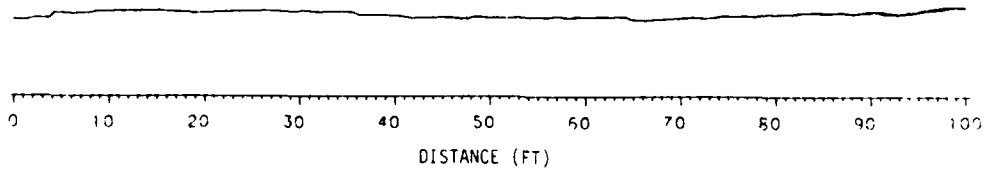
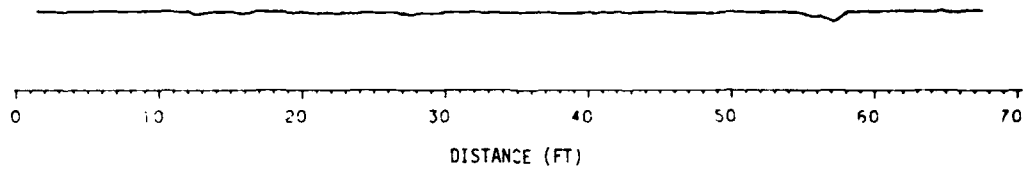
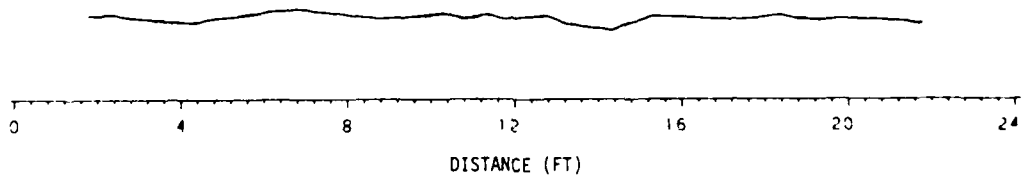


Figure 30. Plot of string line cross sections:
Island Notch (joint); DS + 122 (minor joint);
and DS + 122 (joint No. 2)

914 RIB (JOINT)



DUNN CREEK NOTCH (JOINT)



930 JOINT (UPPER END)

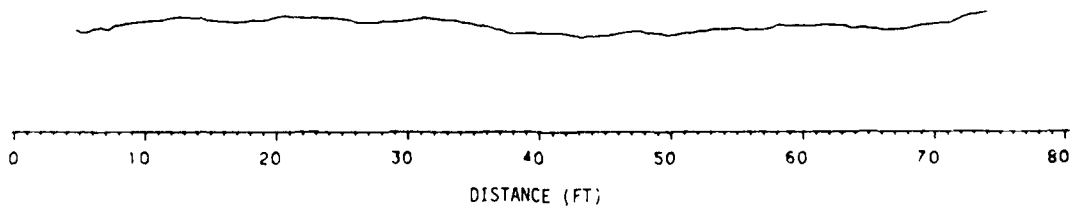
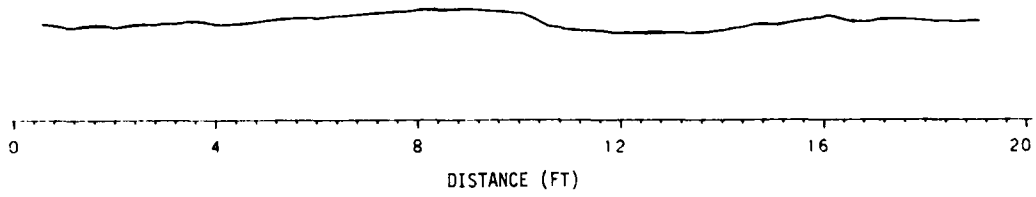
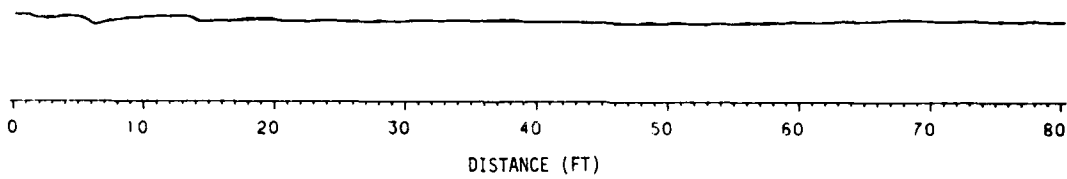


Figure 31. Plot of string line cross sections: 914 Rib (joint);
Dunn Creek Notch (joint); and 930 (joint)

ISLAND NOTCH (UTG)



ISLAND NOTCH (BEDDING)



WOLF CREEK JCT (JOINT)

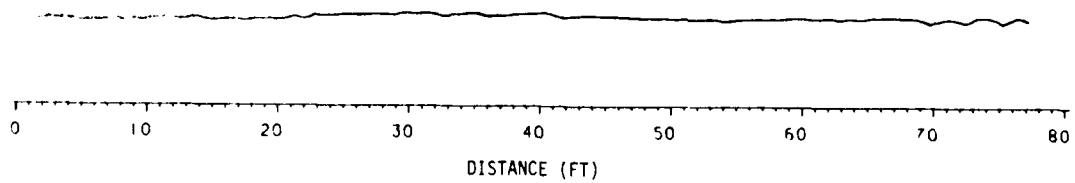
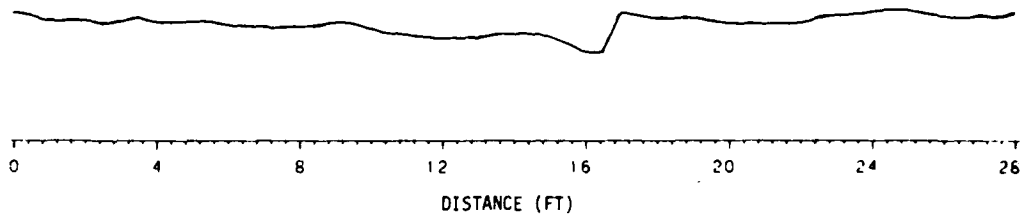
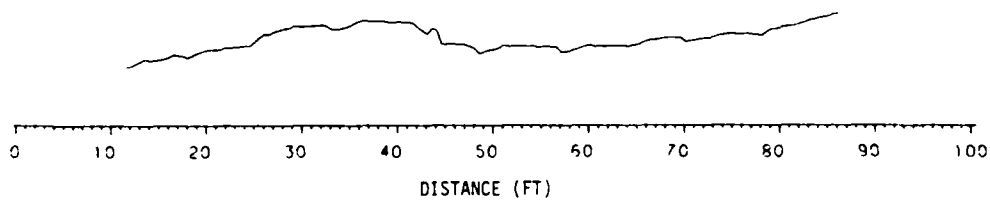


Figure 32. Plot of string line cross-sections: Island Notch (joint/bedding plane intersection); Island Notch (bedding); and Wolf Creek Jct. (joint)

DUNN CREEK NOTCH (BEDDING)



OLD NOTCH #1 (JOINT)



BACKUS NOTCH (JOINT)

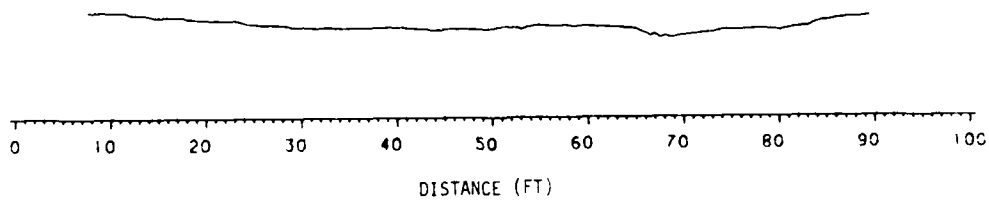


Figure 33. Plot of string line cross sections: Dunn Creek Notch (bedding); Old Notch No. 1 (joint); and Backus Notch No. 1 (joint)

Table 6

Fractal Dimension Calculation for String Line Cross Section

Rock Surface	Number of Counts, N				Fractal Dimension
	*y = 2.0	y = 1.5	y = 1.0	y = 0.5	
Backus Notch No. 1 (bed)	46.375	61.847	92.790	185.84	1.001320
Backus Creek Notch (bed)	31.835	42.493	63.615	127.80	1.002256
DS + 122 (C joint)	50.330	67.093	100.73	201.99	1.002557
Island Notch (joint)	10.265	13.690	20.580	40.210	1.002831
DS + 122 (minor joint)	50.070	66.860	100.38	201.13	1.002907
DS + 122 (joint No. 2)	50.175	66.893	100.52	201.52	1.003175
914 Rib (joint)	33.080	44.173	66.370	132.92	1.003190
Dunn Creek Notch (joint)	10.020	13.400	20.050	40.300	1.003220
930 (joint)	35.025	46.720	70.280	141.08	1.005294
Island Notch (joint/bed)	9.290	12.380	18.680	37.420	1.005762
Island Notch (bed)	42.625	56.840	85.280	171.970	1.006291
Wolf Creek Jct. (joint)	37.750	50.490	76.180	152.84	1.008842
Dunn Creek Notch (bed)	14.165	18.990	28.400	57.560	1.010249
Old Notch No. 1 (joint)	38.305	51.487	77.700	157.20	1.017850
Backus Notch No. 1 (joint)	41.230	54.980	82.730	166.08	1.005408

*y values are in feet; these correspond to 60.96 cm, 45.72 cm, 30.48 cm, and 15.24 cm.

approach was used to calculate the fractal dimension. A linear regression equation is assumed of the form:

$$\log_{10}(N) = D_0 + D_1 \log_{10}(y) \quad (6)$$

In this equation, D_0 is the value of $\log_{10}(N)$ when $\log_{10}(y)$ is zero and D_1 is the slope of this line. Because the fractal dimension, D , is the negative of the slope of this line, then

$$D = -D_1 \quad (7)$$

46. Using the principle of least squares regression, D is calculated as (McCuen 1985, p 187):

$$D = -D_1 = - \frac{\Sigma(\text{Log}_{10}(N)\text{Log}_{10}(y)) - (\Sigma\text{Log}_{10}(N)\Sigma\text{Log}_{10}(y))/K}{\Sigma(\text{Log}_{10}(y))^2 - (\Sigma\text{Log}_{10}(y))^2/K} \quad (8)$$

where K is the number of different trial segment lengths, y , used to calculate D . In Table 6, for example K is equal to 4 and the fractal dimension values listed were calculated using equation (8). The fractal dimension values range from 1.000132 for the Backus Notch No. 1 bedding surface to 1.01785 for the Old Notch No. 1 joint surface. These values are comparable to those determined for the DS + 122 joint surface listed in Table 2 for the Method 2 calculation.

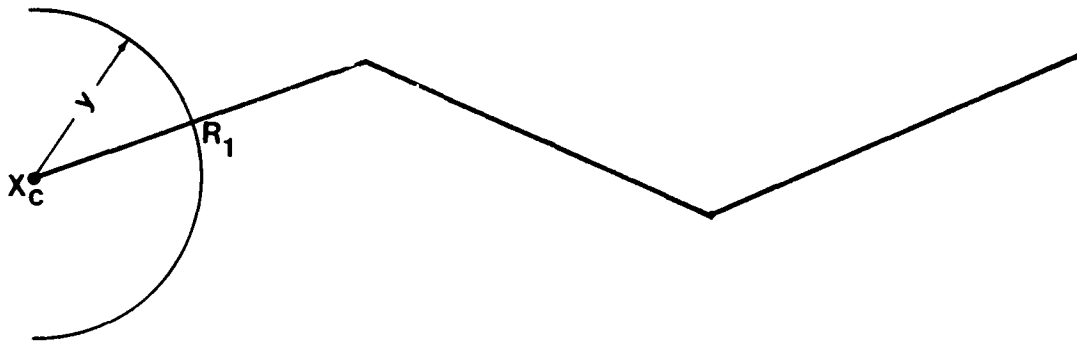
Computer Calculation of the Fractal Dimension

47. Results presented in Tables 2 and 6 were developed by selecting a segment length, y , then physically walking a pair of dividers opened a distance equal to y along a plotted cross section or string line. This is a tedious task and is susceptible to error during the counting of the number of steps, N ; the calculation of the remainder at the end of the plot; or from stretching of the paper on which the cross sections are plotted due to humidity; etc. A computer program was developed to enable easier calculation of the fractal dimension by a numerical algorithm of counting segment lengths in addition to equation (8). This program is presented in Appendix E.

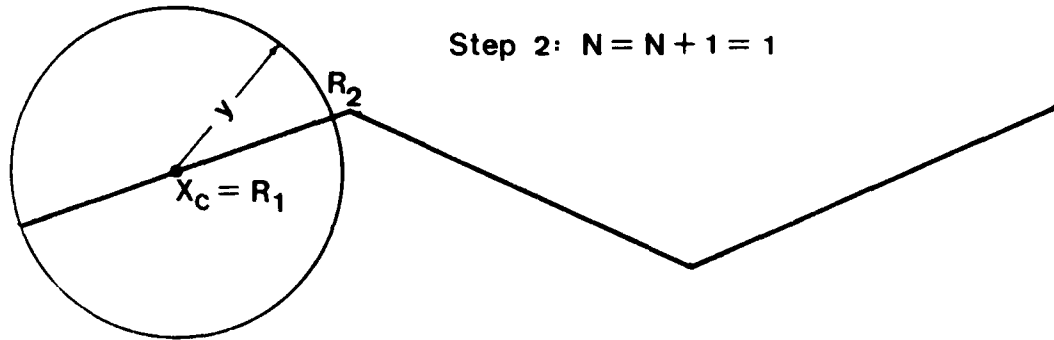
48. Input to the program consists of the number of segment lengths, y , to be considered; specification of these segment lengths; and the elevation and distance coordinates along a cross section or string line. This program is limited at present to one dimensional analyses. The algorithm on which the program is based is graphically presented in Figure 34.

49. Fractal dimensions calculated for the rock surfaces listed in Table 5 using the computer program of Appendix E are listed in Table 7. Although the fractal dimension values do not appear to be much different than those shown in Table 6, a different result was obtained when analyzing the cross sections in terms of roughness. The fractal dimension values are so

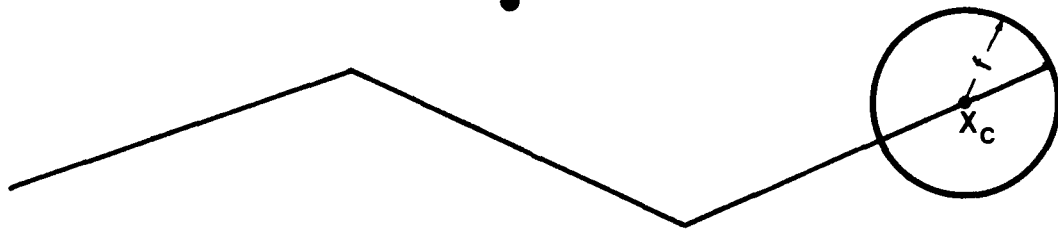
Step 1: $N = 0$



Step 2: $N = N + 1 = 1$



•
etc
•



Final Step $N + 1$: $N = N + \frac{f}{y}$

Figure 34. Algorithm for fractal dimension calculation program

Table 7
Computer Calculation of String Line Fractal Dimensions

Rock Surface	Number of Counts, N				Fractal Dimension
	*y = 2.0	y = 1.5	y = 1.0	y = 0.5	
Backus Notch No. 1 (bed)	46.303	61.755	92.682	185.48	1.001059
Backus Creek Notch (bed)	31.785	42.391	63.603	127.30	1.000891
DS + 122 (C joint)	50.334	67.105	100.78	202.14	1.003045
Island Notch (joint)	10.252	13.670	20.504	41.013	1.000107
DS + 122 (minor joint)	50.089	66.824	100.337	201.28	1.003369
DS + 122 (joint No. 2)	50.127	66.887	100.55	201.44	1.003469
914 Rib (joint)	33.048	44.171	66.248	132.88	1.003334
Dunn Creek Notch (joint)	10.028	13.387	20.110	40.377	1.004735
930 (joint)	35.018	46.731	70.256	140.93	1.004516
Island Notch (joint/bed)	9.278	12.389	18.586	37.285	1.003104
Island Notch (bed)	42.592	56.829	85.272	170.72	1.001409
Wolf Creek Jct. (joint)	37.850	50.555	76.094	152.57	1.005641
Dunn Creek Notch (bed)	14.189	19.076	28.458	57.588	1.008608
Old Notch No. 1 (joint)	38.345	51.624	77.055	158.28	1.021994
Backus Notch No. 1 (joint)	41.231	55.004	82.666	166.86	1.004233

* Units for y are in feet; these correspond to 60.96 cm, 45.72 cm, 30.48 cm, and 15.24 cm.

close in value to 1 that considerable error can occur when measuring these values by hand. Small changes in the number of counts, N, determined for a segment length, y, can result in a significantly different fractal dimension. A computer calculation of the fractal dimension is, therefore, preferred over a hand calculation procedure.

Variogram Analysis of String Line Cross Sections

50. Variograms were calculated for each rock surface listed in Table 5. These variograms are presented in Appendix F. Table 8 lists the string line cross sections, their fractal dimensions, and variogram characteristics. The following observations are made of these variograms:

- a. The variogram nugget is strongly correlated with the fractal dimension (the correlation coefficient is 0.979).
- b. The variogram sill is strongly correlated with the fractal dimension (the correlation coefficient is 0.914).

Table 8
Variogram Results for String Line Cross Sections

<u>Rock Surface</u>	<u>Fractal Dimension*</u>	<u>Variogram</u>			
		<u>Nugget</u>	<u>Sill</u>	<u>Range</u>	<u>Behavior</u>
Backus Notch No. 1 (bed)	1.001059	0.0009	0.0149	10.00	2 periods
Backus Creek Notch (bed)	1.000891	0.0008	0.0848	27.00	0 periods
DS + 122 (C joint)	1.003045	0.0039	0.0450	16.00	4 periods
Island Notch (joint)	1.000107	0.0001	0.0010	7.20	1 period
DS + 122 (minor joint)	1.003369	0.0026	0.0651	16.00	0 periods
DS + 122 (joint No. 2)	1.003469	0.0027	0.1590	25.00	0 periods
914 Rib (joint)	1.003334	0.0028	0.0200	30.00	2 periods
Dunn Creek Notch (joint)	1.004735	0.0035	0.0200	6.50	2 periods
930 (joint)	1.004516	0.0050	0.2680	14.00	0 periods
Island Notch (joint/bed)	1.003104	0.0025	0.0552	6.00	0 periods
Island Notch (bed)	1.001409	0.0016	0.0164	23.00	2 periods
Wolf Creek Jct. (joint)	1.005641	0.0040	0.0349	14.00	0 periods
Dunn Creek Notch (bed)	1.008608	0.0134	0.0677	5.50	2 periods
Old Notch No. 1 (joint)	1.021994	0.0254	1.8800	12.20	0 periods
Backus Notch No. 1 (joint)	1.004233	0.0045	0.3840	16.20	0 periods

Correlation Coefficient

1. Fractal Dimension and Nugget	0.979
2. Fractal Dimension and Sill	0.914
3. Fractal Dimension and Range	-0.217
4. Fractal Dimension and Behavior	-0.206

* The fractal dimension values shown are from Table 7. Units for the range are feet. The behavior category describes the appearance of the variogram relative to Figure 25.

- c. There is a poor correlation between variogram periodicity (a behavior similar to Figure 25) and the fractal dimension; the correlation coefficient is -0.206 ; hence, the variogram is less likely to be periodic for large fractal dimensions (a negative correlation).
- d. The variogram range is poorly correlated with the fractal dimension (the correlation coefficient is -0.217).

From these variogram analyses, the strongest correlation is found between the variogram nugget (an indicator of data randomness) and the fractal dimension. A strong correlation is also found between the variogram sill and the fractal dimension. Other variogram characteristics are seemingly unrelated to the fractal dimension.

51. A numerical example is forwarded to explain the relationship between the fractal dimension and variogram nugget. A random number generator was used to simulate elevation values at a spacing of 0.5 ft along a fictitious 50 ft string line. These simulated elevation values were scaled to have a range between 0 and 4 ft. The result is plotted in Figure 35. Using the computer program listed in Appendix E, the fractal dimension was calculated to be 1.2952. The variogram of this cross section, shown in Figure 36, is random, as expected for random numbers; the nugget value is equal to sample variance, 1.20.

52. Three different low pass filters were applied to these random elevation values. These filtered results are plotted in Figure 37, and variograms are plotted in Figures 38 through 40. The filtering process results in spatially correlated elevation values; hence, the variograms develop an appearance similar to the spherical shape (Appendix B). As the filter size increases, the variance of the data decreases; thus, the variogram sill decreases. This smoothing results in a lower fractal dimension and a reduction in data randomness; hence, the nugget value decreases. This demonstrates that the nugget and sill values of a variogram are directly proportional to the fractal dimension; as the fractal dimension approaches unity, the variogram nugget and sill approach zero.



$D = 1.30$

Figure 35. Artificial string line cross section formed using random elevation values

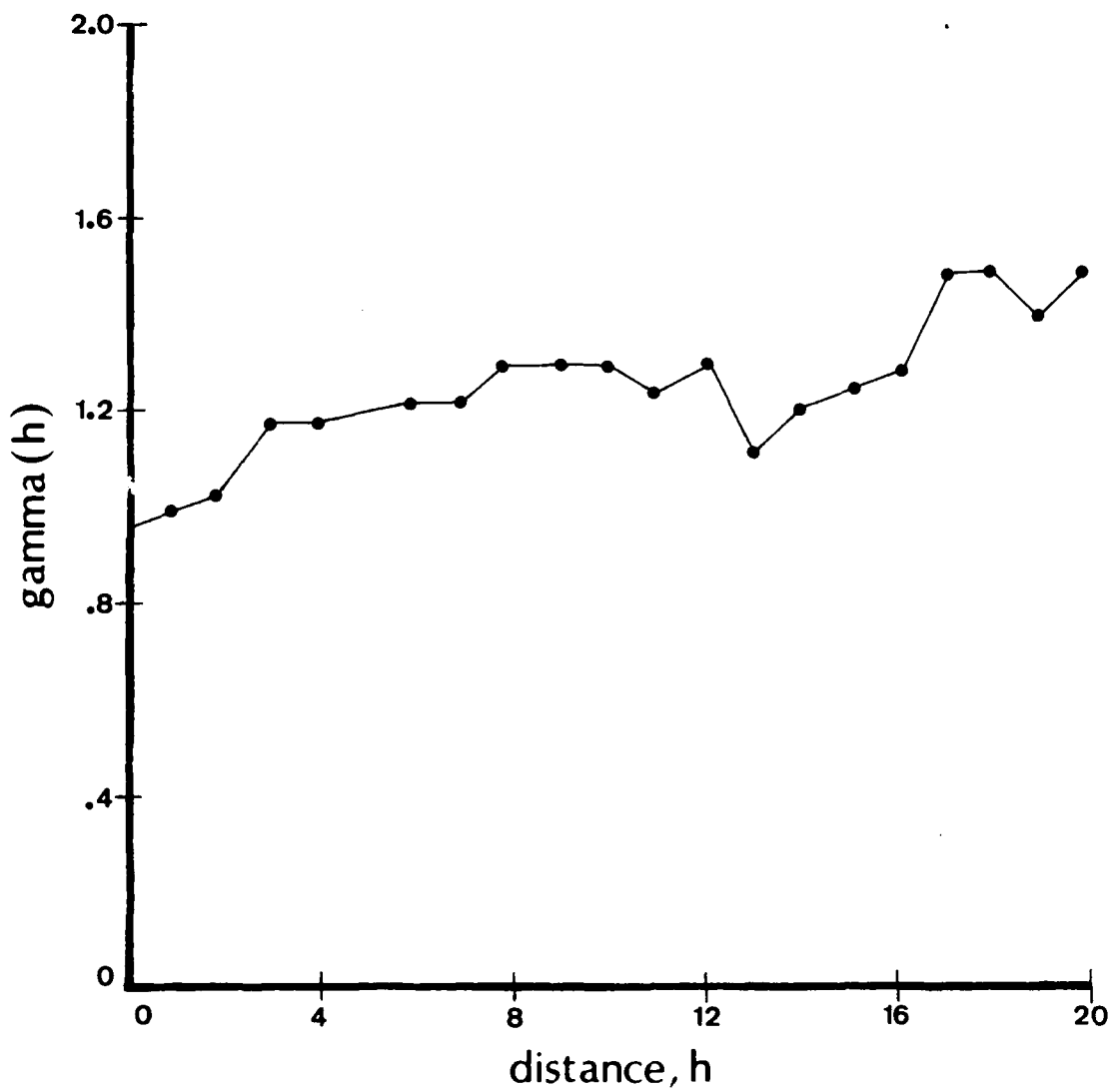


Figure 36. Variogram for string line cross section shown in Figure 35

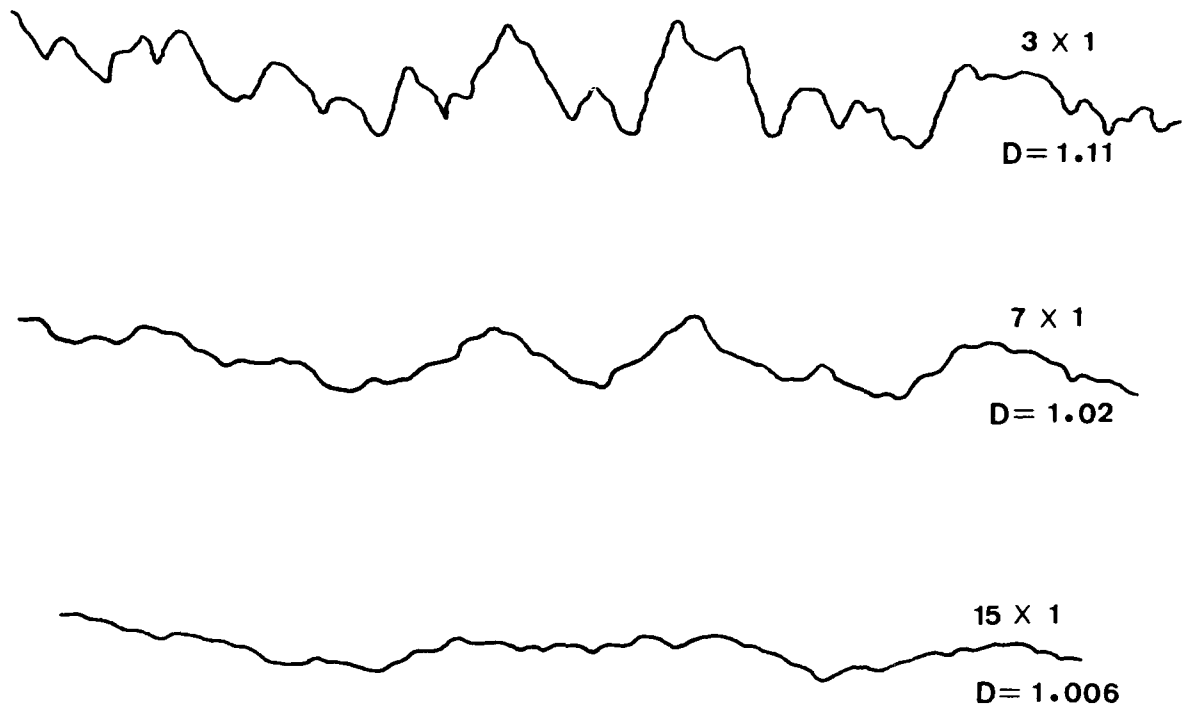


Figure 37. Three filtered results developed from the string line cross section shown in Figure 35; filter sizes are shown

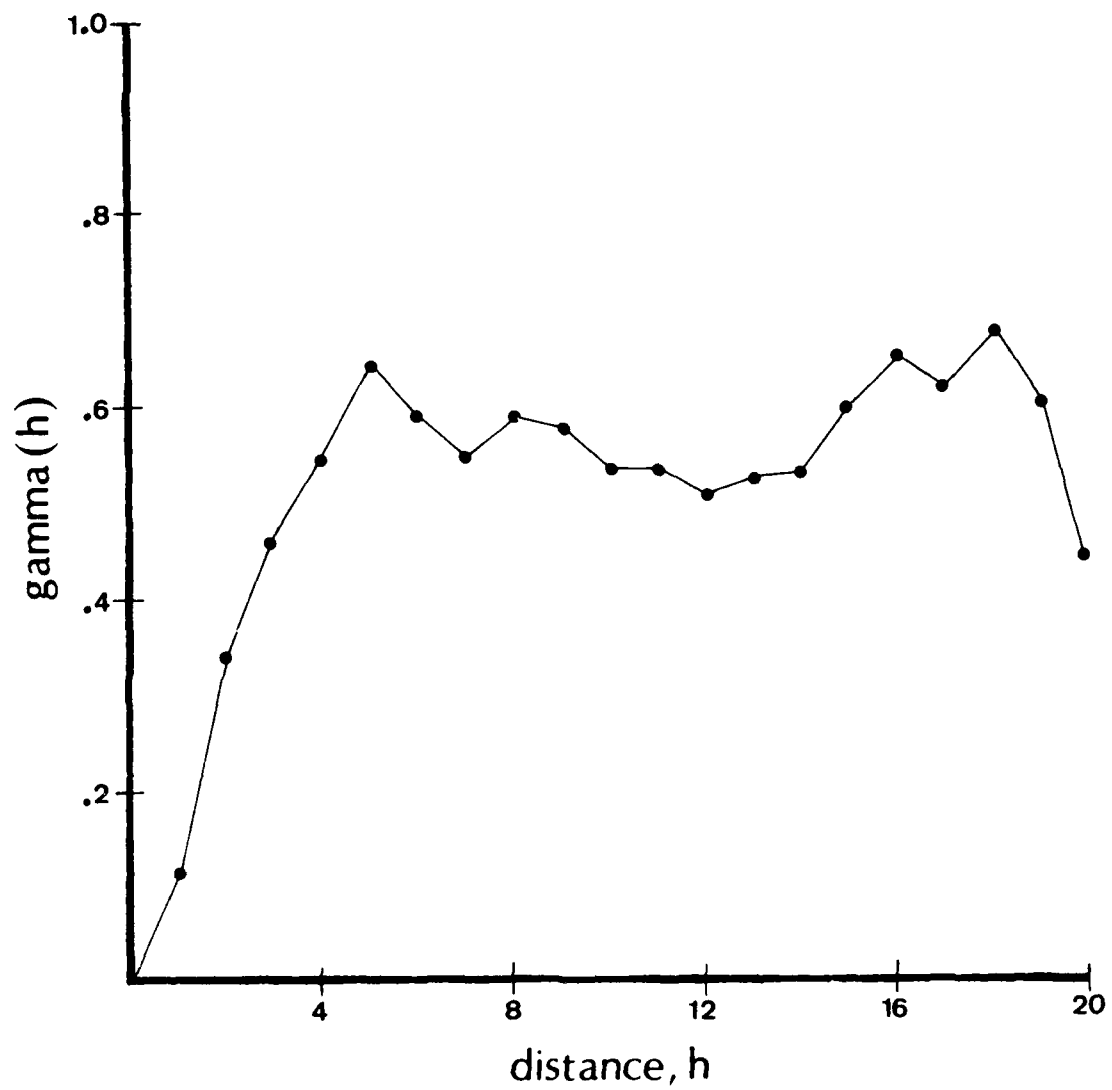


Figure 38. Variogram for the 3X1 filtered string line cross section

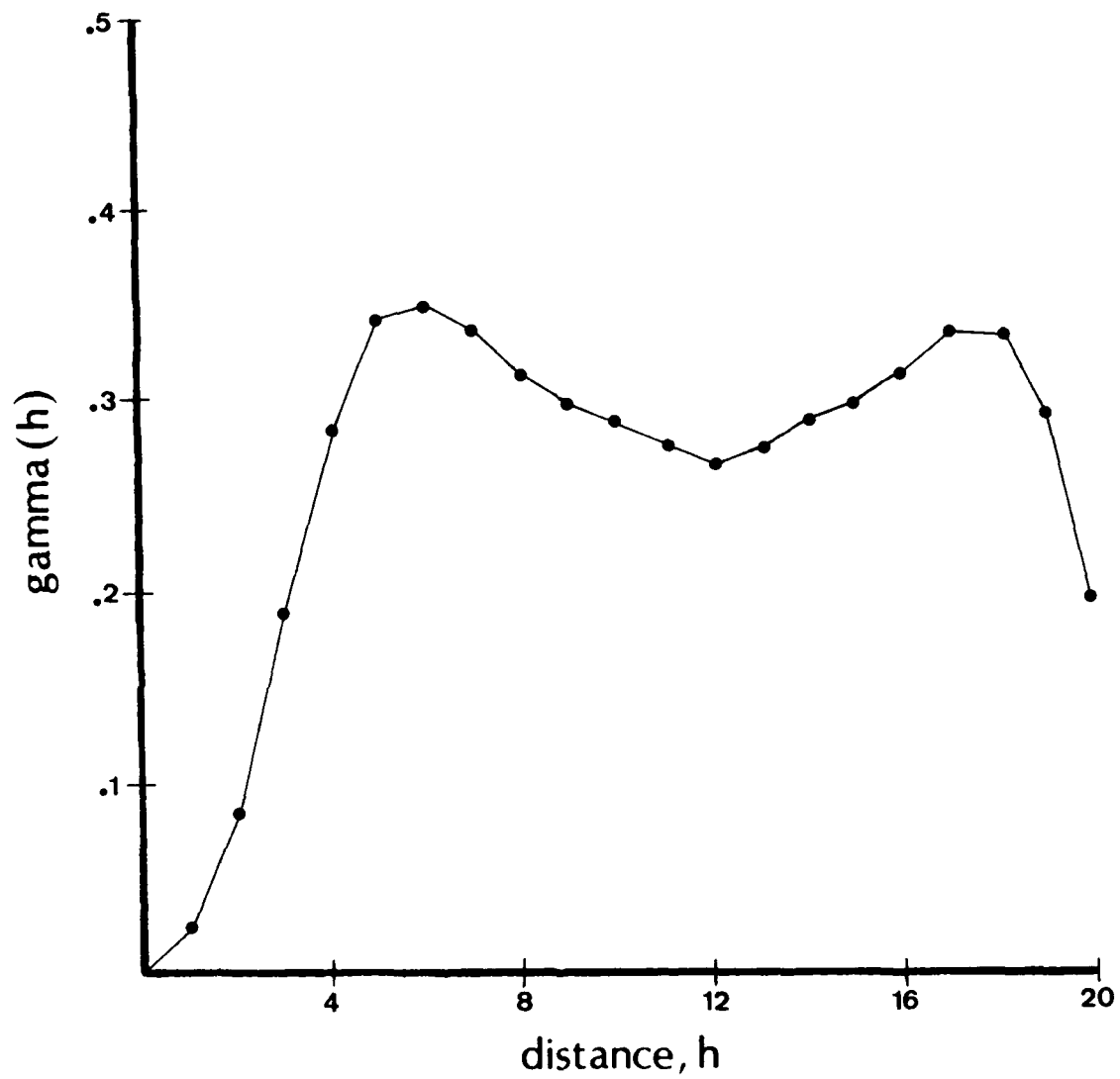


Figure 39. Variogram for the 7X1 filtered string line cross section

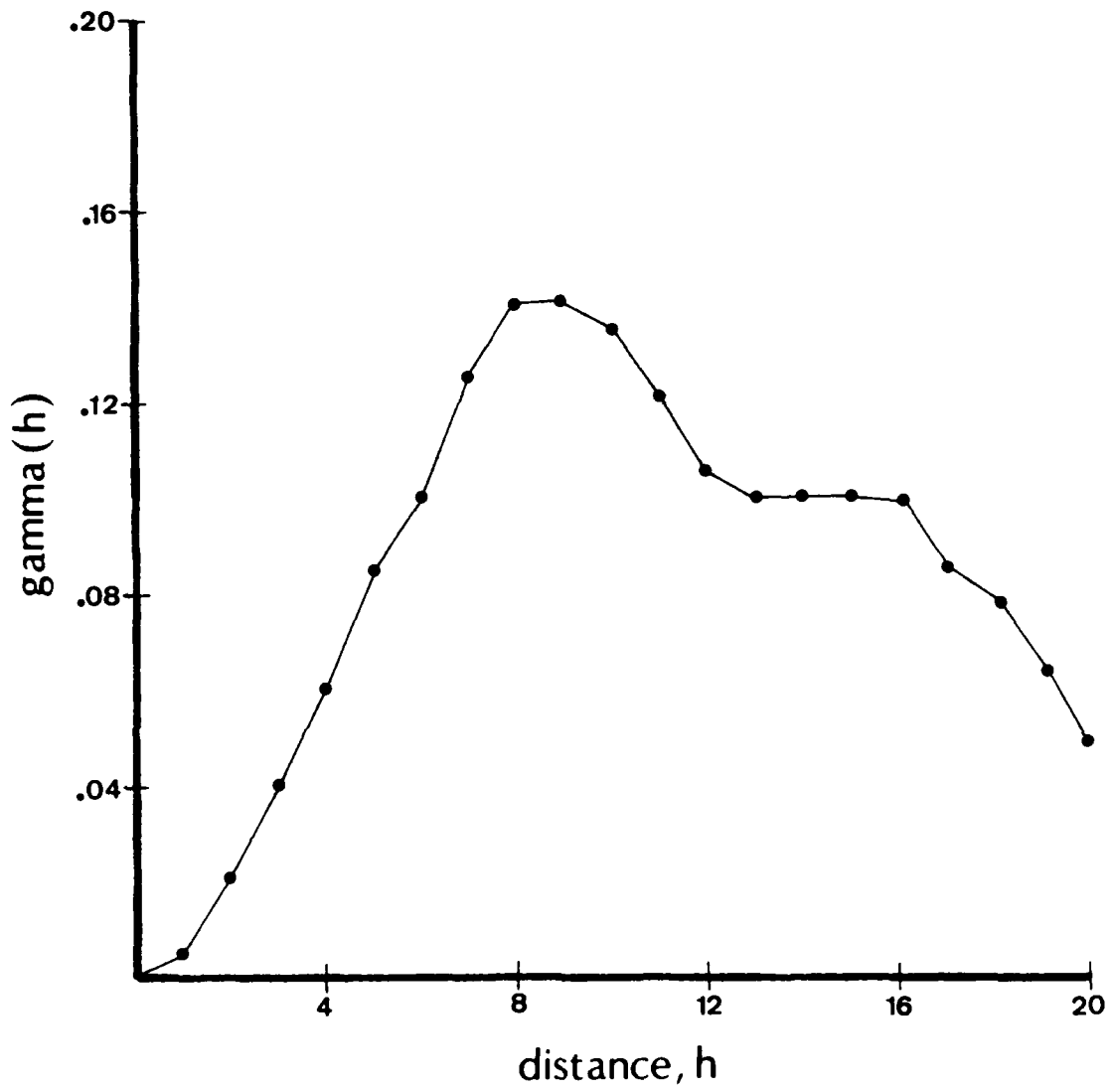


Figure 40. Variogram for the 15X1 filtered string line cross section

PART VI: REGRESSION: THE RELATIONSHIP BETWEEN THE FRACTAL DIMENSION AND JOINT ROUGHNESS COEFFICIENT

53. Joint roughness (and the roughness of bedding planes) is a factor in the sliding stability of rock masses. The rougher the surface of a joint is, the greater stability it has against sliding. An accepted value which describes the roughness of rock surfaces is known as the Joint Roughness Coefficient or JRC (Barton and Choubey 1977).

54. Typical roughness profiles for various JRC values are shown in Figure 41, reproduced from Barton and Choubey (1977). JRC values were assigned to each cross section listed in Table 5 using Figure 41. This assignment is

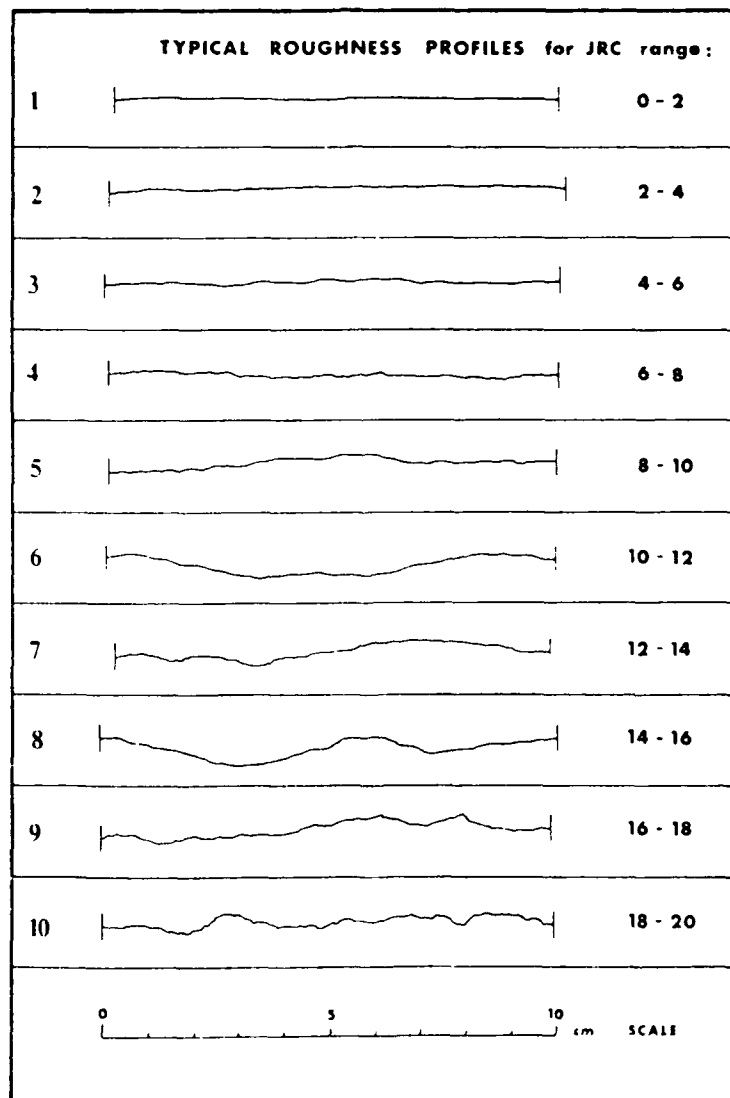


Figure 41. JRC profiles (Barton and Choubey 1977)

shown in Table 9. It is noted that one cross section is assigned a value of 22, which is larger than any profile shown by Barton and Choubey (1977). This high value was extrapolated based on the nature of the other Libby Dam area sections. Moreover, the sections shown by Barton and Choubey (1977) refer to the laboratory specimens they examined and are not thought to represent maximum possible values. Each cross section is listed along with the assigned JRC value, the fractal dimension and the variogram nugget. A fictitious, ideal cross section is also included for the subsequent discussion. This fictitious rock surface is an ideal plane with a JRC value equal to zero, a fractal dimension equal to one, and a nugget equal to zero. The purpose of including this ideal surface is explained subsequently.

55. From the information listed in Table 9, a regression equation can be developed to predict a JRC value based on:

- a. The fractal dimension alone.
- b. The variogram nugget alone.
- c. The fractal dimension and variogram nugget.

The development of such a regression equation has a simple objective. It is a difficult exercise in judgment to use Figure 41 to assign a JRC value to a specific cross section. By developing a regression of JRC on the fractal dimension and/or the variogram nugget, the JRC value can be estimated rather than visually assigned.

56. The calculation of JRC is not a new approach. A calculation procedure was developed based on laboratory shear tests of rock samples (Barton and Choubey 1977):

$$JRC = \frac{\arctan(\tau/\sigma_N) - \phi_b}{\log_{10}(JCS)/\sigma_N} \quad (9)$$

where

- τ = shear stress
- σ_N = effective normal stress
- ϕ_b = basic friction angle
- JCS = joint wall compression strength

The solution to equation (9) requires the use of laboratory rock shear tests.

57. The development of a regression equation based on the fractal dimension and variogram nugget requires only elevation data measured along a

Table 9
Joint Roughness Coefficient (JRC) for String Line Cross Section

<u>Rock Surface</u>	<u>JRC*</u>	<u>D</u>	<u>CO</u>
Fictitious Ideal	0	1.0000	0.0000
Backus Notch No. 1 (bedding)	3	1.0011	0.0009
Backus Creek Notch No. 1 (bedding)	2	1.0009	0.0008
DS + 122 (C joint)	4	1.0031	0.0039
Island Notch (joint)	1	1.0001	0.0001
DS + 122 (minor joint)	4	1.0034	0.0026
DS + 122 (joint No. 2)	5	1.0035	0.0027
914 Rib (joint)	3	1.0033	0.0028
Dunn Creek Notch (joint)	7	1.0047	0.0035
930 (joint)	8	1.0045	0.0050
Island Notch (joint/bed)	5	1.0031	0.0025
Island Notch (bedding)	2	1.0014	0.0016
Wolf Creek Jct. (joint)	8	1.0056	0.0040
Dunn Creek Notch (bedding)	13	1.0086	0.0134
Old Notch No. 1 (joint)	22	1.0220	0.0254
Backus Notch No. 1 (joint)	6	1.0042	0.0045

* JRC is the Joint Roughness Coefficient; D is the fractal dimension; and CO is the variogram nugget. For this table, N is 16.

consistent linear direction. These data can be collected in the field without the need for expensive laboratory equipment. The development of such an equation will not duplicate, but will supplement or be an alternative to equation (9).

Regression Analysis

58. Regression analysis involves the estimation of a dependent variable using one or several independent variables. Such a procedure begins by plotting the dependent variable versus the independent variables, one plot per independent variable. Such a plot reveals the type of correlation between the

dependent and independent variables. There may be a lack of correlation, or the relationship may be linear, quadratic or some other functional form.

59. Suppose, for example, the two variables are linearly correlated and only one independent variable is considered. Figure 42 is an example. In this case, the dependent variable, y , can be estimated from the independent variable, x , as

$$y = A_0 + A_1x \quad (10)$$

Once the form of this equation has been chosen, it remains to solve for the coefficients, A_0 and A_1 , to define the equation explicitly.

60. In regression analysis, one possible method for the solution of the coefficients is the method of least squares. This involves the minimization

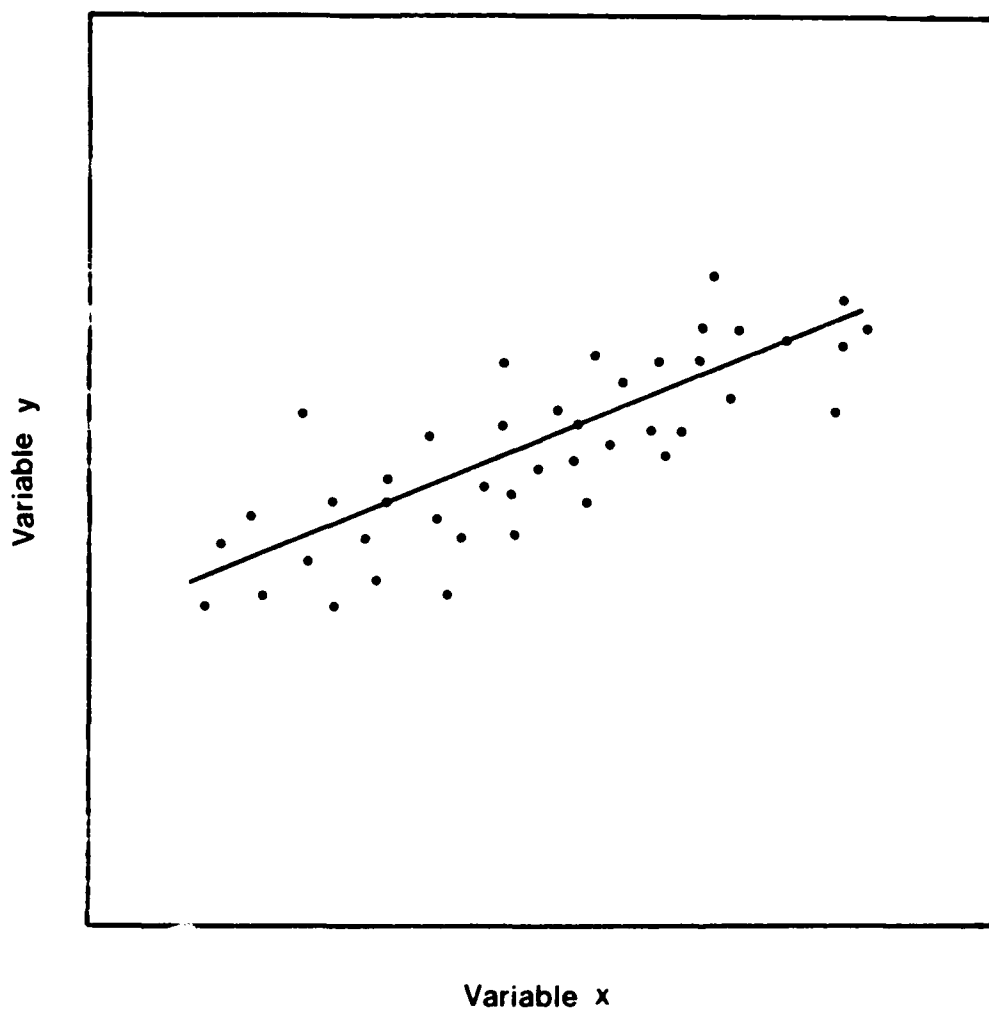


Figure 42. Example case of two linearly correlated variables

of the errors when estimating the dependent variable, y . To explain this procedure, Figure 42 is recalled. Each point plotted on this figure is associated with two known values, x and y . At each of these points, an estimate of y can be calculated as

$$y^* = A_0 + A_1 x \quad (11)$$

with an error, e , calculated as $e^2 = (y - y^*)^2$

61. Using this procedure, a regression equation is defined which, when applied, has a zero mean error and a minimum error variance. The same procedure outlined above is used for linear equations of more than one independent variable or for nonlinear functional equations. A modification is required, however, to accommodate additional variables or to introduce the nonlinear functional form.

Regression Analysis for Estimation of the Joint Roughness Coefficient

62. Plots of JRC versus fractal dimension and JRC versus variogram nugget are shown in Figure 43. A linear correlation is observed between the JRC and each of the independent variables. Based on this preliminary visual analysis, three forms of a regression equation are proposed:

- a. $JRC = A_0 + A_1 D.$
- b. $JRC = A_0 + A_1 CO.$
- c. $JRC = A_0 + A_1 D + A_2 CO.$

where

D = fractal dimension

CO = variogram nugget

Each of these functional forms was tested to determine the optimal regression equation.

63. The data used to define the coefficients of these equations are presented in Table 9. The fictitious, ideal cross section was used to include the ideal case where JRC is equal to zero. Each equation was evaluated for accuracy relative to the mean square error resulting from its application.

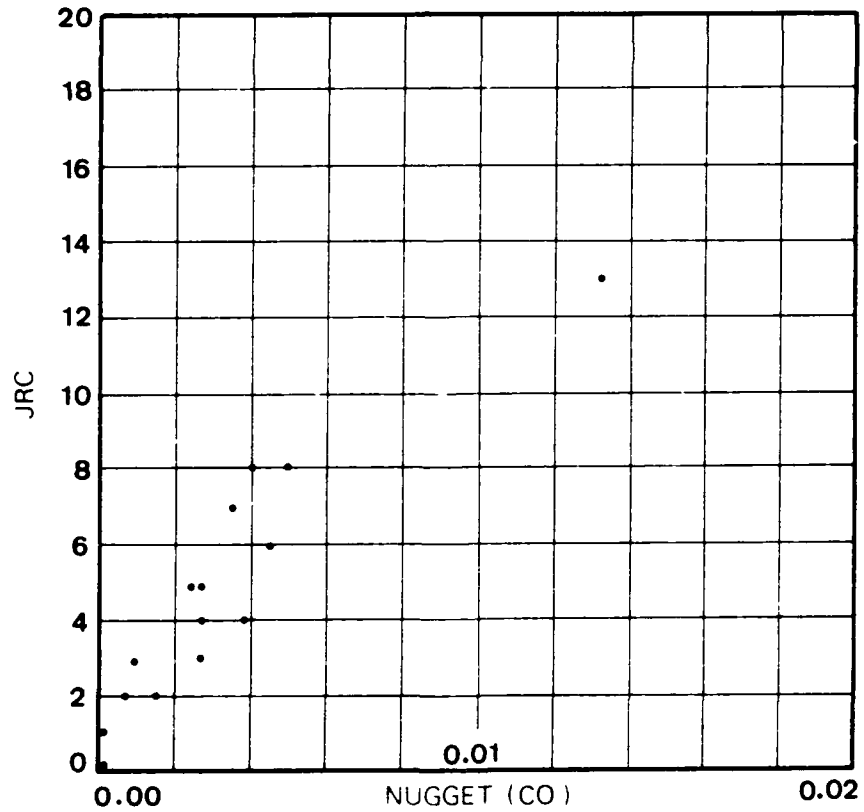
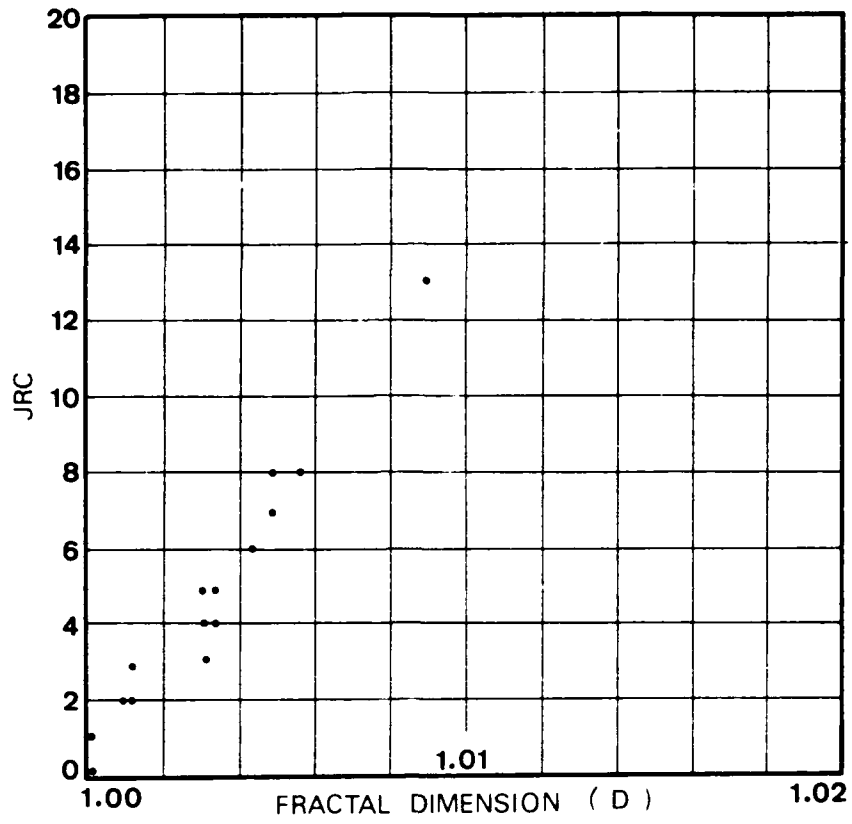


Figure 43. Two regression plots: JRC versus fractal dimension and JRC versus variogram nugget

64. Using the method of least squares, the following regression equations were derived:

a. For the fractal dimension only:

$$JRC = -1022.55 + (1023.92)D \quad (19)$$

b. For the variogram nugget only:

$$JRC = 2.042 + (818.53)CO \quad (20)$$

c. For the fractal dimension and variogram nugget:

$$JRC = -758.41 + (759.93)D + (215.05)CO \quad (21)$$

For each of these equations, D and CO must be represented by at least four digit precision after the decimal point. Table 10 lists the results of the application of each equation for the estimation of JRC. The most accurate equation is the one based on the two independent variables.

65. It is acknowledged that the accuracy of the three equations is similar. Moreover, these equations are empirical and are forwarded only as a procedure for the estimation of JRC. It is difficult for users unfamiliar with variograms to interpret the nugget value. It is therefore recommended to use the regression equation based solely on the fractal dimension to estimate JRC. This equation, in review, is

$$JRC = -1022.55 + (1023.92)D \quad (19)$$

This equation has an error standard deviation equal to 1.24 JRC values. When using this equation, it is essential that the fractal dimension, D, be represented by at least four digit precision after the decimal point, even though the coefficients have a precision less than this. For rock surfaces, the fractal dimension has a range from 1 to about 1.03; hence, these values are small and the precision is therefore necessary.

66. A rough approximation of equation (19) is developed as

$$JRC = 1000(D - 1) \quad (22)$$

Table 10

Application of Regression Equations for the Estimation of JRC

<u>Rock Surface</u>	<u>JRC</u>	<u>JRC^{1*}</u>	<u>JRC²</u>	<u>JRC³</u>
Fictitious Ideal	0	1.37	2.04	1.52
Backus Notch No. 1 (bedding)	3	2.50	2.78	2.55
Backus Creek Notch No. 1 (bedding)	2	2.29	2.70	2.38
DS + 122 (C joint)	4	4.54	5.23	4.71
Island Notch (joint)	1	1.47	2.12	1.62
DS + 122 (minor joint)	4	4.85	4.17	4.66
DS + 122 (joint No. 2)	5	4.95	4.25	4.76
914 Rib (joint)	3	4.75	4.33	4.63
Dunn Creek Notch (joint)	7	6.18	4.91	5.84
930 (joint)	8	5.98	6.13	6.01
Island Notch (joint/bed)	5	4.54	4.09	4.41
Island Notch (bedding)	2	2.80	3.35	2.93
Wolf Creek Jct. (joint)	8	7.10	5.32	6.64
Dunn Creek Notch (bedding)	13	10.18	13.01	10.94
Old Notch No. 1 (joint)	22	23.90	22.83	23.70
Backus Notch No. 1 (joint)	6	<u>5.67</u>	<u>5.73</u>	<u>5.68</u>
Mean Square Error		1.54	1.77	1.39
Mean Standard Deviation		1.24	1.33	1.18

* Superscripts on the JRC headings represent the equation used for estimation. Superscript 1 represents the equation based on the fractal dimension alone; superscript 2 represents the equation based on the variogram nugget alone; and superscript 3 represents the equation based on the fractal dimension and variogram nugget.

and this equation is more conservative than equation (19); that is, a lower estimate of JRC results from equation (22). Moreover, this equation is useful for the calculation of other rock surface parameters, such as shear stress. For example, equation (9) is recalled:

$$JRC = \frac{\arctan(\tau/\sigma_N) - \phi_b}{\text{Log}_{10}(\text{JCS})/\sigma_N} \quad (9)$$

If the shear stress, τ , is to be calculated based on a known JRC value, then

$$\tan^{-1}(\tau/\sigma_N) = JRC(\text{log}_{10}(\text{JCS}/\sigma_N)) + \phi_b \quad (23)$$

or

$$\tau = \sigma_N \tan(\text{JRC}(\log_{10}(\text{JCS}/\sigma_N)) + \phi_b) \quad (24)$$

Incorporating the fractal dimension, D , into the equation is most easily done using equation (22):

$$\tau = \sigma_N \tan(100(D - 1)(\log_{10}(\text{JCS}/\sigma_N)) + \phi_b) \quad (25)$$

Equation (25) is an expression for the calculation of shear stress as a function of the fractal dimension.

67. An additional study was made to investigate the accuracy of equations (19) and (22). An enlargement of Figure 41 was made, and a fractal dimension was computed for each of the ten profiles. The results of these calculations are presented in Table 11 with a plot of JRC versus fractal dimension shown in Figure 44. It is interesting that through the JRC range of 14, the plot of JRC versus fractal dimension is steeper in Figure 44 than what is shown by Figure 43; i.e., based on Figure 41, an increase in the fractal dimension should indicate a larger increase in the JRC value than what is predicted by equations (19) and (22). For the JRC range greater than 14, however, Figure 44 shows a distinct change in the slope of the plot of JRC versus fractal dimension. Several explanations are possible. The resolution of the enlargement (a photographic enlargement) was poor, and this might account for the change. Barton and Choubey (1977) seemed to assign high JRC values to profiles which had a sinusoidal shape but were otherwise smooth (i.e., similar to a sine curve). A low fractal dimension would result for such a curve. Some of the profiles for higher JRC values appear to have such a shape (Figure 41). It is observed from Table 12 that the application of equations (19) and (22) to the profiles of Figure 41 result in lower estimates of JRC than what is shown in Table 11. Thus, equations (19) and (22) are useful for a conservative analysis of joint surface roughness.

Table 11

Fractal Dimension Calculations for Profiles of Figure 41

JRC Range	Number of Segments, N					Fractal Dimension
	y = 1 cm	y = 2 cm	y = 3 cm	y = 4 cm	y = 5 cm	
0-2	173.267	86.589	57.708	43.277	34.621	1.000603
2-4	178.600	89.242	59.465	44.570	35.656	1.001199
4-6	178.408	89.047	59.332	44.450	35.552	1.002287
6-8	176.569	88.117	58.691	43.948	35.138	1.003124
8-10	176.468	88.036	58.616	43.893	35.073	1.003822
10-12	177.890	88.701	59.028	44.207	35.301	1.004689
12-14	172.990	86.251	57.401	42.963	34.317	1.005596
14-16	184.614	92.123	61.238	45.788	36.560	1.006203
16-18	182.133	90.697	60.244	44.942	35.874	1.009647
18-20	184.560	91.550	60.686	45.321	36.205	1.012453

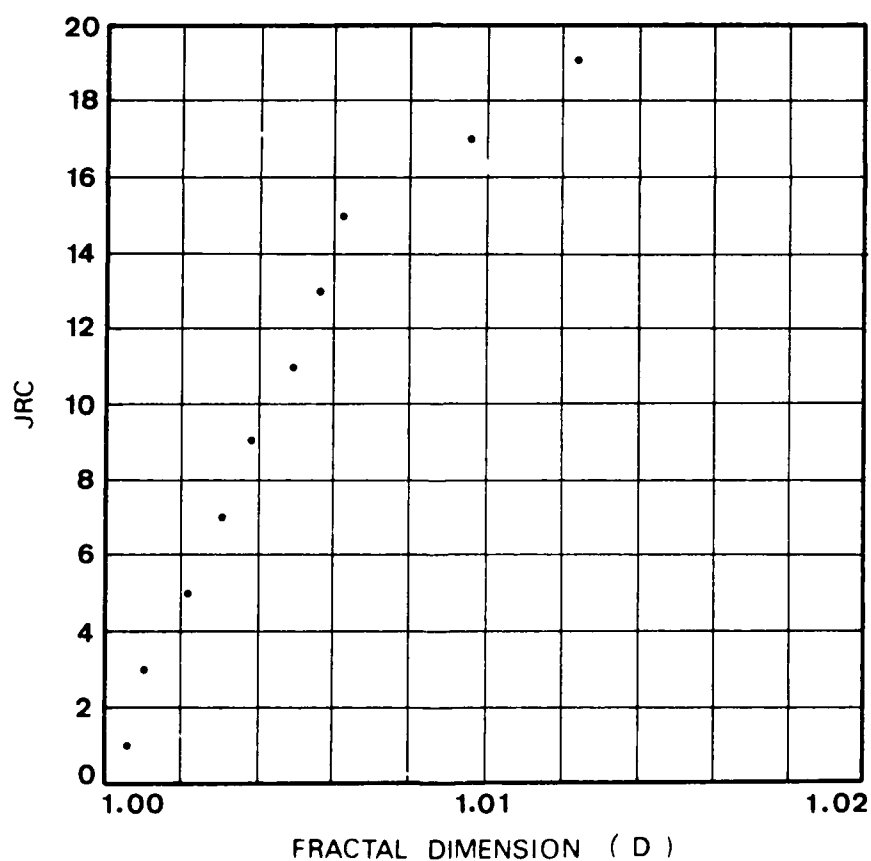


Figure 44. Plot of JRC versus fractal dimension for the profiles shown in Figure 41

Table 12
Predicted JRC Values for Profiles of Figure 41

<u>JRC Range (actual)</u>	<u>Fractal Dimension</u>	<u>Predicted JRC Values</u>	
		<u>Eq. (19)</u>	<u>Eq. (22)</u>
0-2	1.000603	1.99	0.60
2-4	1.001199	2.60	1.20
4-6	1.002287	3.71	2.29
6-8	1.003124	4.57	3.12
8-10	1.003822	5.28	3.82
10-12	1.004689	6.17	4.69
12-14	1.005596	7.10	5.60
14-16	1.006203	7.72	6.20
16-18	1.009647	11.25	9.65
18-20	1.012453	14.12	12.45

PART VII: CONCLUSIONS

Implication of Results

68. Applications of both the fractal dimension and the variogram were novel for the analysis of the texture of a joint surface. The objective of this study was to evaluate each of these techniques for the description of rock surfaces. As was reviewed in this report, both of these techniques are valuable for rock mass characterization.

69. The fractal dimension accurately measured the roughness of discrete cross sections across the DS + 122 joint surface. Regions which appeared to be smooth on the contour map were found to have a lower fractal dimension compared with regions of greater complexity. Moreover, the value of the fractal dimension is directly proportional to surface roughness. The greater the difference, $D - 1$, the rougher is the surface. The fractal dimension offers a unique approach to the quantitative description of surface roughness, which has otherwise been qualitatively described. These results were also verified for the string line cross sections.

70. As a complement to the fractal dimension, variograms for selected cross sections demonstrated that elevation values were spatially correlated. The variance in elevation values along each cross section presented in this report is a function of the asperities along the joint surface. Variograms were able to show that asperities are spatially correlated and have a finite spatial continuity. Moreover, at least for the example of Figure 25, the variogram is useful for the investigation of asperity magnitude differences across a joint surface. Occasionally, the variogram yields ambiguous results concerning asperity magnitude and spatial structure. This ambiguity was evident for some of the string line cross sections.

Problems Encountered in this Research

71. The only problems which occurred during this research resulted from the application of existing techniques to a novel problem. The concept of the fractal dimension is a recent development. The literature, except for publications by Mandelbrot, only sparsely contains publications which discuss the fractal dimension. It is therefore difficult, at present, to check the

correctness of a research procedure which involves the calculation of a fractal dimension. Such verification was provided in this report using a control calculation.

72. With respect to the variogram, geostatistical techniques are based on the principle of the Intrinsic Hypothesis. This hypothesis simply requires that the local mean of the data in one location be identical to the local mean in a different location. This is an hypothesis required by the geostatistical techniques. For this study, the elevation data for some of the cross sections conformed to the hypothesis. Elevation values for other cross sections, however, did not conform well to this hypothesis. In these latter cases, it was necessary to filter the data to allow a conformity with the Intrinsic Hypothesis. This was not necessary for the string line data. These data were sampled relative to a string stretched above and parallel to the rock surface. This method of data collection yields stationary data.

Solutions to Research Problems

73. For the calculation of the fractal dimension, some experimentation is required. The better approach to this calculation involves four steps: (a) select a finite, small segment length, y ; (b) count the number of times, N , the segment length, y , can be laid, end to end, along an irregular line; at the end of this irregular line, add the remainder, k , normalized by y to the counts, N (i.e., $N = N + k/y$); (c) repeat steps a and b for different segment lengths, y ; (d) plot $\log_{10}(N)$ versus $\log_{10}(y)$; the negative of the slope of this line is the fractal dimension. As an alternative, the fractal dimension can be calculated using the computer program listed in Appendix E.

Research Contribution

74. Once the fractal dimension has been calculated, a JRC value can be estimated using the fractal dimension. This study found that JRC and the fractal dimension are strongly correlated. This is a contribution to the state-of-the-art in rock mechanics because a procedure is now available to estimate, or calculate, the JRC rather than guessing its value from a figure, such as Figure 41. The relationship between JRC and the fractal dimension is

$$\text{JRC} = -1022.55 + (1023.92)D$$

(19)

with D , the fractal dimension, having a precision of at least four digits after the decimal point. Such precision is easily obtained from the computer program listed in Appendix E.

REFERENCES

- Banks, D. C., and Strohm, W. E., Jr. 1974. "Calculation of Rock Slide Velocities," 3rd Congress of the International Society for Rock Mechanics, pp 839-847.
- Barton, N., and Choubey, V. 1977. "The Shear Strength of Rock Joints in Theory and Practice," Rock Mechanics, Vol 10, pp 1-54.
- Dewdney, A. K. 1985. "Computer Recreations: A Microcomputer Zooms in for a Look at the Most Complex Object in Mathematics," Scientific American, Vol 253, No. 2, pp 16-24.
- Goodman, R. E. 1976. Methods of Geological Engineering in Discontinuous Rocks, West Publishing Co., St. Paul, MN.
- Hamel, James V. 1974. "Rock Strength from Failure Cases: Left Bank Slope Stability Study, Libby Dam and Lake Koocanusa, Montana," Technical Report MRD-1-74, US Army Engineer Division, Missouri River, Omaha, NE.
- Hoek, E., and Bray, J. 1974. Rock Slope Engineering, The Institution of Mining and Metallurgy, London.
- Journel, A. G., and Huijbregts, Ch. J. 1978. Mining Geostatistical, Academic Press, London.
- LaPoint, P. R. 1980. "Analysis of the Spatial Variations in Rock Mass Properties Through Geostatistics," Proceedings of the 21st U.S. Symposium on Rock Mechanics, pp 570-580.
- Mandelbrot, Benoit B. "How Long is the Coast of Great Britain? Statistical Self-Similarity and Fractional Dimension," Science, Vol 156, pp 636-638.
- _____. 1982. The Fractal Geometry of Nature, Freeman, San Francisco.
- _____. 1985. Personal communication.
- McCuen, Richard H. 1985. Statistical Methods for Engineers, Prentice-Hall, Englewood Cliffs, NJ.
- Miller, S. M., and Borgman, L. E. 1985. "Spectral-Type Simulation of Spatially Correlated Fracture Set Properties," Journal of the International Association for Mathematical Geology, Vol 17, No. 1 pp 41-52.
- Olea, R. A. 1974. "Optimal Contour Mapping Using Universal Kriging," Journal of Geophysical Research, Vol 79, No. 5, pp 695-702.
- Patton, F. D. 1966. "Multiple Modes of Shear Failure in Rock and Related Materials," Ph.D. Thesis, Department of Geology, University of Illinois, Urbana.
- Patton, F. D., and Deere, D. U. 1970. "Significant Geologic Factors in Rock Slope Stability," Planning Open Pit Mines: Proceedings of the Symposium on the Theoretical Background to the Planning of Open Pit Mines with Special Reference to Slope Stability, Balkema, Amsterdam, pp 143-151.
- Piteau, D. R. 1970. "Geological Factors Significant to the Stability of Slopes Cut in Rock," Planning Open Pit Mines: Proceedings of the Symposium on the Theoretical Background to the Planning of Open Pit Mines with Special Reference to Slope Stability, Balkema, Amsterdam, pp 33-53.

Van Besien, Alfonse C. 1985. "A Statistical Analysis of Subsidence Type and Delays Over Room and Pillar Coal Mines," Ph.D. Thesis, Department of Geological Engineering, University of Missouri-Rolla.

BIBLIOGRAPHY

Geostatistics:

Carr, J. R., and Glass, C. E. 1985. "Treatment of Earthquake Ground Motion Using Regionalized Variables," Journal of the International Association for Mathematical Geology, Vol 17, No. 5, pp 221-241.

David, Michel. 1977. Geostatistical Ore Reserve Estimation, Elsevier, Amsterdam.

Davis, John C. 1986. Statistics and Data Analysis in Geology, (2nd ed.), John Wiley and Sons, New York.

Journel, A. G., and Huijbregts, C. J. 1978. Mining Geostatistics, Academic Press, London.

Matheron, G. 1963. "Principles of Geostatistics," Economic Geology, Vol 58, pp 1246-1266.

Fractals:

Dewdney, A. K. 1985. "Computer Recreations: A Microcomputer Zooms in for a Look at the Most Complex Object in Mathematics," Scientific American, Vol 253, No. 2, pp 16-24.

Mandelbrot, Benoit B. 1977. Fractals: Form, Chance and Dimension, Freeman, San Francisco.

_____. 1982. The Fractal Geometry of Nature, Freeman, San Francisco.

Mark, D. M., and Aronson, P. B. 1984. "Scale-Dependent Fractal Dimensions of Topographic Surfaces: An Empirical Investigation, with Applications in Geomorphology and Computer Mapping," Journal of the International Association for Mathematical Geology, Vol 16, No. 7, pp 671-684.

APPENDIX A: THE CONCEPT OF THE FRACTAL DIMENSION

Introduction

1. Geometry is the branch of mathematics that addresses the measurement, properties, and relationships of points, lines, angles, surfaces and solids. In a broad context, this branch of mathematics studies the properties of given elements which remain invariant under specified transformations. Geometry also represents an arrangement of objects or parts which suggest a particular shape or figure.

2. In nature, shapes are geometrically unique. The shapes of the Amazon drainage system, a butterfly's wings, a blood cell, or a cubic crystal of galena are unique. Moreover, these shapes are often difficult to describe. The crystal of galena is geometrically familiar: a cube. A blood cell, although more complex in shape than a cube, is described well as a thin, hollowed cylinder or disk. In contrast, there is no easy geometrical way to describe the shape of the Amazon drainage system.

3. From a topological viewpoint, the shape of the Amazon River is a curve. The same is true of any coastline. A curve is a line, a one dimensional entity. Hence, the topological dimension of a river system or a coastline is one. This characterization is, however, disturbing. The Amazon drainage system does not look like a familiar curve or line. It looks instead like a complex system of smaller curves and lines, randomly oriented into a dendritic collage. As a result of this example, a topological description of a river system is incomplete.

Fractal Dimension

4. Rather than attempting to describe the shape of the Amazon River system, or any other natural and irregular form, an effort can be made to classify this irregularity. This effort can be achieved through the attempt to measure the length of the irregular form, in this case, the length of the Amazon River.

5. The Amazon River is shown to scale in Figure A1. The length of this stream can be approximated by selecting a particular ruler length, y , then

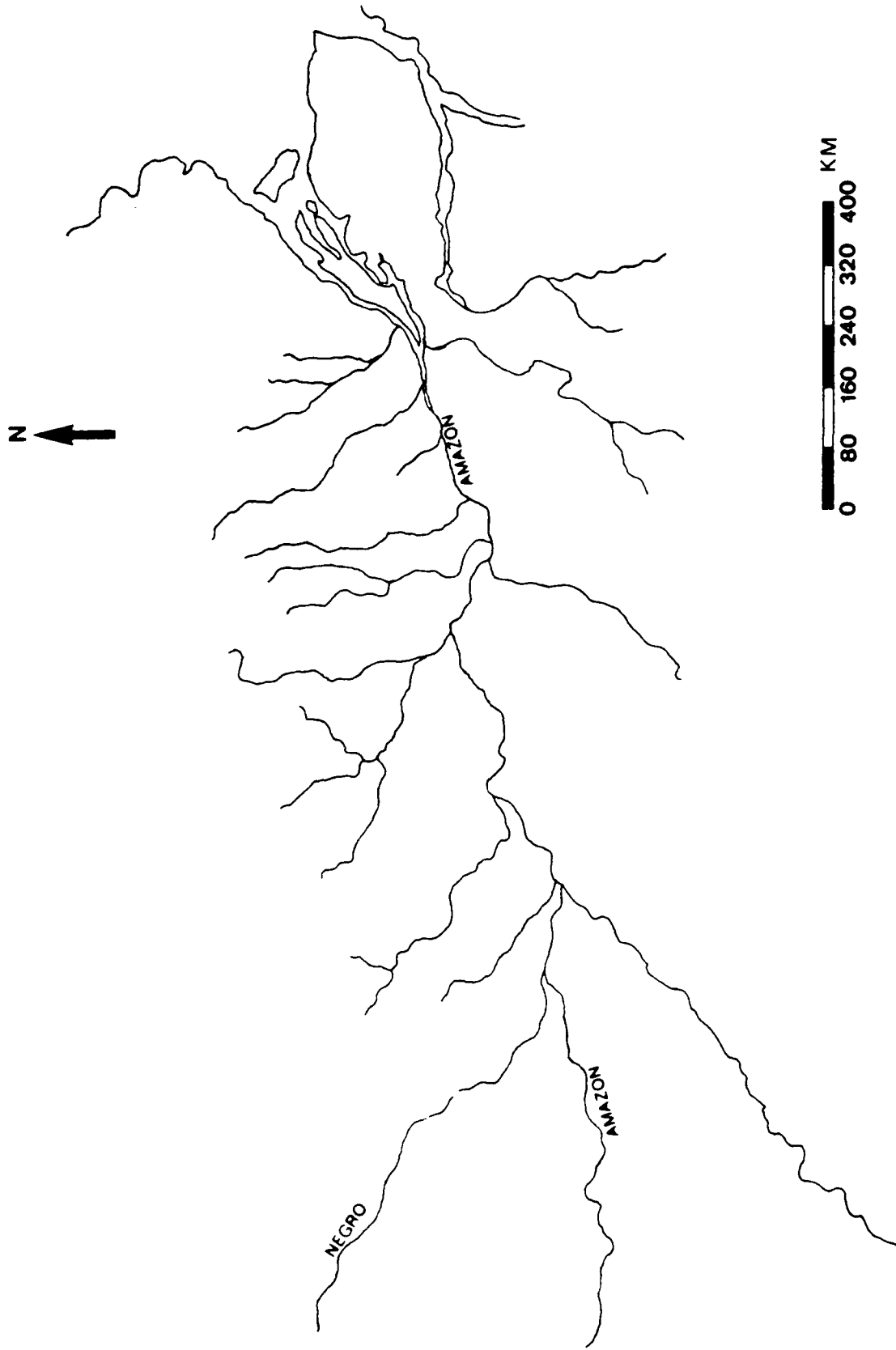


Figure A1. Trace of the Amazon River system, Brazil

counting the number of times, N , the length, y , can be laid along the stream. The length of the stream, L , is approximated as Ny .

6. If the ruler length, y , is progressively decreased and allowed to converge to zero, the length, L , of the stream is found to increase without bound (Mandelbrot 1967)*. This statement seems to be incorrect because it is thought that L converges to some finite value as y converges to zero. This is not the case, however, as is graphically demonstrated in Figure A2. Imagine if one were to measure the length of the Amazon in situ, not from a map trace. If y is 1 km, one result for L would be obtained. As y is decreased, say to 1 m, a different result for L would be obtained because features, such as embankment undulations, become important at the scale of 1 m that were overlooked at the scale of 1 km. As y is further decreased, say to 1 mm, individual rock fragments in the embankment of the river become important and add to the length, L . This describes the unbounded increase in the length, L .

7. Because of the unbounded increase of the global length, L , this parameter is not satisfactory for the description of natural shapes. The relationship between the ruler length, y , and the global length, L , is valuable, however, for the description of natural shapes. This relationship was given before as

$$L = Ny \tag{A1}$$

This relationship can be expressed in a slightly different fashion as

$$L = Ny^D \tag{A2}$$

where D is called the Hausdorff-Besicovitch dimension (Mandelbrot 1982). In equation (A1), this dimension is equal to 1.

8. For the Amazon River, each of the ruler lengths, y , (1 km, 1 m, 1 mm), is associated with a particular number of steps, N , used to approximate the global length, L . Figures A3 through A5 show the results for the Amazon River less its tributaries with ruler lengths of 160 km, 80 km and

* References cited in this appendix are included in the references at the end of the main text.

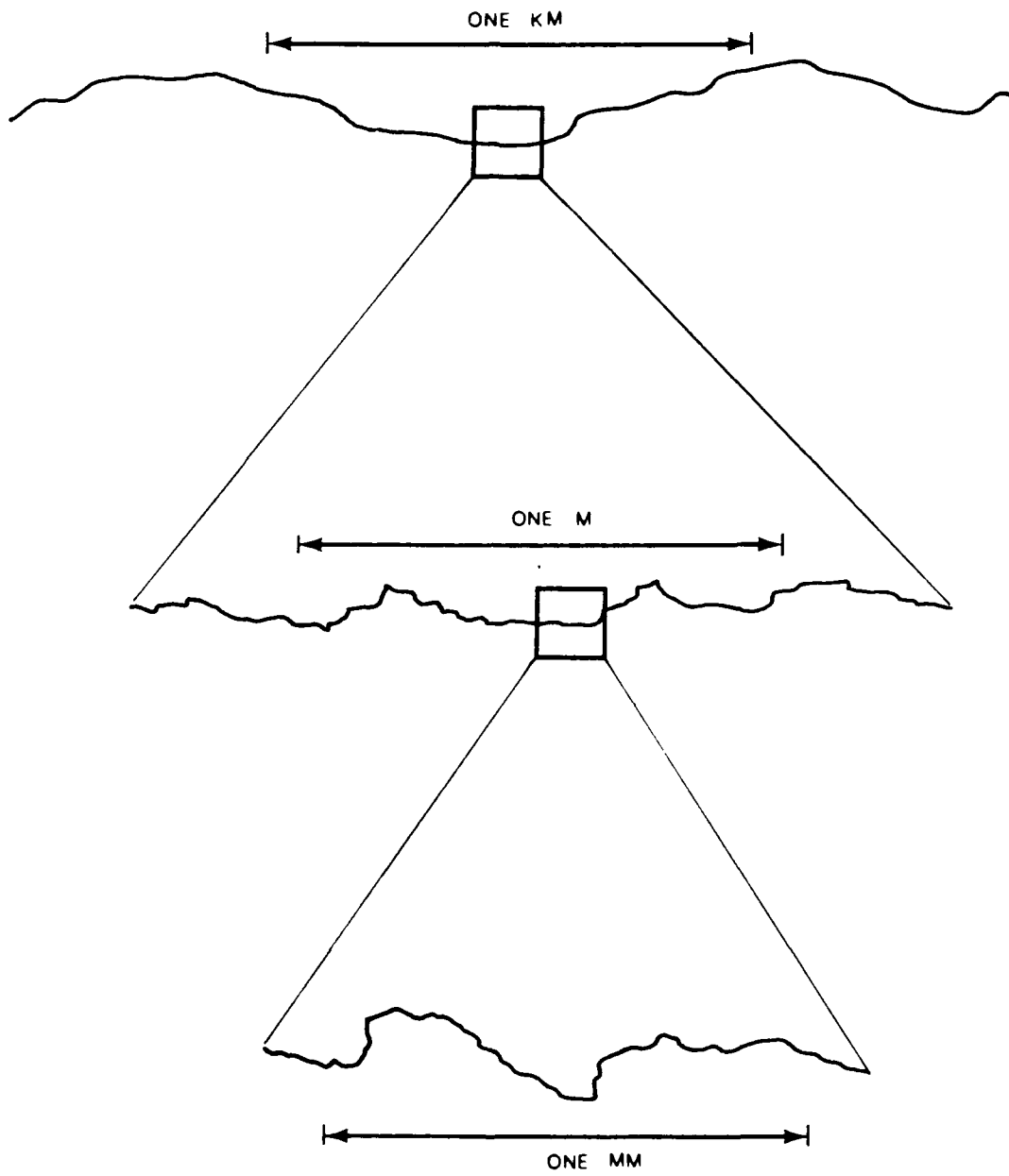


Figure A2. Schematic representation of the unbounded increase in length as the ruler measure, y , decreases

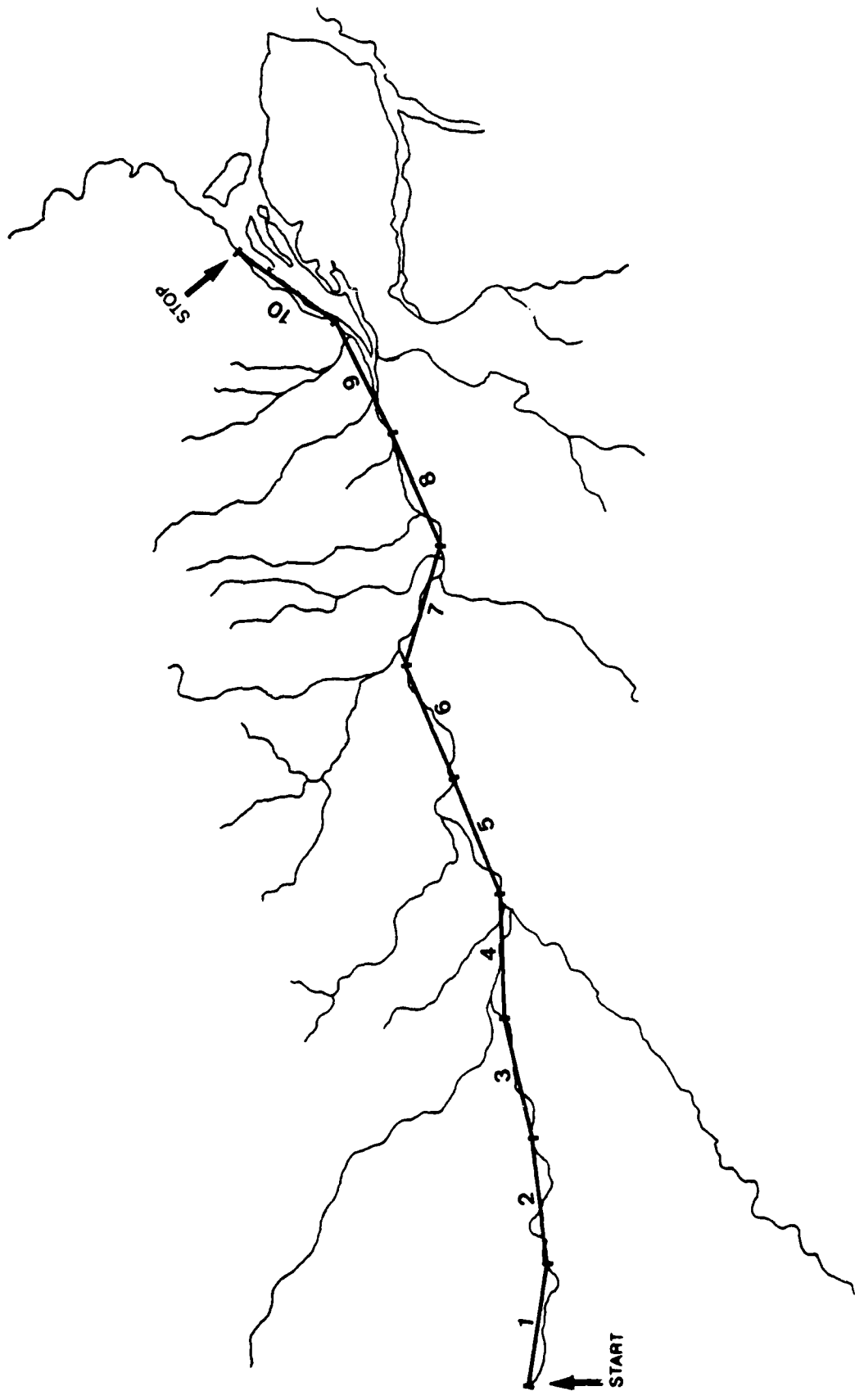


Figure A3. Amazon River trace, showing the measurement of its length using 160 km step sizes (y)

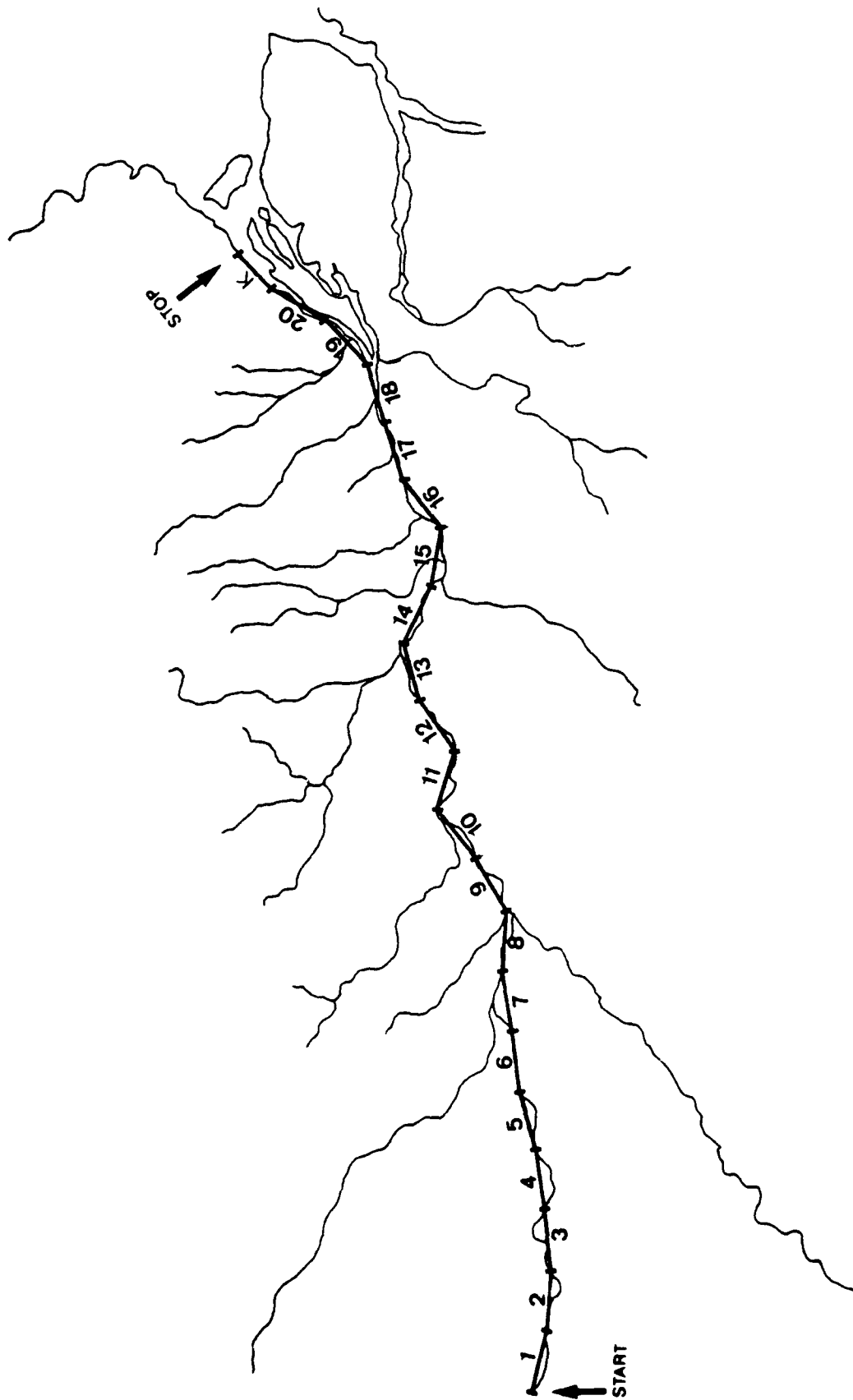


Figure A4. Amazon River trace, showing the measurement of its length using 80 km step sizes (y). Here, $20 + K$ steps are shown, where k is a remainder

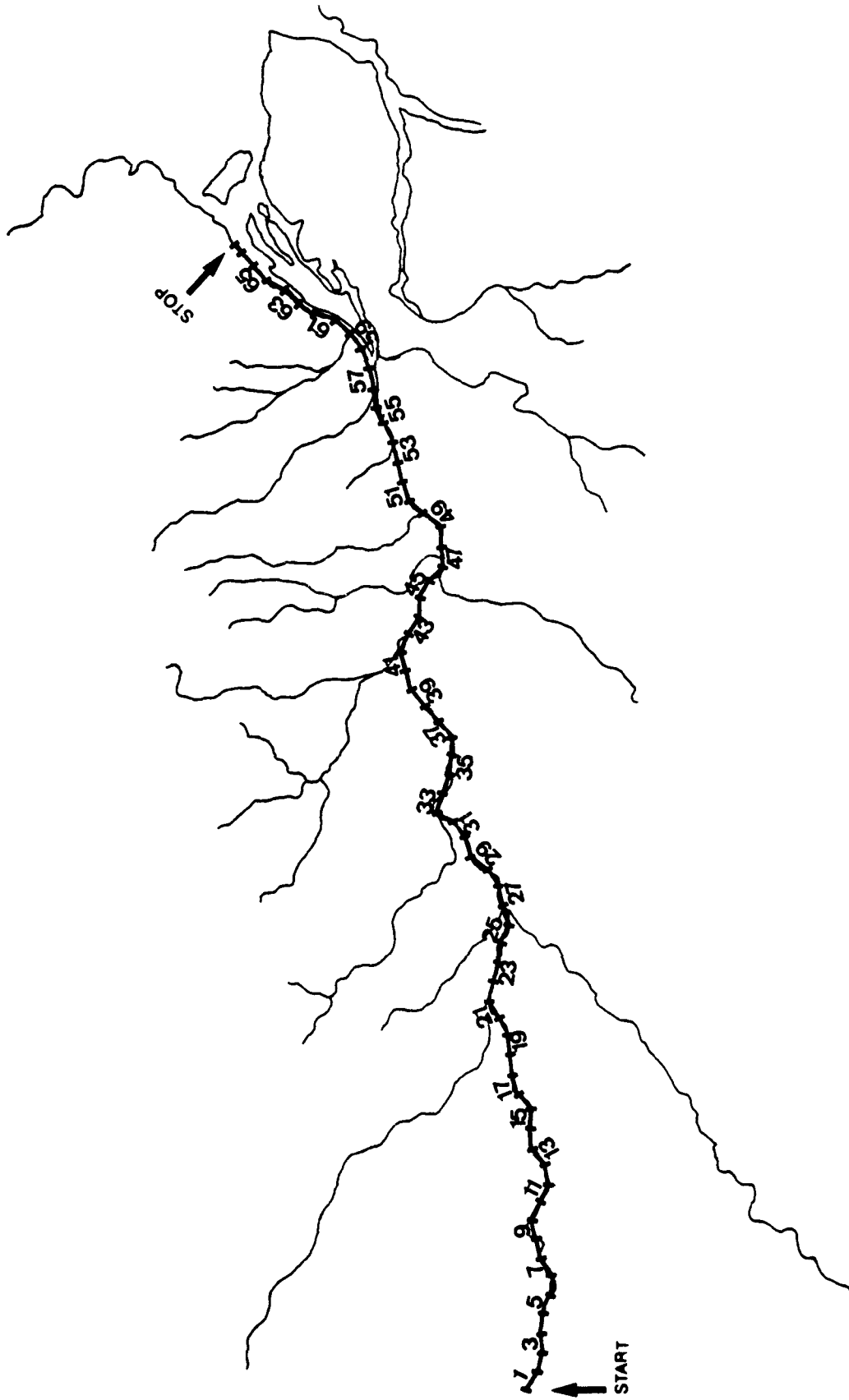


Figure A5. Amazon River trace, showing the measurement of its length using 25 km step sizes (y). Here, 66 + k steps are shown, where K is a remainder

25 km. As y decreases, N increases without bound; hence, L increases without bound.

9. By examining equation (A2), however, and rearranging terms, the following relationship is found:

$$Ly^{-D} = N \quad (A3)$$

and there is a constant relationship between y and N . If the base-ten log of N is plotted against the base-ten log of y , the slope of this plot is $-D$. This relationship is expressed by equation (A3). Moreover, the slope of this plot is a straight line; hence, it is constant. Therefore, despite the divergent behavior of the global length, L , the Hausdorff-Besicovitch dimension is constant.

10. The results from Figures A3 through A5 are plotted in Figure A6. From this plot, it is evident that the relationship between $\log_{10}(N)$ and $\log_{10}(y)$ is constant. The slope of this line is -1.02 . Therefore, the Hausdorff-Besicovitch dimension is 1.02 .

11. If the Amazon River were perfectly straight, as shown in Figure A7, a different result would be obtained for the Hausdorff-Besicovitch dimension. The $\log_{10}(N)$ versus $\log_{10}(y)$ plot for this idealized river is shown in Figure A8. The slope of this plot is exactly -1 , thus, the Hausdorff-Besicovitch dimension is 1 .

12. The hypothetical stream of Figure A7 is represented perfectly by the topological line. For this stream, $D = 1$; therefore, equation (A1) accurately measures the length. As was stated before, the topological dimension of any river is 1 . For the stream of Figure A7, the Hausdorff-Besicovitch dimension is exactly equivalent to the topological dimension.

13. This is not the case for the Amazon River. Its Hausdorff-Besicovitch dimension was found to be 1.02 . This value is greater than 1 . In nature, any curve, surface, or volume whose Hausdorff-Besicovitch dimension exceeds its topological dimension is a fractal. Furthermore, the Hausdorff-Besicovitch dimension is known as the fractal dimension (Mandelbrot 1982).

14. The fractal dimension provides the capability for the description of irregular, natural shapes. Whereas the fractal dimension is simply a numerical value and does not describe a shape such as a line, it does describe

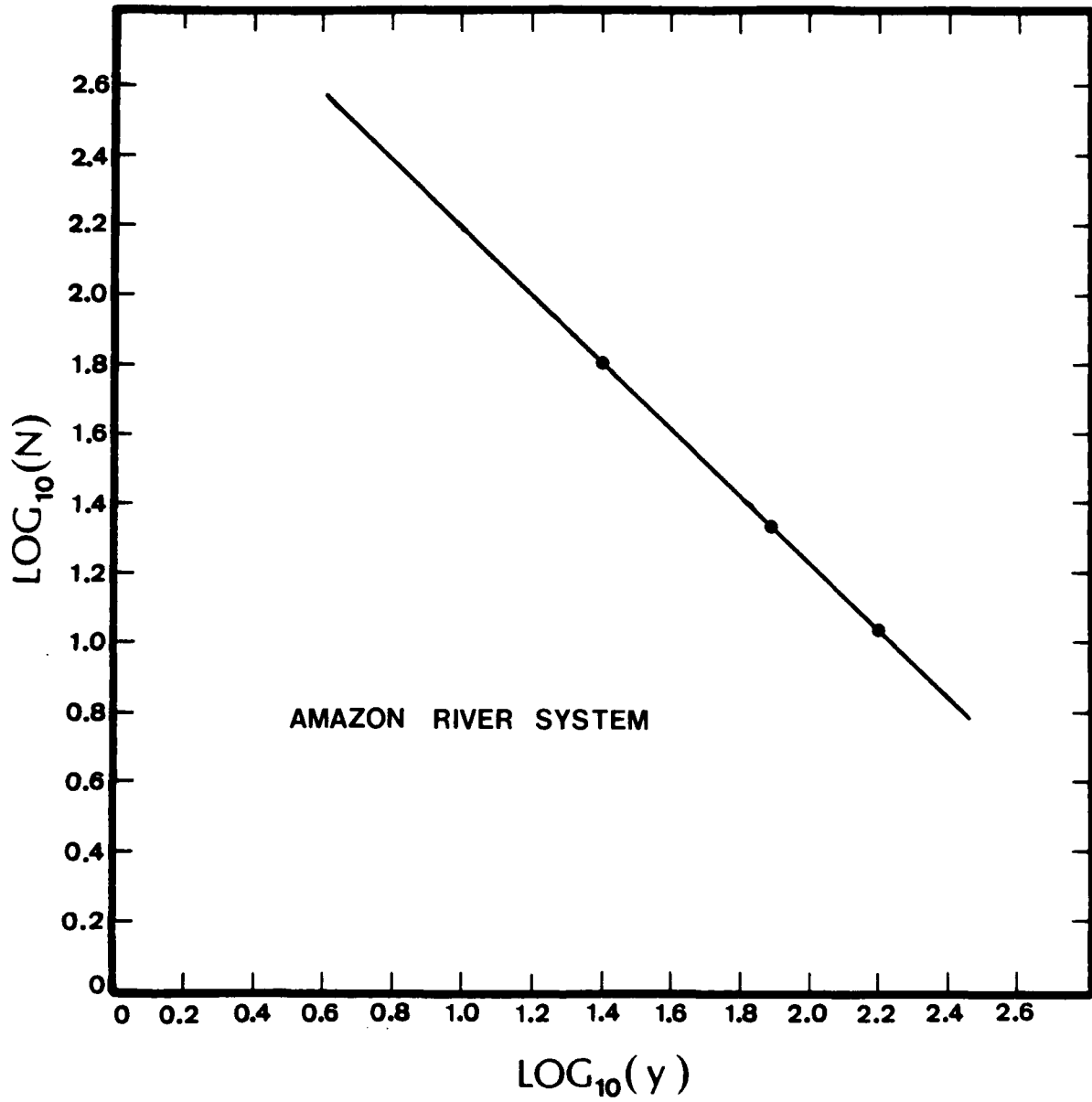


Figure A6. $\text{Log}_{10}(N)$ versus $\text{Log}_{10}(y)$ plot for the Amazon River.
The fractal dimension, D , is 1.02

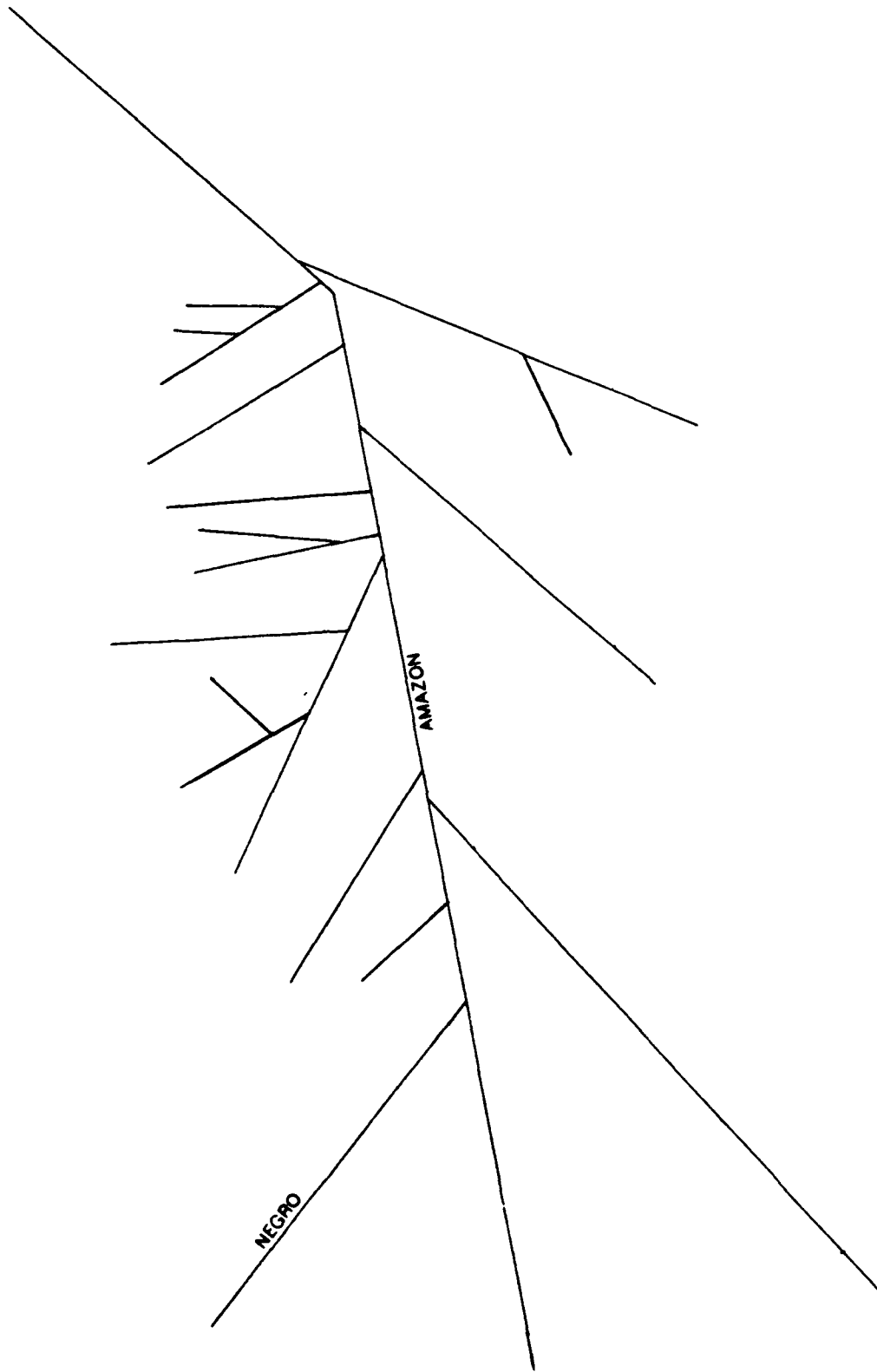


Figure A7. Linear idealization of the Amazon drainage system

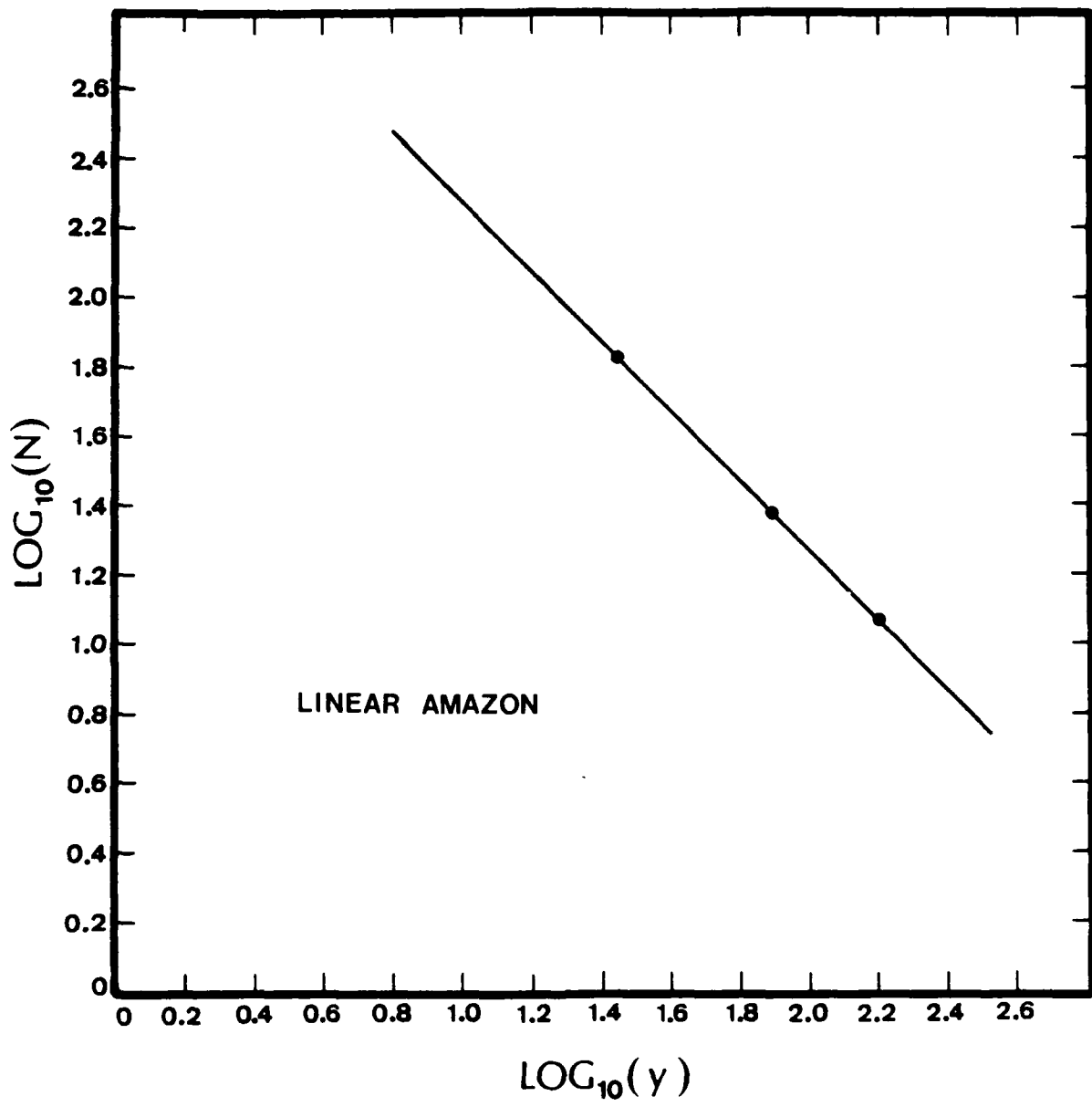


Figure A8. $\text{Log}_{10}(N)$ versus $\text{Log}_{10}(y)$ plot for the linear Amazon.
The fractal dimension, D , is 1.00

the complexity or irregularity of a curve, a surface, or a volume. This offers considerable capability for the description of natural surfaces.

Example Calculations

15. An example calculation of the fractal dimension has been provided in Figures A3 through A6. The concept of the fractal dimension has also been applied previously for the description of coastlines (Mandelbrot 1967).

16. Two coastlines are chosen as examples. Figure A9 shows the west coast of Great Britain; Figure A10 shows the coast of southern California. The southern California coast qualitatively appears to be smoother than the west coast of Great Britain. Therefore, it is expected that the fractal dimension of the southern California coast will be less than the fractal dimension for the west coast of Great Britain.

17. Using the scales plotted on each map, the selection of the ruler length, y , is as shown in Tables A1 and A2. The technique for determining N for each y is the same as was reviewed in Figures A3 through A5. The only difference in the procedure involved the use of different ruler lengths, y .

18. From Tables A1 and A2, the $\log_{10}(N)$ versus $\log_{10}(y)$ plots for each coastline are shown in Figures A11 and A12. From these plots, the fractal dimension for the west coast of Great Britain is 1.25. The fractal dimension of the southern California coast is 1.02. Hence, the fractal dimension verified the intuition that the southern California coast is smoother than the west coast of Great Britain.

Mandelbrot Set

19. The Mandelbrot Set is a recent discovery in mathematics. This set consists of a region at the contact between the plane of real numbers and the plane of complex numbers. Within this region, numerical vectors defined by the real and complex planes remain of finite numerical value following an infinite number of iterations in which the value of each vector is consistently squared.

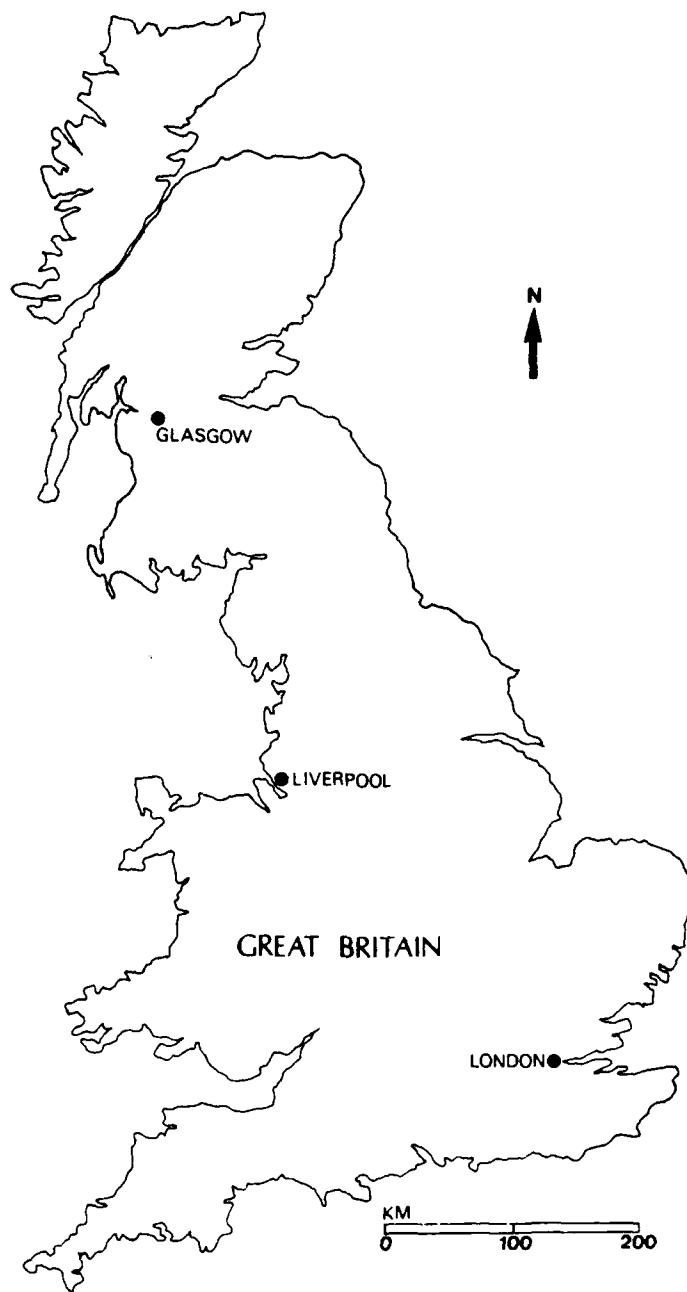


Figure A9. Outline of the coast of Great Britain

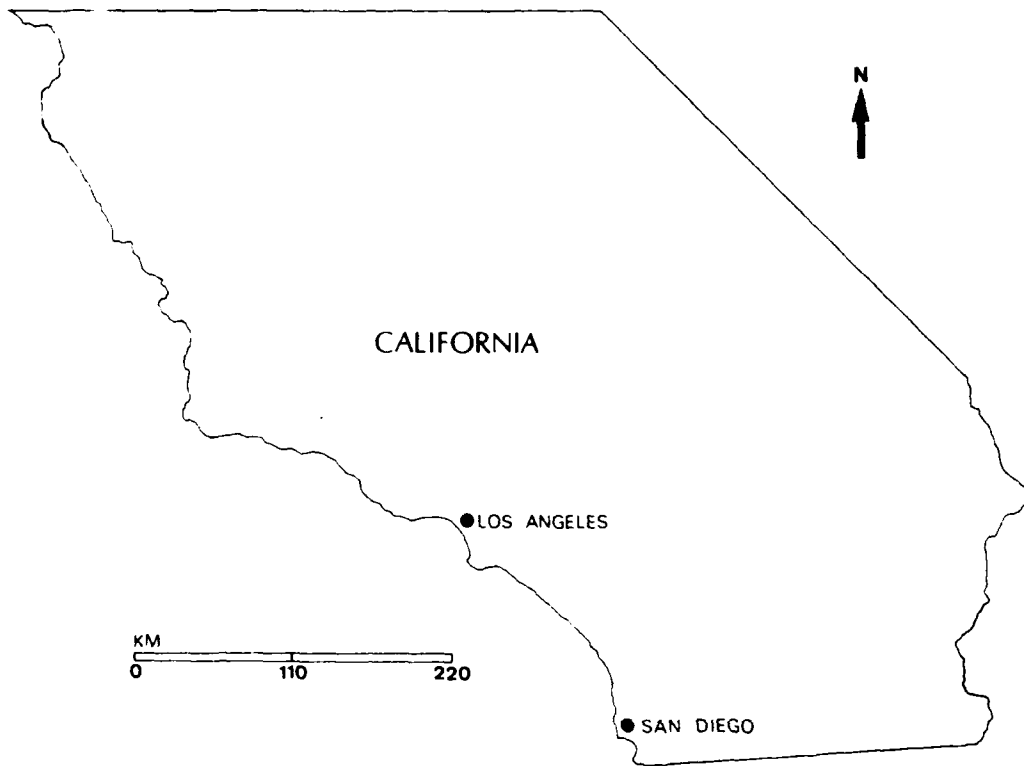


Figure A10. Outline of the coast of southern California

Table A1

Fractal Dimension* Calculation, West Coast of Great Britain

<u>Ruler Length</u> <u>y (km)</u>	<u>$\log_{10}(y)$</u>	<u>Segment Counts, N</u>	<u>$\log_{10}(N)$</u>
125	2.097	7.57	0.879
50	1.699	24.25	1.385
25	1.398	56.10	1.749

* Fractal Dimension is 1.25.

Table A2

Fractal Dimension* Calculation, Southern California Coast

<u>Ruler Length</u> <u>y (km)</u>	<u>$\log_{10}(y)$</u>	<u>Segment Counts, N</u>	<u>$\log_{10}(N)$</u>
100	2.000	7.600	0.880
40	1.600	19.330	1.290
10	1.000	80.000	1.903

* Fractal Dimension is 1.02.

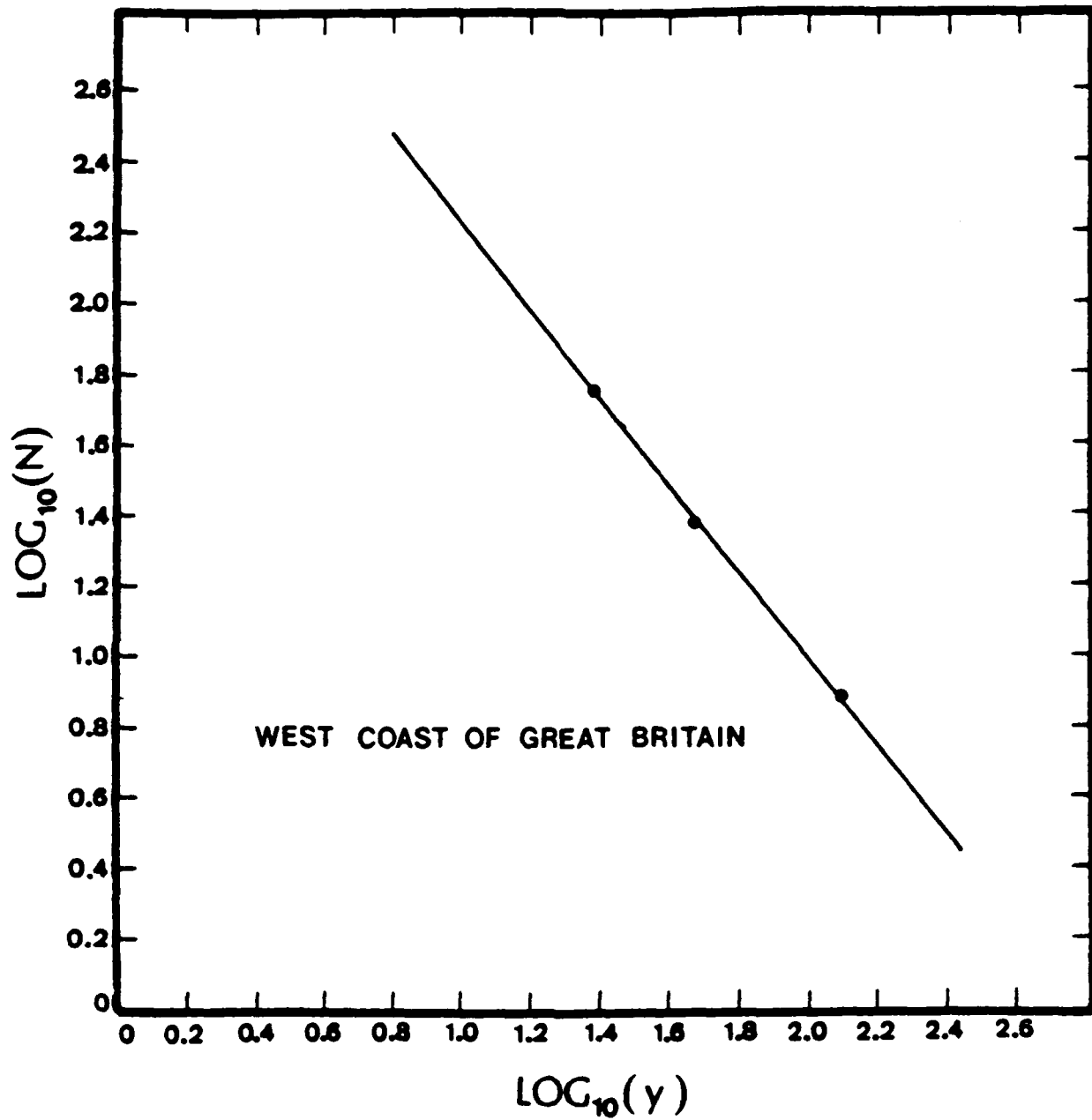


Figure A11. $\text{Log}_{10}(N)$ versus $\text{Log}_{10}(y)$ plot for the western coast of Great Britain. The fractal dimension is 1.25

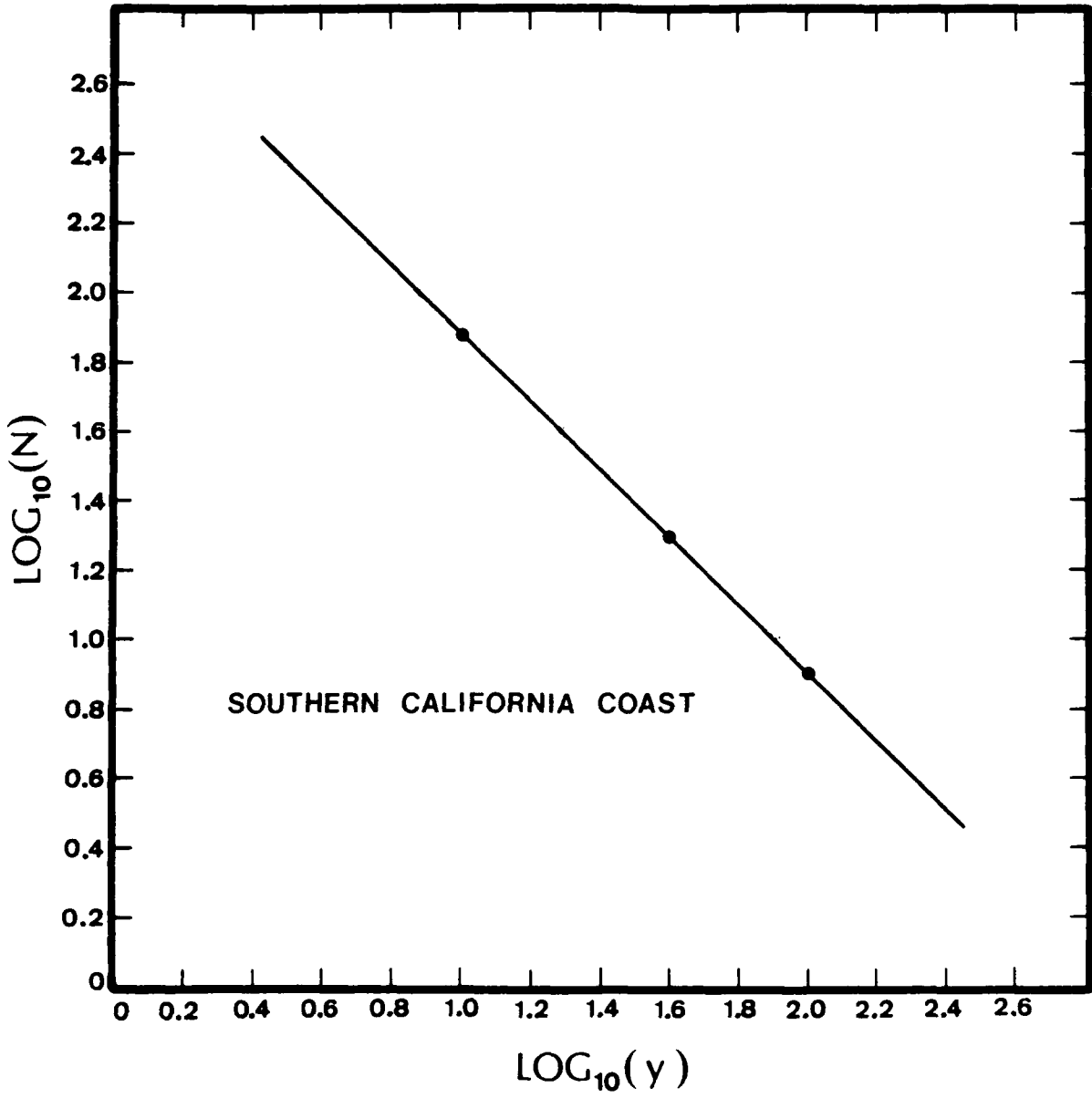


Figure A12. $\text{Log}_{10}(N)$ versus $\text{Log}_{10}(y)$ plot for the southern California coast. The fractal dimension is 1.02

20. An example of the fringe surrounding the Mandelbrot Set is shown in Figure A13. The fringe (shaded region) is not part of the Mandelbrot Set; this set resides inside this fringe. The IBM-PC compatible, BASIC language program used to create this figure (Dewdney 1985) is listed in Figure A14.

21. The Mandelbrot Set is a fractal. This set is not the result of a contrived mathematical function used to create an interesting graphical image. This set is, instead, a fascinating property of real and complex numbers. This set provides one more example of the fractal geometry of nature.

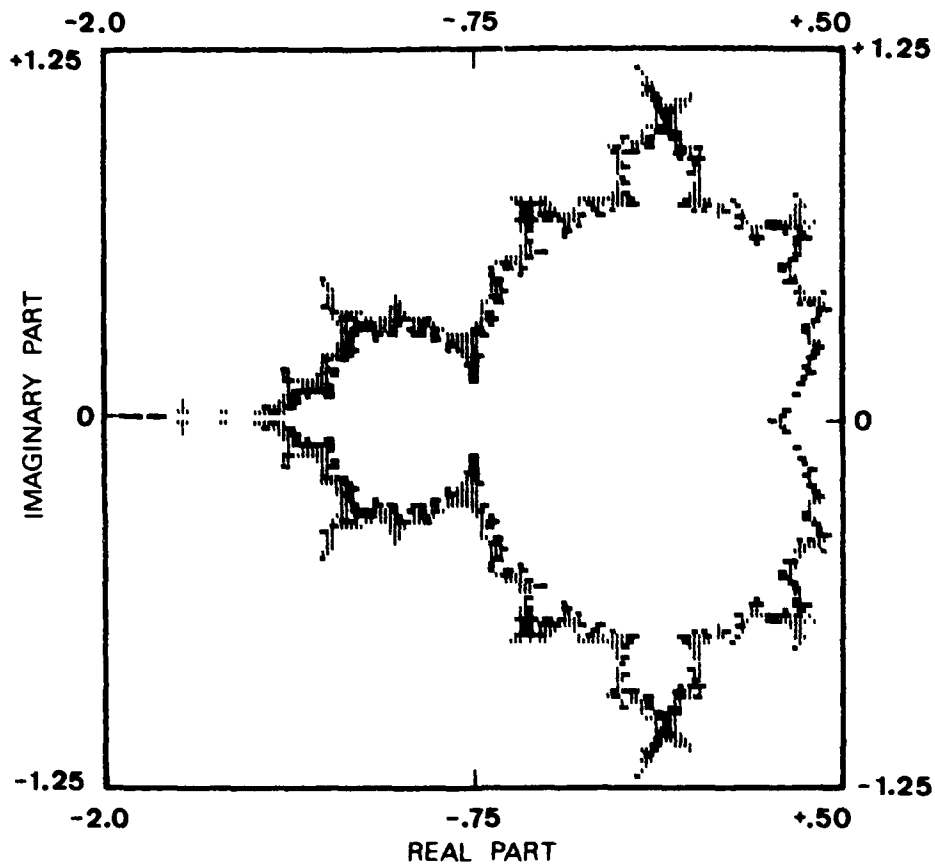


Figure A13. Mandelbrot Set. The border shows the range of real and imaginary numbers used to create this object.
(ACORNER = -2.0, BCORNER = 1.25, SIDE = 2.5)

```

5  KEY OFF:  SCREEN 1:  COLOR 0,0
10 INPUT "ENTER THE VALUE:  ACORNER";  ACORNER
20 INPUT "ENTER THE VALUE:  BCORNER";  BCORNER
50 INPUT "ENTER THE VALUE:  SIDE   ";  SIDE
55 GAP = SIDE / 150.0
56 CLS
60 FOR I = 1 TO 150
70 FOR J = 1 TO 150
90 C = (J * GAP + ACORNER)
95 E = (BCORNER - I * GAP)
96 R = C
97 W = E
100 ICOUNT = 0
101 U = (R^2 - W^2 + C)
102 V = (2*R*W + E)
110 Z = SQR(U^2 + V^2)
120 ICOUNT = ICOUNT + 1
130 IF Z > 2 THEN 150
135 IF ICOUNT > 90 THEN 150
136 R = U
137 W = V
138 GO TO 101
150 L = 0
151 IF ICOUNT < 10 THEN 164
152 IF ICOUNT > 16 THEN 155
153 L = 1
154 GO TO 164
155 IF ICOUNT > 23 THEN 158
156 L = 2
157 GO TO 164
158 IF ICOUNT > 30 THEN 164
159 L = 3
164 PSET (J,I), L
170 NEXT J
175 NEXT I
180 STOP

```

Figure A14. IBM compatible BASIC language program used to create the Mandelbrot Set of Figure A13

APPENDIX B: THE THEORY OF REGIONALIZED VARIABLES,
A GEOSTATISTICAL TECHNIQUE

1. The theory of regionalized variables was developed by Georges Matheron in the late 1950's. Matheron demonstrated that spatially dependent variables can be estimated on the basis of this spatial structure and known samples (Matheron 1963)*. This estimation is one aspect of geostatistics, a concept concerned with describing the distribution, in space, of geologic phenomena.

2. A random variable distributed in space is said to be regionalized. These variables, because of their spatial aspect, possess both random and structured components. On a local scale, regionalized variables can behave randomly or erratically. Two regionalized variables separated by a distance, h , however, are not independent, but are related by a structured aspect dependent upon h . Usually, as the length of h increases, the similarity between two regionalized variables decreases.

3. At first glance, a regionalized variable appears to be a contradiction. In one sense, it is a random variable which locally may have no relation to surrounding variables. On the other hand, there is a structured aspect to a regionalized variable which depends on the distance separating the variables. Both of these characteristics can, nevertheless, be described by a random function of which each regionalized variable is a single realization. By incorporating both the random and structured aspects of a regionalized variable in a single function, spatial variability can be accommodated on the basis of the spatial structure shown by these variables.

Variogram

4. One way to examine the spatial structure of a regionalized variable is to analytically relate the change in samples, or measurements, of the variable as a function of distance separating the samples. In general, if the average difference between samples increases as their distance of separation increases, a spatial structure exists, and the variable is regionalized.

* References cited in this appendix are included in the references at the end of the main text.

5. The function which defines the spatial correlation, or structure, of a regionalized variable is the variogram. This function is denoted as γ and is defined as

$$\gamma(h) = \frac{1}{2N} \sum_{i=1}^N \left[Z(X_i) + Z(X_i + h) \right]^2 \quad (B1)$$

where N is the total number of data pairs separated by a distance, h . The variogram is simply one half the average square of the difference between samples, $Z(X_i)$, separated by a distance, h . If a spatial relationship exists, the value of $\gamma(h)$ increases as the separation distance, h , increases. This implies that samples located close in space are more similar in value than those separated by a considerable distance.

6. For most geostatistical applications, the variogram has a spherical shape (Journel and Huijbregts, 1978). This function can be modeled by the following equation:

$$\begin{aligned} \text{Nugget} + C \frac{1.5h}{R} - \frac{0.5h^3}{R^3}, \quad h < R \\ \gamma(h) = & \hspace{15em} (B2) \\ \text{Nugget} + C, \quad h \geq R \end{aligned}$$

Each component of this equation is illustrated in Figure B1. The "nugget" value indicates the amount of white, or random, noise present in a set of data. This value is the intercept of the variogram with the abscissa axis. The value, R , is the distance at which the variogram stops increasing and becomes flat; this value is known as the range. The quantity, C , is obtained by subtracting the nugget from the sill. The sill is the variogram value at the distance, $h = R$, and is usually equal to the sample variance.

Linear Estimation of the Regionalized Variables: Kriging

7. Once the spatial structure of a regionalized variable has been determined through computation of the variogram, the spatial structure can be

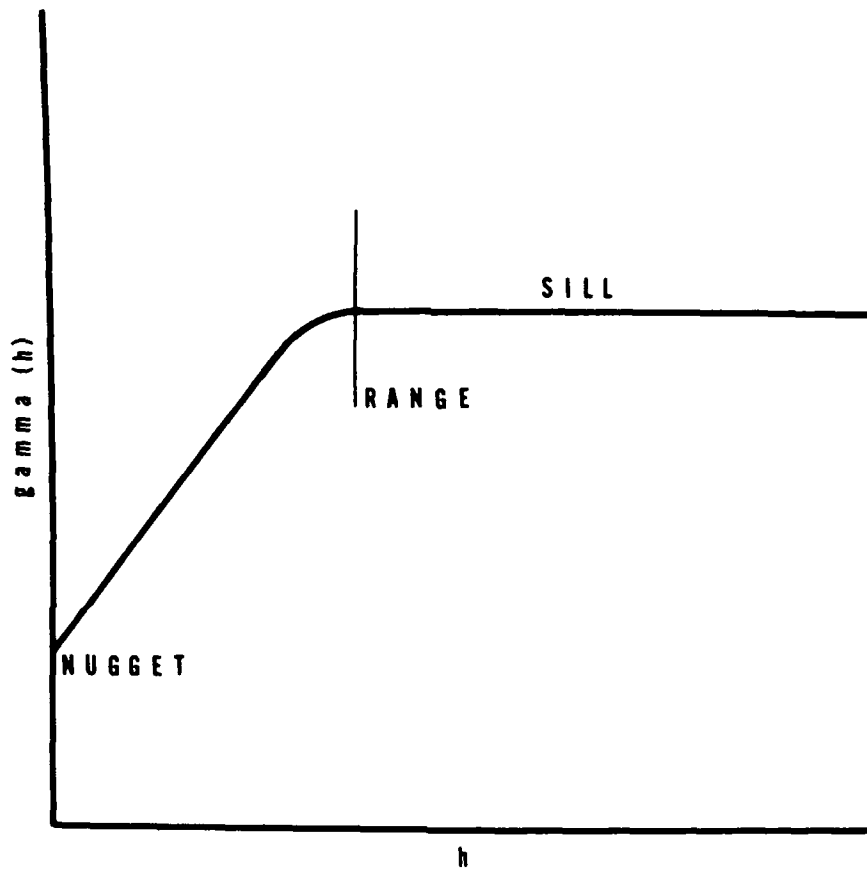


Figure B1. Example of a spherical variogram showing the nugget, range, sill and shape

used to estimate the value of a variable at an unsampled location. This estimation, or interpolation process, is known as kriging (Matheron, 1963).

8. The estimate, $Z^*(X_0)$, of a regionalized variable at a location, X_0 , is given by

$$Z^*(X_0) = \sum_{i=1}^N \lambda_i Z(X_i) \quad (B3)$$

where N is the number of closest surrounding locations used for estimation.

9. In equation (B3), λ is the vector of weights applied to each of the closest surrounding locations. Generally, the largest weights are assigned to the closest locations. Kriging is an unbiased estimator and results in a minimum variance of the error. These objectives are controlled by the weights, λ . For the unbiased condition, the sum of the weights is unity:

$$\sum_{i=1}^N \lambda_i = 1 \quad (B4)$$

where N is the same as for equation (B3). To compute the vector, λ , the following procedure is used:

$$\sum_{i=1}^N \lambda_i \sigma_{ij} - \mu = \sum_{i=1}^N \sigma_{oi} \quad (B5)$$

Where μ is an unknown, solved along with λ , and is the Lagrangian multiplier used to achieve a minimum error variance. In equation (B5), σ_{oj} and σ_{oi} are respectively the intersample and point-sample covariances. These are obtained by solving

$$\sigma(h) = Sill - \gamma(h) \quad (B6)$$

For the intersample covariance matrix, σ_{ij} , the distance, h , is that separating each of the N known locations used for estimation. For the

point-sample covariance vector, σ_{oi} , the distance, h , is that between the location, X_0 , and each of the N known locations used for estimation. In equation (B6), γ is obtained from equation (B2).

10. Once the weighting vector, λ , is known, the kriging variance, which is the variance of the estimation error, is computed as

$$\text{Krig Var} = \text{Sill} - \sum_{i=1}^N \lambda_i \sigma_{i0}^{-\mu} \quad (\text{B7})$$

where the terms sill, λ , σ_{oi} , and μ are defined as above. In a practical sense, the kriging variance is analogous to the mean square error of the estimate.

Intrinsic Hypothesis

11. This hypothesis is also known as the concept of data stationarity (Journel and Huijbregts 1978). The Intrinsic Hypothesis holds that the mean of the data in one location, X_1 , is equivalent to the mean at another location, X_2 . This requires that data values be more or less equal throughout a space, except for their natural variation (variance).

12. Kriging is a technique which expects each estimate to be the mean of the data. This explains why kriging is most accurate where the Intrinsic Hypothesis holds. The natural variability in the data is captured by the variogram. Thus, kriging is really attempting to model data fluctuations.

13. The Intrinsic Hypothesis cannot hold everywhere in space; otherwise, a natural phenomenon would be ubiquitous throughout the universe. Eventually, a natural phenomenon diminishes and becomes non-existent. An ore body gradually grades to barren country rock; earthquake ground motion gradually diminishes away from an epicenter; and the concentration of oxygen in the earth's atmosphere gradually lessens as one ascends through the atmosphere. These are all examples of nonstationary data behavior. That is, the mean is not constant, but gradually decreases. For these examples, the Intrinsic Hypothesis does not hold.

14. Despite the examples of non-stationary behavior, the data will still show natural fluctuations. By invoking the concept of quasi-stationary

behavior (Journel and Huijbregts 1978), we can restrict the size of the space over which we require the Intrinsic Hypothesis to hold. This allows us to analyze most natural situations, including those listed above.

Example Calculations

15. The previous description of a variogram is admittedly confusing. To better explain the variogram function, a short numerical example is forwarded. Let a linear arrangement of data be as shown in Figure B2. At each data location, A through G, a numerical value is given. These locations and data values provide the information needed to compute a variogram.

16. This computation is given in Table B1. We begin by examining a separation distance that is close, but not equal, to zero. (For a separation distance of zero, we would be looking at the difference between a data value with itself, which is zero. Hence, no useful information is really obtained for h equal to zero). This example begins with a separation distance of one unit ($h=1$). All data pairs separated by this distance are obtained as shown in Table B1; in this case, six pairs are found. For each pair, the difference between values is squared. These squared differences are then summed and divided by twice the number of pairs. This becomes the variogram value for a particular separation distance.

17. Subsequent to this, the separation distance is incremented until a distance is reached which exceeds the separation distance between the farthest spaced pairs. For real data whose locations are irregularly spaced, the separation distance h , is incremented in the same manner from a small value to a larger value. An exception is that h is considered to be an average value. For example, for $h = 2$, we would find all pairs separated by a distance between 1.5 and 2.5 with an average separation distance of 2.0.

18. The results of a variogram calculation are displayed graphically. For the computation developed in Table B1, the graphical result is shown in Figure B3. This variogram is seen to increase from the origin as expected. Beyond a separation distance of three units, however, the variogram begins to decrease. This is occasionally encountered with variogram computation and, in this instance, shows that data locations are similar at the ends of this linear array. It is essential to remember, nevertheless, that each set of data has a unique variogram. This is a valuable aspect of geostatistics.

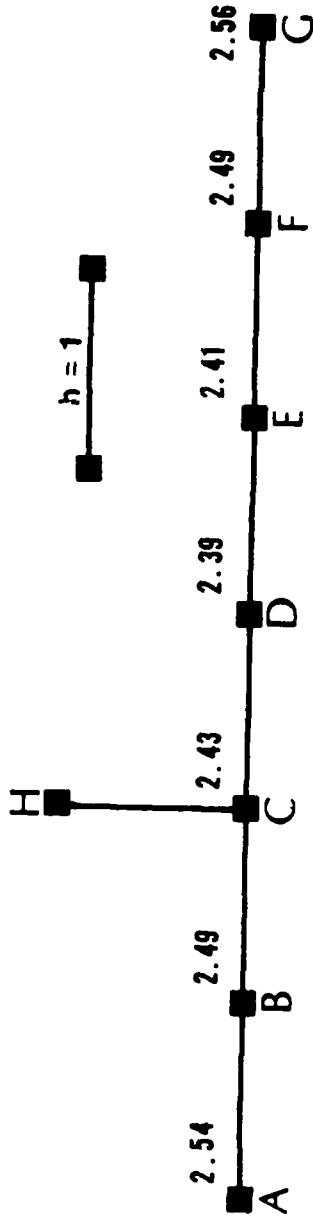


Figure B2. Example arrangement of sample locations and values

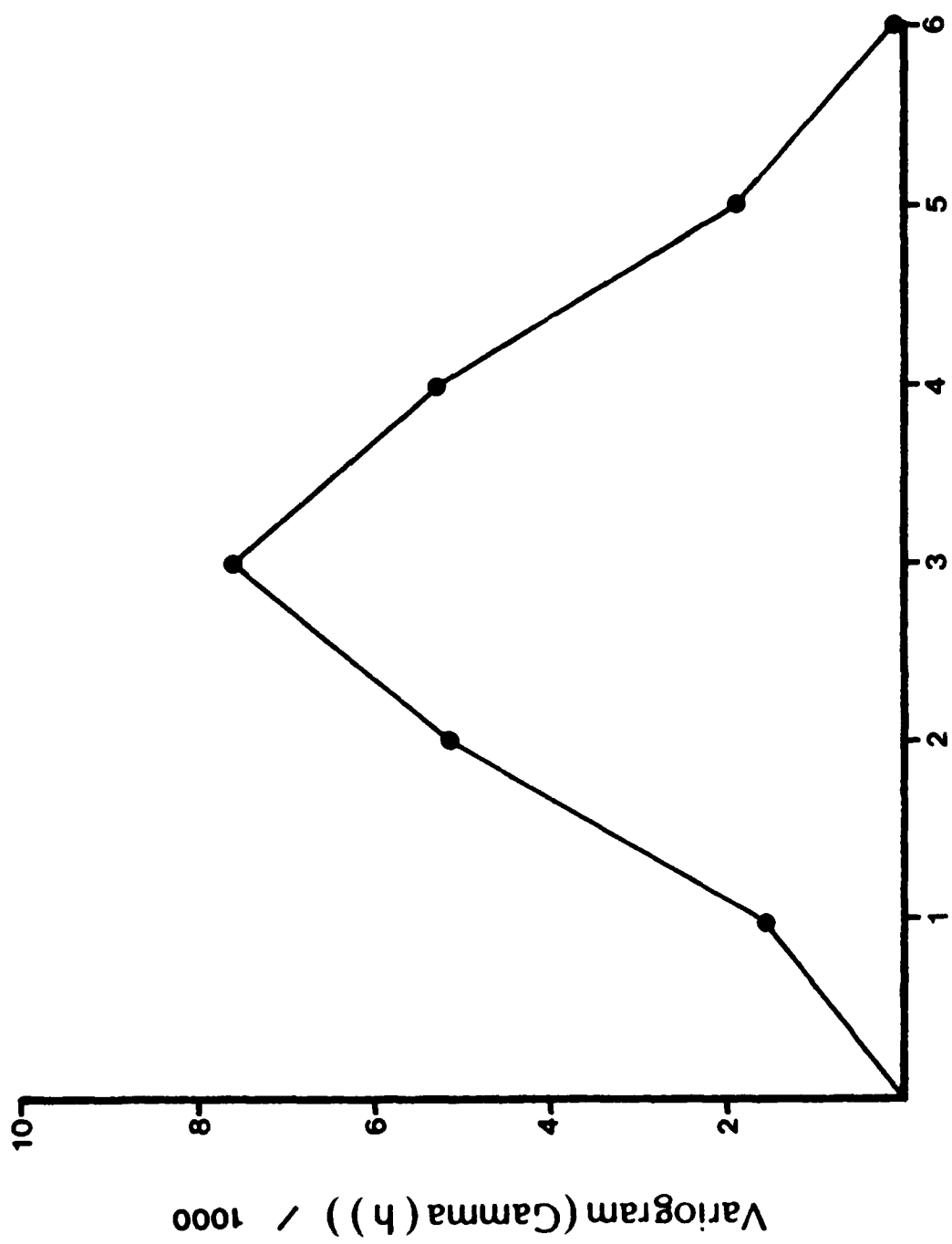
Table B1
Computation of a Variogram for the Data of Figure B1

h	<u>Pairs</u>	<u>Difference (Squared)</u>
1	A - B	$(2.54 - 2.49)**2 = 0.0025$
	B - C	$(2.49 - 2.43)**2 = 0.0036$
	C - D	$(2.43 - 2.39)**2 = 0.0016$
	D - E	$(2.39 - 2.41)**2 = 0.0004$
	E - F	$(2.41 - 2.49)**2 = 0.0064$
	<u>F - G</u>	$(2.49 - 2.56)**2 = \underline{0.0049}$
	N = 6	sum = 0.0194 $\gamma(1) = 0.0194/2(6) = 0.0016$
2	A - C	$(2.54 - 2.43)**2 = 0.0121$
	B - D	$(2.49 - 2.39)**2 = 0.0100$
	C - E	$(2.43 - 2.41)**2 = 0.0004$
	D - F	$(2.39 - 2.49)**2 = 0.0100$
	<u>E - G</u>	$(2.41 - 2.56)**2 = \underline{0.0225}$
	N = 5	sum = 0.055 $\gamma(2) = 0.055/2(5) = 0.0055$
3	A - D	$(2.54 - 2.39)**2 = 0.0225$
	B - E	$(2.49 - 2.41)**2 = 0.0064$
	C - F	$(2.43 - 2.49)**2 = 0.0036$
	<u>D - G</u>	$(2.39 - 2.56)**2 = \underline{0.0289}$
	N = 4	sum = 0.0614 $\gamma(3) = 0.0614/2(4) = 0.0077$
4	A - E	$(2.54 - 2.41)**2 = 0.0169$
	B - F	$(2.49 - 2.49)**2 = 0$
	<u>C - G</u>	$(2.43 - 2.56)**2 = \underline{0.0169}$
	N = 3	sum = 0.0338 $\gamma(4) = 0.0338/2(3) = 0.0056$
5	A - F	$(2.54 - 2.49)**2 = 0.0025$
	<u>B - G</u>	$(2.49 - 2.56)**2 = \underline{0.0049}$
	N = 2	sum = 0.0074 $\gamma(5) = 0.0074/2(2) = 0.0019$
6	<u>A - G</u>	$(2.54 - 2.56)**2 = \underline{0.0004}$
	N = 1	$\gamma(6) = 0.0004/2(1) = 0.0002$
7	No pairs found	

(Continued)

Table B1 (Concluded)

<u>h</u>	<u>Summary</u>	<u>$\gamma(h)$</u>
1		0.0016
2		0.0055
3		0.0077
4		0.0056
5		0.0019
6		0.0002



Distance of Separation - h

Figure B3. Variogram for the data of Figure B2

19. Variogram estimation is fundamental to the understanding of spatial structure. Moreover, because the variogram is estimated from data representing a particular spatial phenomenon, geostatistics is adaptable to any spatial situation without the need for modification. The variogram is, as a result, a powerful analytical procedure.

20. The variogram is the foundation of the regionalized variables estimator, known as kriging (Matheron 1963). Kriging is developed for one primary objective: everywhere estimates are made, the variance of the error of these estimates is a minimum. Further, this noble objective must be achieved within the constraint that estimation proceeds without changing the mean value of the spatial phenomenon. Hence, kriging is a constrained, optimal estimator.

21. A numerical example is useful for showing how the weights, λ_i , are computed in the kriging system. Returning to Figure B2, suppose an estimate is to be made at location H on the basis of locations B, C, and D. The geometry of this example is simple and allows for a clear description of kriging. This does not suggest, however, that kriging always requires such regular geometries.

22. For this example, a function is required to model the variogram of Figure B3. For most applications of kriging, a spherical variogram model is useful. Such a model has the form of equation (B2).

23. In this example, let equation (B2) be adapted to fit the variogram of Figure B3. For this simple case, the following is true:

- a. Nugget = 0.
- b. Sill = 0.0077.
- c. Range = 3.

On this basis, equation (B2) becomes

$$\gamma(h) = \begin{cases} 0.0077(h/2 - h^3/54), & h < 3 \\ 0.0077, & h \geq 3 \end{cases} \quad (\text{B8})$$

This is the variogram model for this example.

24. The procedure used to form the kriging system for this example is shown in Table B2. Some explanation is required concerning the formation of the matrix system. For the matrix, $[\sigma_{Z_i Z_j}]$, the last row, (1 1 1 0), assures that the sum of the weights is equal to 1. Further, with respect to

Table B2
Example Kriging Computation

Step 1. Form intersample covariance matrix

$$\begin{bmatrix} \sigma_{Z_1 Z_1} & \sigma_{Z_1 Z_2} & \sigma_{Z_1 Z_3} & 1 \\ \sigma_{Z_2 Z_1} & \sigma_{Z_2 Z_2} & \sigma_{Z_2 Z_3} & 1 \\ \sigma_{Z_3 Z_1} & \sigma_{Z_3 Z_2} & \sigma_{Z_3 Z_3} & 1 \\ 1 & 1 & 1 & 0 \end{bmatrix}$$

where

1) $\sigma_{Z_i Z_i} = \text{sill} = 0.0077$

2) $\sigma_{Z_i Z_j} = \sigma_{Z_j Z_i} = \text{sill} - \gamma(h_{ij})$

From this

i	j	h_{ij}	γ_{ij} (equation 12)	$\sigma_{Z_i Z_j}$
1=B	2=C	1	0.0037	0.0040
1=B	3=D	2	0.0065	0.0012
2=C	3=D	1	0.0037	0.0040

Hence

$$\begin{bmatrix} \sigma_{Z_1 Z_1} & \sigma_{Z_1 Z_2} & \sigma_{Z_1 Z_3} & 1 \\ \sigma_{Z_2 Z_1} & \sigma_{Z_2 Z_2} & \sigma_{Z_2 Z_3} & 1 \\ \sigma_{Z_3 Z_1} & \sigma_{Z_3 Z_2} & \sigma_{Z_3 Z_3} & 1 \\ 1 & 1 & 1 & 0 \end{bmatrix}$$

(Continued)

(Sheet 1 of 3)

Table B2 (Continued)

Step 2. Form point - sample covariance vector

$$\sigma_{Z^*(H)Z} = \begin{Bmatrix} \sigma_{Z^*(H)Z_1} \\ \sigma_{Z^*(H)Z_2} \\ \sigma_{Z^*(H)Z_3} \\ 1 \end{Bmatrix}$$

Z*(H)	Z _i	Distance, h	γ(h)	σ(h)
H	B	1.414	0.0050	0.0027
H	C	1.000	0.0037	0.0040
H	D	1.414	0.0050	0.0027

Hence

$$\sigma_{Z^*(H)Z} = \begin{Bmatrix} 0.0027 \\ 0.0040 \\ 0.0027 \\ 1 \end{Bmatrix}$$

Step 3. Solve the following system

$$\begin{bmatrix} 0.0077 & 0.0040 & 0.0012 & 1 \\ 0.0040 & 0.0077 & 0.0040 & 1 \\ 0.0012 & 0.0040 & 0.0077 & 1 \\ 1 & 1 & 1 & 0 \end{bmatrix} \begin{Bmatrix} \lambda_1 \\ \lambda_2 \\ \lambda_3 \\ \mu \end{Bmatrix} = \begin{Bmatrix} 0.0027 \\ 0.0040 \\ 0.0027 \\ 1 \end{Bmatrix}$$

From Gauss Elimination:

$$\lambda_1 = 0.289 \quad \lambda_2 = 0.422 \quad \lambda_3 = 0.289 \quad \mu = -1.56E-03$$

(Continued)

(Sheet 2 of 3)

Table B2 (Concluded)

Step 4. Compute the estimate

$$\begin{aligned} Z^*(H) &= \lambda_1 Z_B + \lambda_2 Z_C + \lambda_3 Z_D \\ &= (0.289)(2.49) + (0.422)(2.43) + (0.289)(2.39) \\ &= 2.44 \end{aligned}$$

Step 5. Compute the kriging variance

$$\begin{aligned} \text{Krig Var} = \text{Sill} &= \sum_{i=1}^N \lambda_i^2 \sigma_{Z^*(H)Z}^2 - \mu \\ &= 0.0077 - [(0.289)(0.0027) + (0.422)(0.0040) \\ &\quad + (0.289)(0.0027)] - (-1.56E-03) \\ &= 0.0060 \end{aligned}$$

$$\text{Standard Deviation} = 0.0060 = 0.078$$

(Sheet 3 of 3)

this matrix, the unity values in the fourth column are included because the Lagrangian multiplier helps relate the covariances of the left hand side of the equation with those of the right hand side. This multiplier assures the minimization of the variance of the error.

25. From this example, it is observed that the largest weight is associated with location C , closest to the estimation location, H . The weights, λ_i , are a function of a separation distance, and closer points will receive greater weight, in general, than farther points. The estimate obtained in this example is 2.44 with an error having a standard deviation of 0.078. Hence, kriging not only yields an estimate but also provides an estimate of its error.

APPENDIX C: FRACTAL DIMENSION CALCULATIONS

1. Table C1 presents the information used to calculate the fractal dimensions of cross sections using the method 1 calculation. Table C2 presents the information used to calculate the fractal dimensions of cross sections using the method 2 calculation. These tables are included to show the significant difference between these techniques for the calculation of the fractal dimension of rock surfaces. The method 2 calculation is the correct procedure.

Table C1
Fractal Dimension Summary (Method 1 Calculation)

<u>Cross Section</u>	<u>Number of Segment Counts, N</u>			<u>Fractal Dimension</u>
	<u>y=305 cm</u>	<u>y=100 cm</u>	<u>y=20 cm</u>	
AB	4	13	65	1.023
AF	4	12	62	1.006
AG	5	15	78	1.008
AH	4	12	64	1.018
AJ	5	15	79	1.013
AN	3	9	46	1.002
AP	3	10	50	1.033
AQ	3	10	51	1.040
AR	4	12	63	1.012
AS	3	10	51	1.040
AT*	2	7	36	1.061
AU*	1	5	25	1.181
AW*	2	8	41	1.109
AX*	2	6	33	1.029
AY*	2	7	39	1.090
AZ*	1	4	24	1.166
BB	8	24	123	1.003
BC	8	24	123	1.003
BD	8	24	125	1.009
BE	7	23	119	1.040
BG	6	19	100	1.033
BH	7	22	113	1.021
BI	6	19	96	1.018
BJ	6	20	101	1.036

* The cross-sectional length of sections AT through AZ is less than that of sections AB through AS. Hence, the segment length, $y = 305 \text{ cm}$, was too large. As a result, the use of whole numbers to represent the number of segment counts, N , was incorrect.

Table C2
Fractal Dimension Summary (Method 2 Calculation)

<u>Cross Section</u>	<u>Number of Segment Counts, N</u>			<u>Fractal Dimension</u>
	<u>y=305 cm</u>	<u>y=100 cm</u>	<u>y=20 cm</u>	
AG	4.951	15.200	77.000	1.0072
AH	4.164	12.750	65.600	1.0119
AJ	4.974	15.480	77.100	1.0060
AN	3.013	9.200	46.100	1.0012
AP	3.328	10.170	50.200	1.0009
AQ	3.302	10.160	51.200	1.0061
AR	4.000	12.490	62.800	1.0107
AT	2.285	7.140	36.800	1.0200
AW	2.551	8.140	41.850	1.0268
AX	2.049	6.290	32.900	1.0189

APPENDIX D: NUMERICAL VARIOGRAM RESULTS

1. This appendix presents the numerical results used to plot the variograms which were presented in Part III. These results are presented to verify each variogram plot and to provide numerical precision beyond what can be interpreted from each plot. Only results for the variograms of Part III are presented.

Table D1
Variogram Results for Cross Section BG

<u>h(cm)</u>	<u>$\gamma(h)$</u>	<u>No. of Pairs (N)</u>
0 - 50	6.00	48
51 - 100	16.96	49
101 - 150	30.32	53
151 - 200	49.38	42
201 - 250	73.94	49
251 - 300	117.47	44
301 - 350	164.15	40
351 - 400	237.89	41
401 - 450	311.95	39
451 - 500	377.23	28
501 - 550	416.96	38
551 - 600	517.00	41
601 - 650	671.00	26
651 - 700	722.03	19
701 - 750	821.73	22
751 - 800	915.75	20
801 - 850	1057.55	22
851 - 900	1161.12	17
901 - 950	1321.39	18
951 - 1000	1474.82	17

Sample Variance = 427.81

Table D2
Variogram Results for Cross Section AF

<u>h(cm)</u>	<u>$\gamma(h)$</u>	<u>No. of Pairs (N)</u>
0 - 80	85.71	28
81 - 160	232.26	31
161 - 240	242.19	32
241 - 320	258.33	24
321 - 400	364.58	24
401 - 480	707.14	21
481 - 560	816.67	21
561 - 640	871.88	16
641 - 720	1125.00	18
721 - 800	1635.00	20
801 - 880	2261.77	17
881 - 960	2335.71	14
961 - 1040	2512.50	16
1041 - 1120	2875.00	16
1121 - 1200	3290.00	15
1201 - 1280	4783.33	18
1281 - 1360	5525.00	10
1361 - 1440	4075.00	4
1441 - 1520	6658.33	6

Sample Variance = 1525.64

Table D3
Variogram Results for Cross Section AL

<u>h (cm)</u>	<u>$\gamma(h)$</u>	<u>No. of Pairs (N)</u>
0 - 40	67.38	71
41 - 80	207.85	80
81 - 120	418.24	76
121 - 160	600.19	75
161 - 200	848.87	76
201 - 240	912.32	74
241 - 280	1165.48	65
281 - 320	1217.34	64
321 - 360	1663.28	58
361 - 400	1679.67	61
401 - 440	1581.22	49
441 - 480	1279.12	57
481 - 520	1087.29	42
521 - 560	815.43	42
561 - 600	684.22	37
601 - 640	1034.19	31
641 - 680	1587.79	28
681 - 720	2254.17	24
721 - 760	2758.40	30
761 - 800	4054.22	18

Sample Variance = 1392.00

Table D4
Variogram Results for Cross Section AS'

<u>h(cm)</u>	<u>$\gamma(h)$</u>	<u>No. of Pairs (N)</u>
0 - 40	15.57	54
41 - 80	72.24	59
81 - 120	137.14	61
121 - 160	204.16	55
161 - 200	279.22	48
201 - 240	401.56	47
241 - 280	411.65	44
281 - 320	548.44	48
321 - 360	775.49	41
361 - 400	944.30	33
401 - 440	870.51	45
441 - 480	1029.90	34
481 - 520	1030.64	36
521 - 560	978.05	28
561 - 600	885.94	26
601 - 640	912.30	23
641 - 680	875.28	16
681 - 720	1083.47	17
721 - 760	1511.42	13
761 - 800	2043.61	9

Sample Variance = 649.39

Table D5
Variogram Results for Cross Section BA

<u>h (cm)</u>	<u>$\gamma(h)$</u>	<u>No. of Pairs (N)</u>
0 - 50	26.60	37
51 - 100	93.65	40
101 - 150	129.00	34
151 - 200	127.79	29
201 - 250	108.22	36
251 - 300	75.55	31
301 - 350	41.86	29
351 - 400	49.67	18
401 - 450	78.40	20
451 - 500	45.89	19
501 - 550	39.69	13
551 - 600	44.00	13
601 - 650	55.71	14
651 - 700	128.43	14
701 - 750	86.00	16
751 - 800	32.77	13
801 - 850	60.55	11
851 - 900	28.00	11
901 - 950	20.00	9
951 - 1000	103.14	7

Sample Variance = 105.47

Table D6
Variogram Results for Cross Section BB

<u>h(cm)</u>	<u>$\gamma(h)$</u>	<u>No. of Pairs (N)</u>
0 - 50	10.52	84
51 - 100	28.45	71
101 - 150	38.96	71
151 - 200	42.11	68
201 - 250	49.86	69
251 - 300	66.79	58
301 - 350	80.38	63
351 - 400	85.70	54
401 - 450	91.88	69
451 - 500	110.67	63
501 - 550	175.91	46
551 - 600	196.44	45
601 - 650	256.33	55
651 - 700	292.09	47
701 - 750	323.66	41
751 - 800	394.04	56
801 - 850	436.00	50
851 - 900	579.28	39
901 - 950	509.30	37
951 - 1000	512.12	34

Sample Variance = 263.77

Table D7
Variogram Results, Cross Section From Patton and Deere (1970)

<u>h(cm)</u>	<u>$\gamma(h)$</u>	<u>No. of Pairs (N)</u>
0 - 8	0.25	269
9 - 16	0.75	342
17 - 24	1.68	326
25 - 32	2.53	310
33 - 40	3.35	294
41 - 48	3.76	274
49 - 56	3.84	258
57 - 64	3.71	242
65 - 72	3.28	226
73 - 80	2.63	210
81 - 88	1.90	194
89 - 96	1.14	178
97 - 104	0.78	162
105 - 112	0.86	146
113 - 120	1.70	130
121 - 128	3.04	114
129 - 136	4.32	98
137 - 144	5.11	79
145 - 152	5.17	62
153 - 160	4.13	55

Sample Variance = 2.42

Table D8
Variogram Results for Cross Section BG (Filtered)

<u>h</u>	<u>$\gamma(h)$</u>	<u>No. of Pairs (N)</u>
0 - 20	1.15	15
21 - 40	2.65	23
41 - 60	2.94	20
61 - 80	6.29	21
81 - 100	6.62	18
101 - 120	5.45	20
121 - 140	7.47	20
141 - 160	8.87	19
161 - 180	9.11	19
181 - 200	6.32	17
201 - 220	4.92	21
221 - 240	4.54	19
241 - 260	4.17	19
261 - 280	4.96	18
281 - 300	3.92	16
301 - 320	2.66	14
321 - 340	2.16	18
341 - 360	4.16	16
361 - 380	7.55	15
381 - 400	8.16	22

Sample Variance = 5.92

APPENDIX E: FORTRAN PROGRAM FOR CALCULATION
OF THE FRACTAL DIMENSION

1. This appendix presents a FORTRAN program for the calculation of the fractal dimension of a one-dimensional irregular line. This program was developed to analyze the string line cross sections presented in Part V of this report. A short user's guide follows.

User's Guide

2. Input to this program is afforded through a free format structure; this facilitates data entry. Input consists of three sections:

- a. Record 1: READ(5,*) K
where K is the number of step sizes, y , to be used to calculate the fractal dimension. For Table 6, K is 4.
- b. Record 2: READ(5,*) (SL(I), I = 1,K)
where SL is a vector which contains the step sizes, y . For Table 6, these values are 0.5, 1.0, 1.5, and 2.0.
- c. Record(s) 3: Data entry; one record is required for each coordinate location. For a 50-ft cross section, for example, sampled every 0.5 ft, 100 records are required. Each record is of the form:
READ(5,*) ELEVATION, X-COORDINATE
The last record is

ELEVATION = -999.0

X-COORDINATE = -999.0


```

17      READ(5,*) K
18      READ(5,*) (SL(I), I = 1, K)
19      KOUNT = 0
20 20    READ(5,*) DUM1, DUM2
21      IF(DUM2.LT.0.0) GO TO 30
22      KOUNT = KOUNT + 1
23      Y(KOUNT) = DUM1
24      X(KOUNT) = DUM2
25      GO TO 20
      C
C.... CALCULATE ALL DISTANCES BETWEEN TWO POINTS
      C                                AND FIRST CENTER OF CIRCLE (XC, YC)
      C
26 30    ND = KOUNT
27      N = ND - 1
28      DO 40 I = 1, N
29          XD = X(I) - X(I+1)
30          YD = Y(I) - Y(I+1)
31          DT(I) = DSQRT(XD * XD + YD * YD)
32 40    CONTINUE
      C
C.... LOOP OF NUMBERS OF DIFFERENT SEGMENTS (R)
      C
33      DO 10000 II = 1, K
34      SUM = 0.0
35      NKOUNT = 0
36      R = SL(II)
37      WRITE(6,50) R
38 50    FORMAT(1H1, 5(/), 10X, '***** SEGMENT LENGTH = ', F5.2,
&        '*****', 3(/))
39      WRITE(6,60) ND
40 60    FORMAT(6X, ' THE NUMBER OF DATA = ', I4, 4(/),
&        19X, ' INTERCEPT POINTS', /, 19X, '-----',
&        //, 13X, 'NUMBER', 4X, 'X-COORD', 4X, 'Y-COORD', //)
41      XC = X(1)
42      YC = Y(1)
      C
C.... FIND DT(M) USING COMPARISION OF THE SUM OF EACH DISTANCE
      C
43      J = 1
44 1000 DO 70 I = J, N
45          SUM = SUM + DT(I)
46          IF(SUM.GE.R) GO TO 80
47          IF(I.GE.N) GO TO 3000
48 70    CONTINUE
49 80    M = I
      C
C.... CALL SUBROUTINE TO CALCULATE THE INTERCEPT POINT
      C
50 2000 CALL CROSS (M, R)

```



```

80      EN(1) = DLOG10 (EN(1))
81      5100 CONTINUE
      C
      C.... FORM THE MATRIX {D}
      C
82      D(1,1) = K
83      DO 5200 I = 1, K
84      D(1,2) = D(1,2) + SL(1)
85      D(2,1) = D(1,2)
86      D(2,2) = D(2,2) + SL(1) * SL(1)
87      5200 CONTINUE
      C
      C.... FORM THE VECTOR {XX}
      C
88      DO 5300 I = 1, K
89      XX(1) = XX(1) + EN(1)
90      XX(2) = XX(2) + SL(1) * EN(1)
91      5300 CONTINUE
      C
      C.... SOLVE THE LINER COEFFICIENTS, VECTOR {F}
      C
92      CALL EQSOLD (2, F)
      C
93      FD = - F(2)
94      WRITE(6,5400) FD
95      5400 FORMAT(5(/), 5X, 'FRACTAL DIMENSION = ', F13.9, 5(/))
96      STOP
97      END
      C
      C.... SUBROUTINE TO CALCULATE THE INTERCEPT POINTS
      C          BETWEEN STRAIGHT LINE AND CIRCLE.
      C
98      SUBROUTINE CROSS (M, R)
99      IMPLICIT REAL*8 (A-H,O-Z)
100     COMMON/COORD/ X(1000), Y(1000)
101     COMMON/DIST/ DT(1000), SL(10), EN(10)
102     COMMON/CENTER/ XC, YC, X1, Y1
      C
      C.... CALCULATE THE COEFFICIENTS OF STRAIGHT LINE
      C          USING ( X(M), Y(M) ) & ( X(M+1), Y(M+1) )
      C           $Y = YM / XM * (X - X(M)) + Y(M)$ 
      C
103     XM = X(M+1) - X(M)
104     YM = Y(M+1) - Y(M)
105     A1 = YM / XM
106     A2 = (-A1) * X(M) + Y(M)
      C
      C.... CALCULATE THE COEFFICIENTS OF 2ND-ORDER EQUATION
      C          USING STRAIGHT LINE AND CIRCLE
      C

```

```

C      CIRCLE : (X - XC)**2 + (Y - YC)**2 = R**2
C
C      2ND-ORDER EQ : A * X**2 + B * X + C = 0
C
107      A = A1 * A1 + 1.0
108      B = 2.0 * A1 * A2 - 2.0 * XC - 2.0 * A1 * YC
109      CC = XC * XC + YC * YC - R * R
110      C = A2 * A2 - 2.0 * A2 * YC + CC
C
C....  CALCULATE THE SOLUTION OF 2ND-ORDER EQUATION
C      USING X = (-B +OR- SQRT(B*B-4*A*C)) / (2 * A)
C
111      DR = B * B - 4.0 * A * C
112      DD = DSQRT(DR)
113      X1 = (-B + DD) / (2.0 * A)
114      Y1 = A1 * X1 + A2
115      RETURN
116      END
C
117      SUBROUTINE EQSOLD (N, F)
C
C....  SUBROUTINE TO PERFORM EQUATION SOLUTION
C      USING GAUSS ELIMINAION
C
118      IMPLICIT REAL*8 (A-H,O-Z)
119      COMMON/CONST/ D(10,10), XX(10)
120      DIMENSION TEMP(10,11), F(10), CK(10), LOC(10), B(10)
121      MP = N + 1
122      DO 20 I = 1, N
123          DO 10 J = 1, N
124              TEMP(I,J) = D(I,J)
125      10      CONTINUE
126          TEMP(I,MP) = XX(I)
127      20      CONTINUE
128          DO 30 I = 1, N
129              CK(I) = 0.0
130      30      CONTINUE
131          DO 100 I = 1, N
132              IP = I + 1
C
C....  FIND MAX. NUMBER IN THE ITH COLUMN
C
133      AMAX = 0.0
134      DO 40 K = 1, N
135          IF(AMAX - DABS(TEMP(K,I))) 35, 40, 40
136      35          IF(CK(K)) 36, 36, 40
137      36          LOC(I) = K
138          AMAX = DABS(TEMP(K,I))
139      40      CONTINUE
140          IF(AMAX .EQ. 0.0) GO TO 100

```

```

C
C.... MAX. ELEMENT IN THE ITH COLUMN IS A(L,I)
C
141      L = LOC(I)
142      CK(L) = 1.0
143      DO 50 J = 1, N
144          IF(L-J) 41, 50, 41
145      41      G = -TEMP(J,I) / TEMP(L,I)
146          DO 45 K = IP, MP
147      45      TEMP(J,K) = TEMP(J,K) + G * TEMP(L,K)
148      50      CONTINUE
149      100     CONTINUE
150      DO 200 I = 1, N
151          L = LOC(I)
152          F(I) = TEMP(L,MP) / TEMP(L,I)
153      200     CONTINUE
154      999     CONTINUE
155      RETURN
156      END

```

APPENDIX F: VARIOGRAMS FOR STRING LINE CROSS SECTIONS

1. This appendix presents the variograms for the string line cross sections introduced in Part V of this report. Because these variograms are of minor significance to the conclusions of this report, no further discussion of them is made other than their presentation in this appendix.

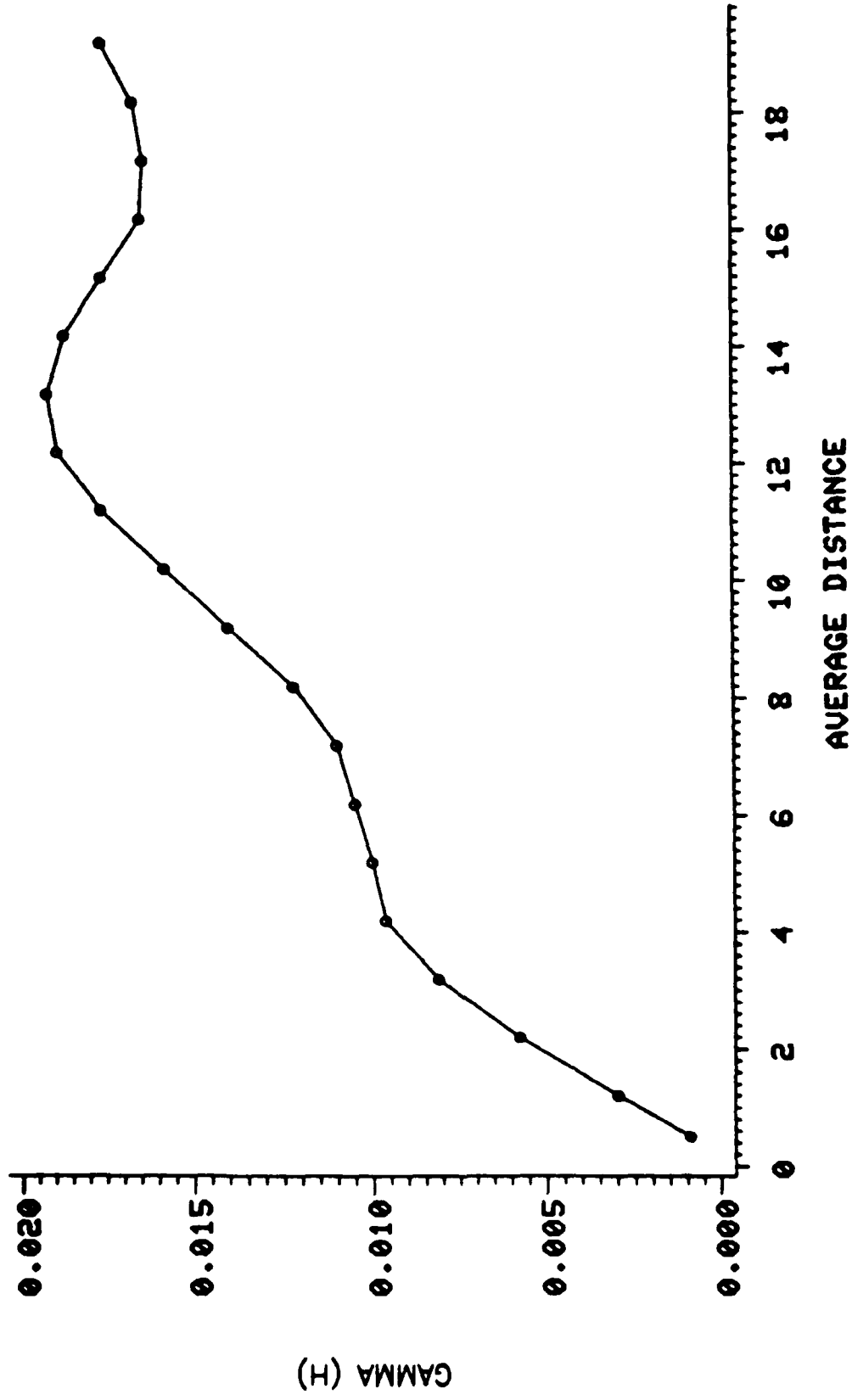


Figure F1. Variogram for the Backus Notch No. 1 bedding surface

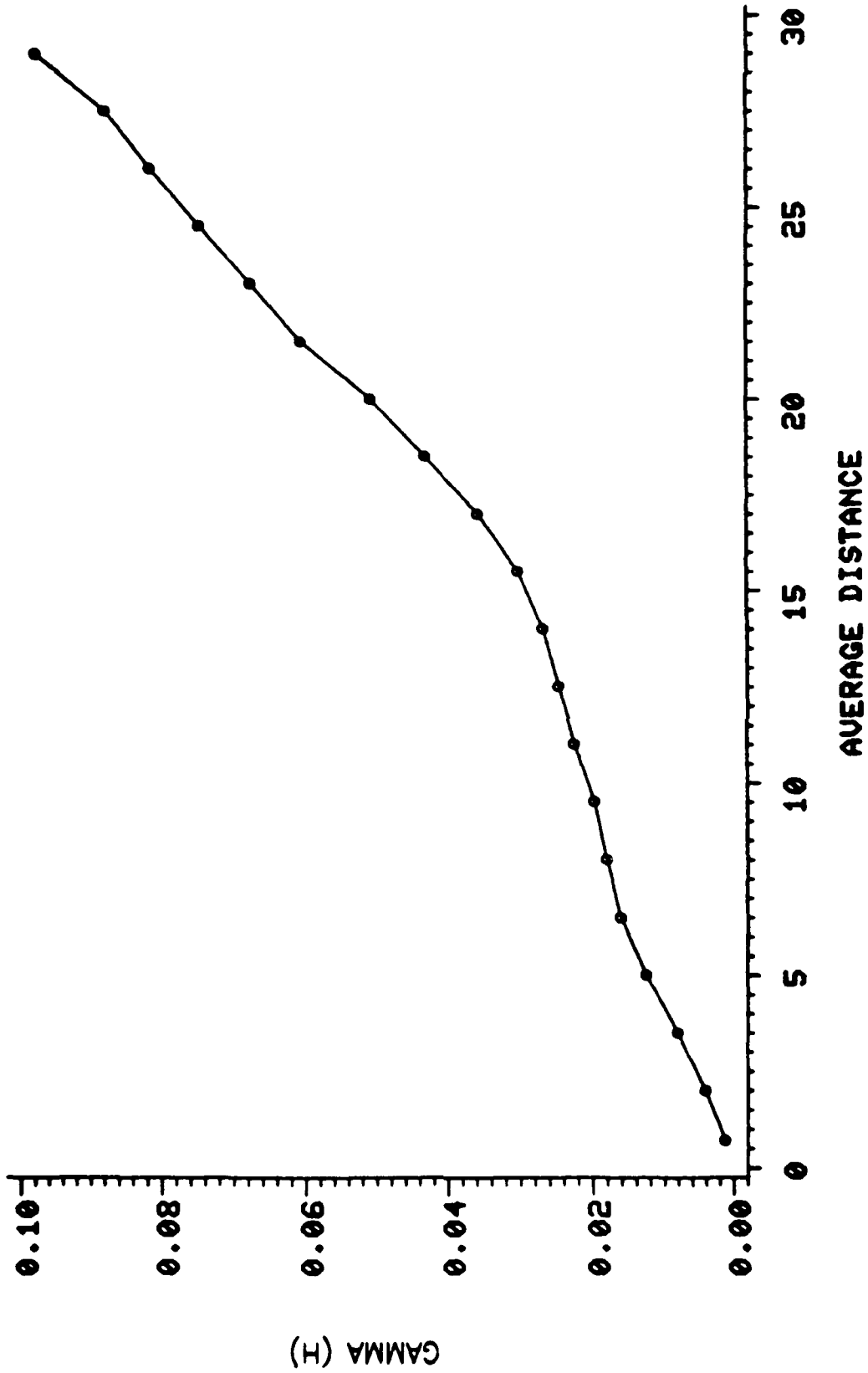


Figure F2. Variogram for the Backus Creek Notch No. 1 bedding surface

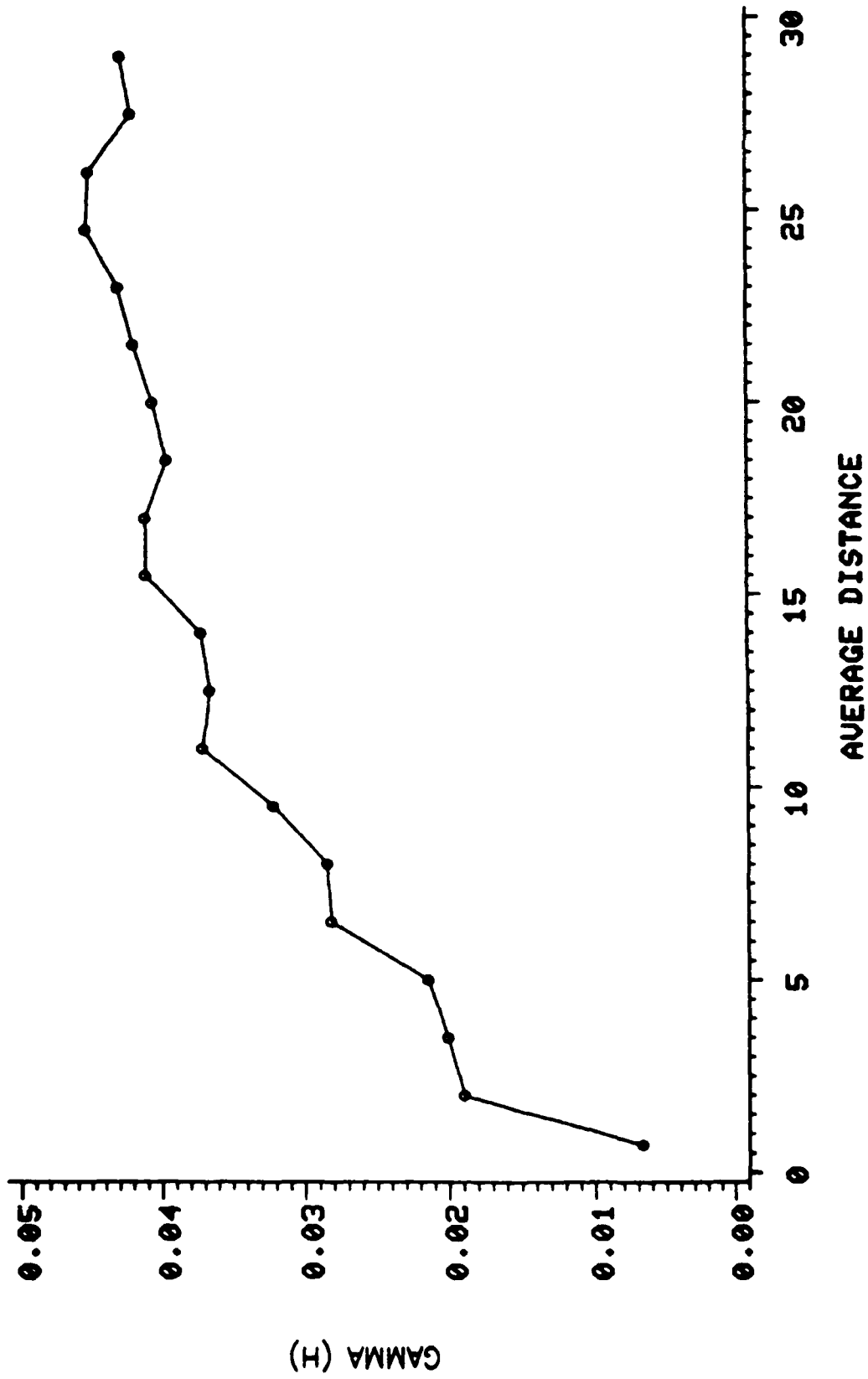


Figure F3. Variogram for the DS + 122, C joint surface

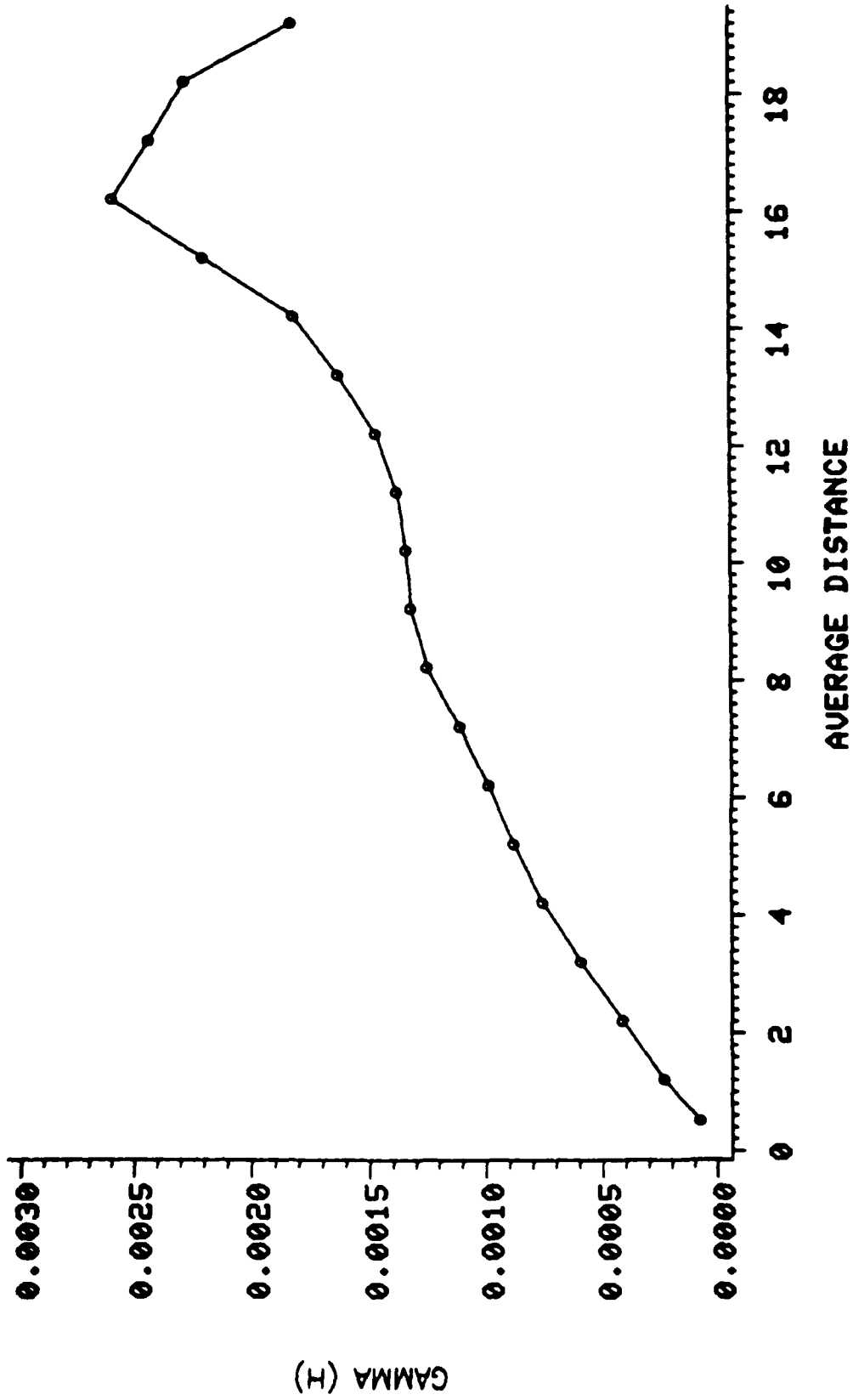


Figure F4. Variogram for the Island Notch joint surface

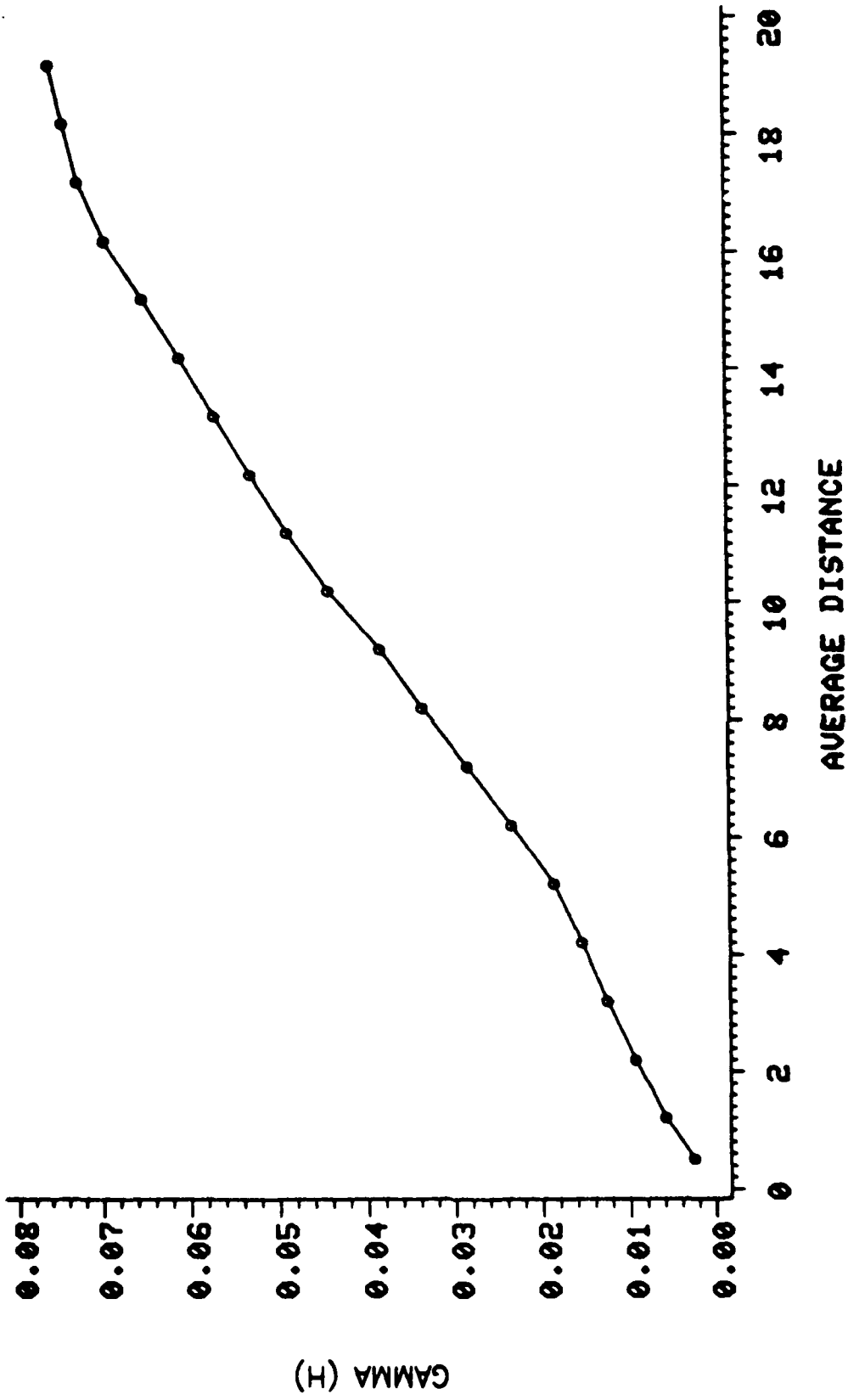


Figure F5. Variogram for the DS + 122 minor joint surface

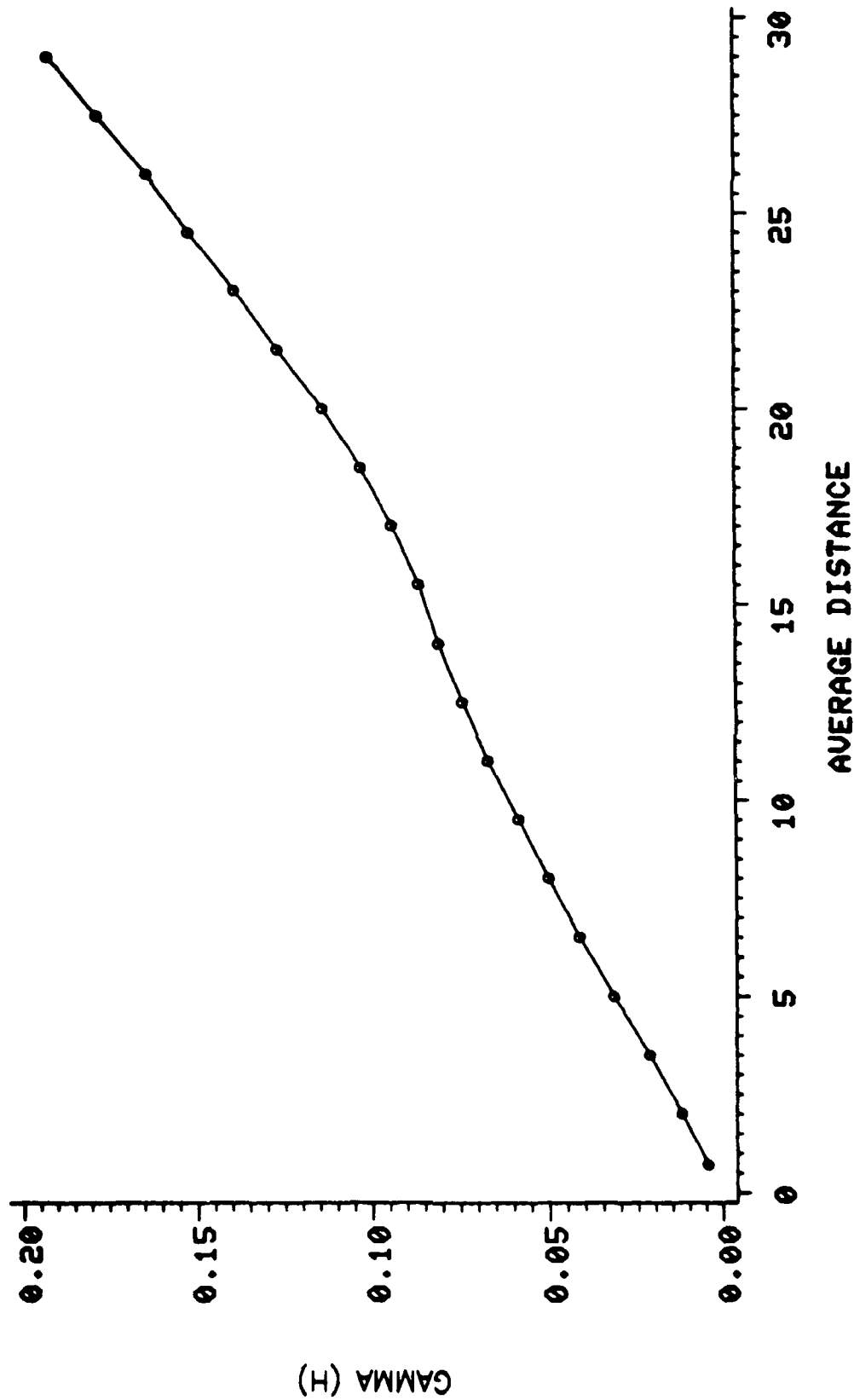


Figure F6. Variogram for the DS + 122 joint No. 2 surface

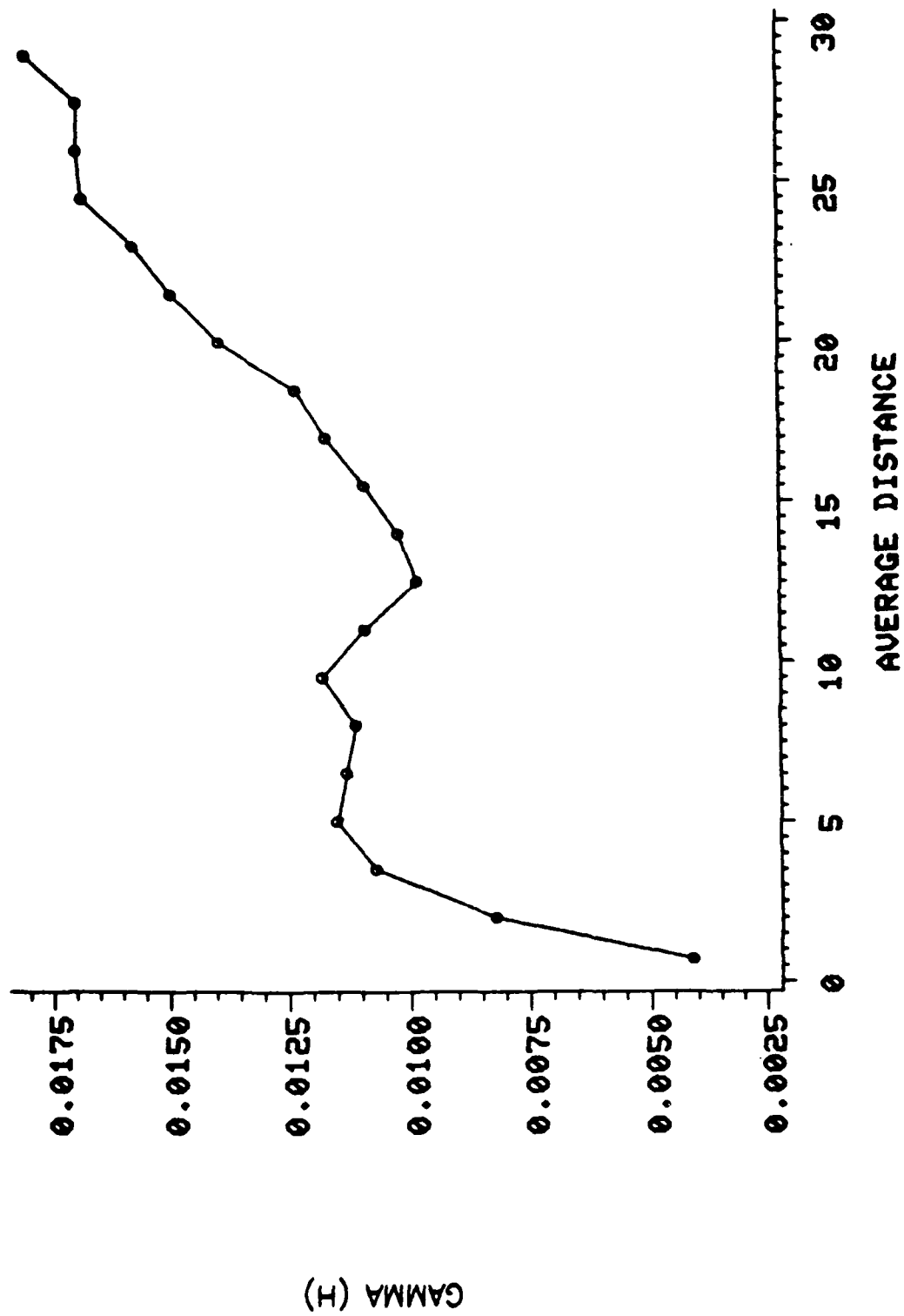


Figure F7. Variogram for the 914 Rib joint surface

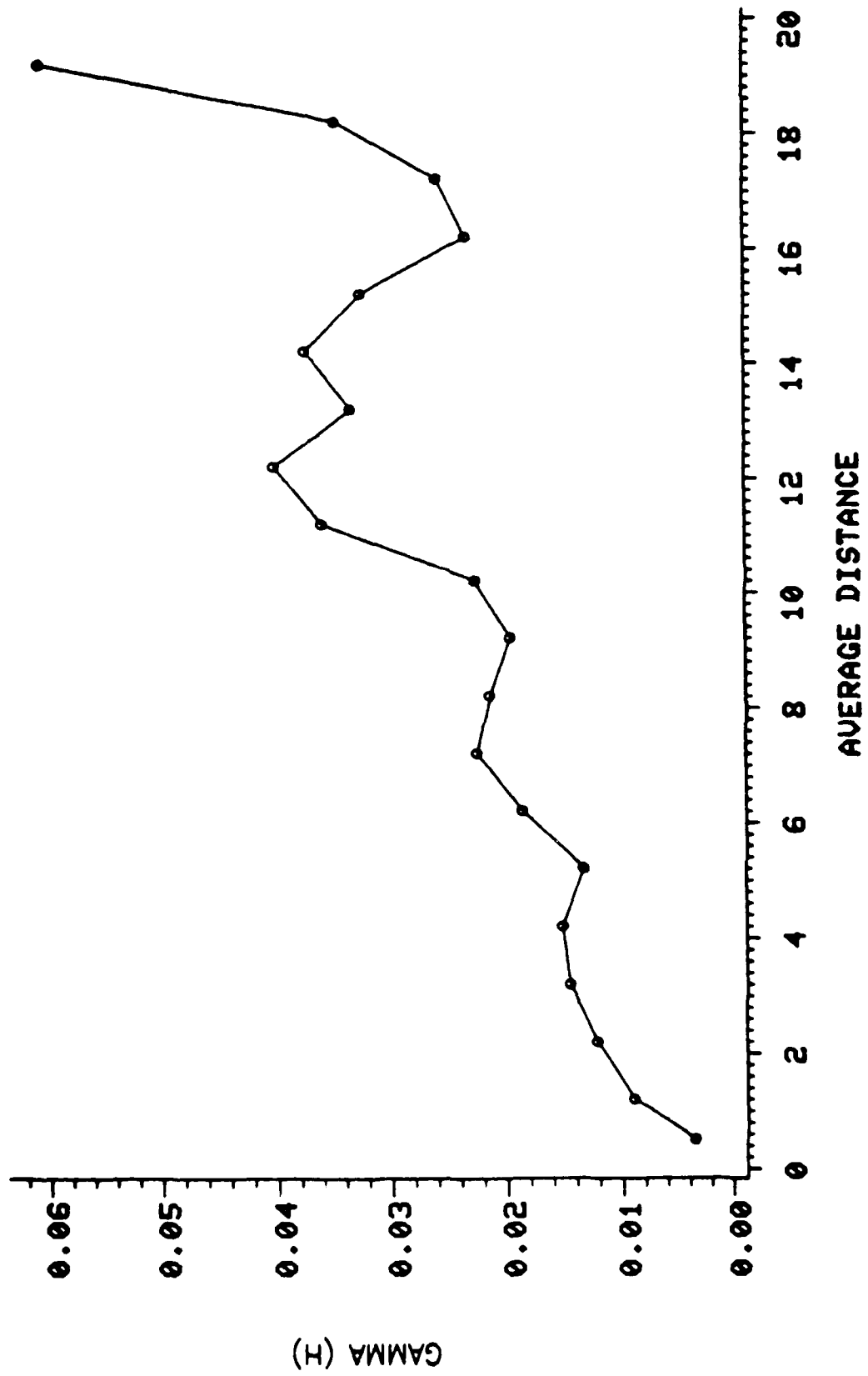


Figure F8. Variogram for the Dunn Creek Notch joint surface

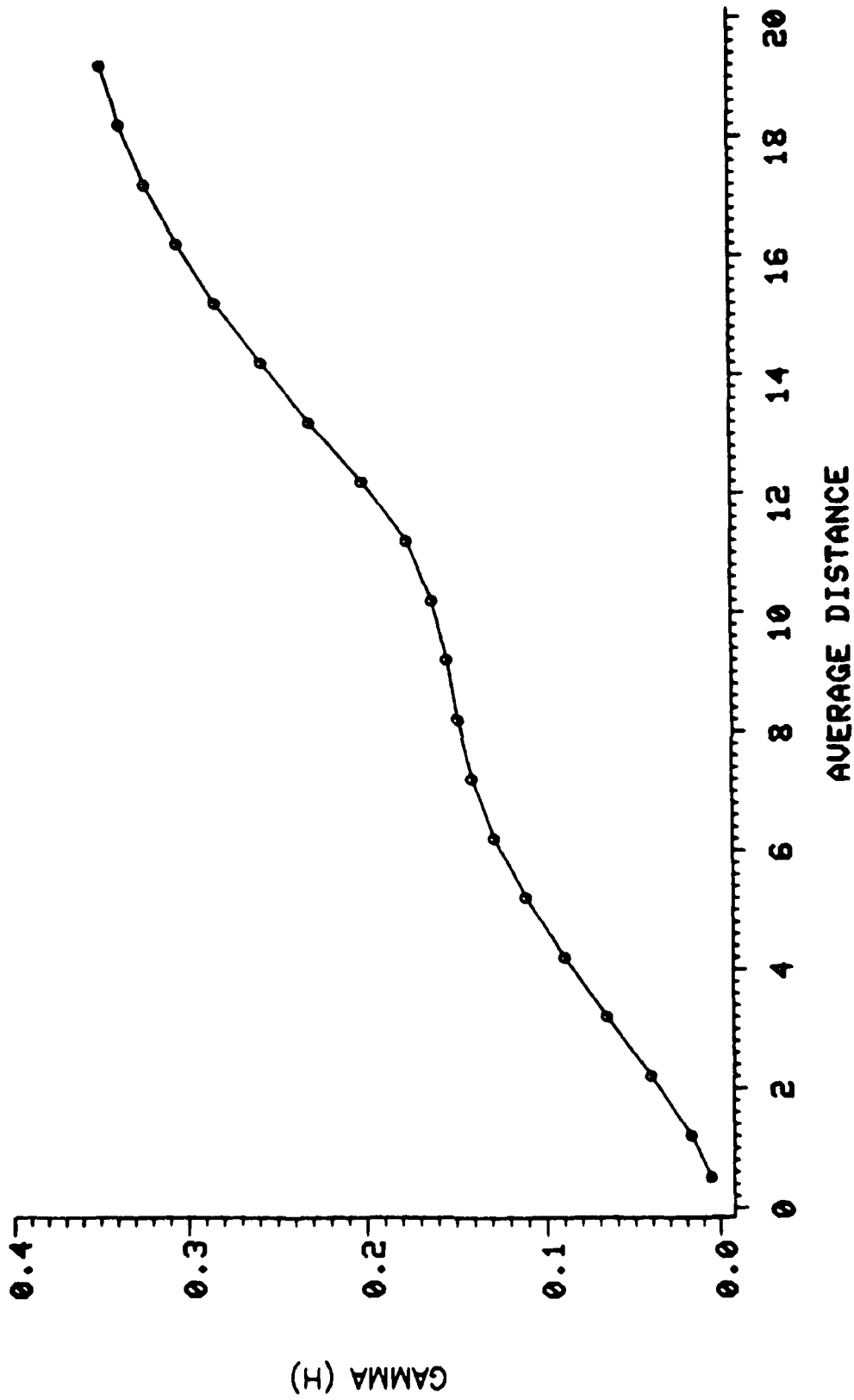


Figure F9. Variogram for the 930 joint surface

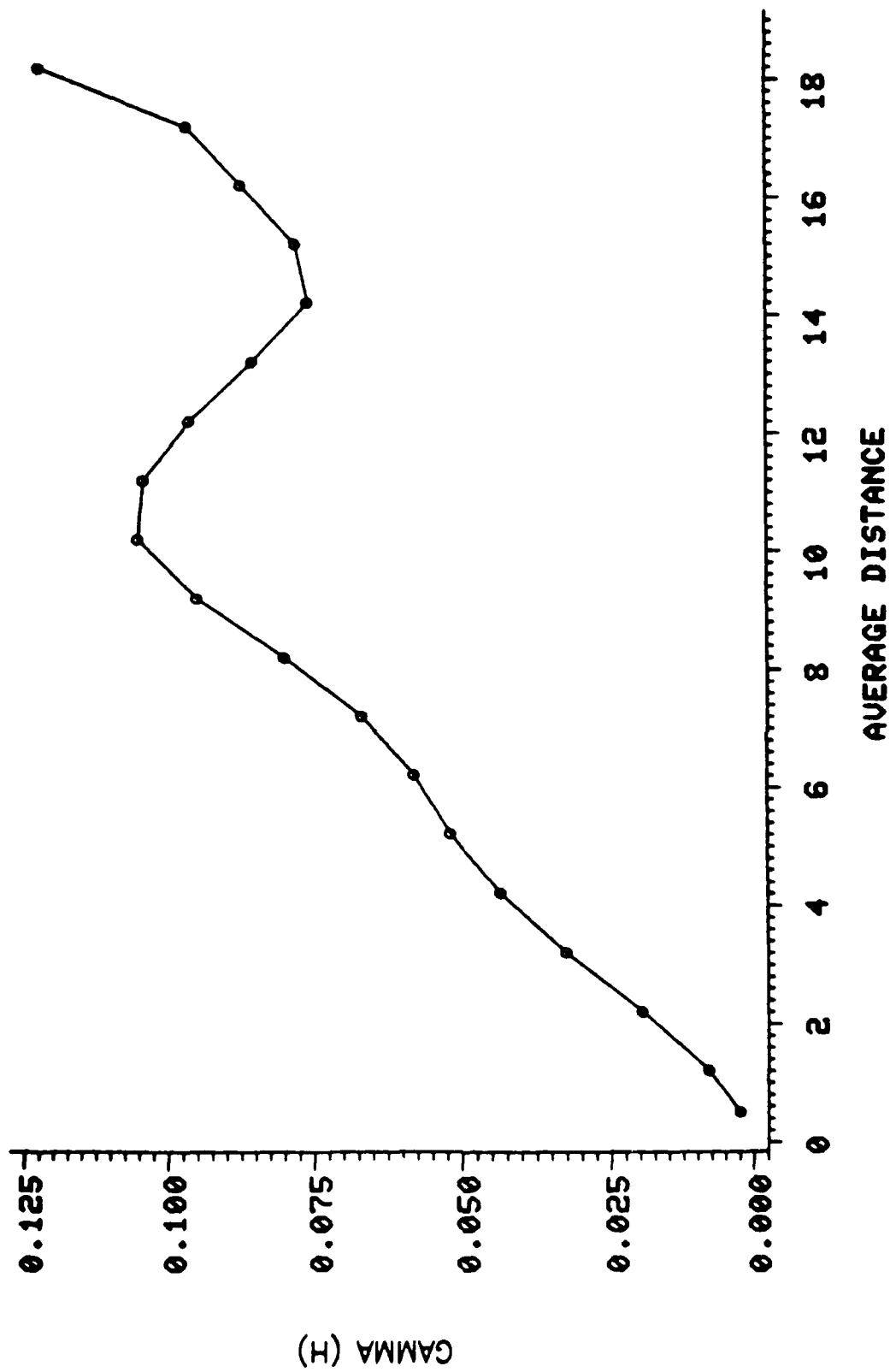


Figure F10. Variogram for the Island Notch joint/bedding plane intersection

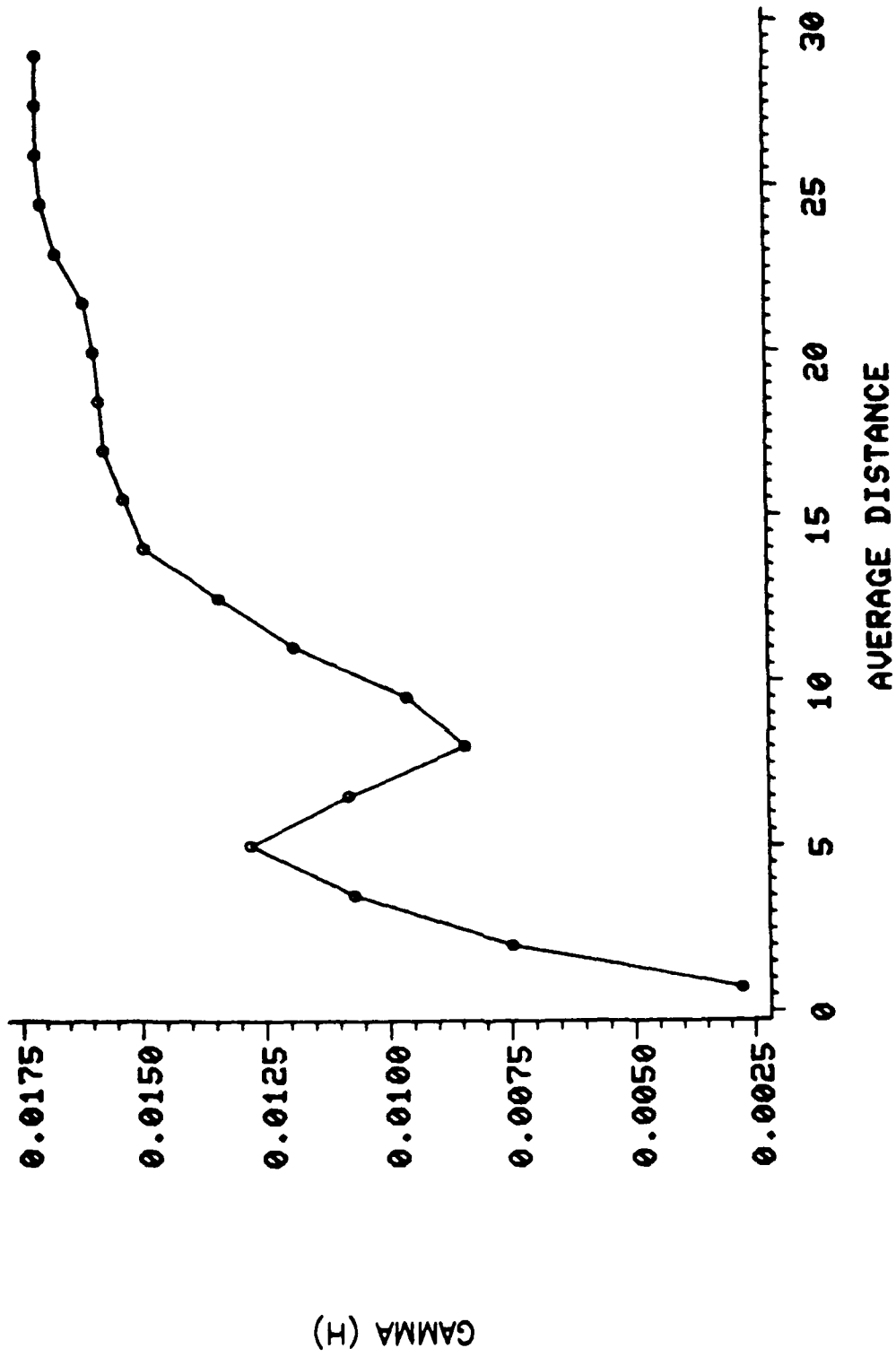


Figure F11. Variogram for the Island Notch bedding surface

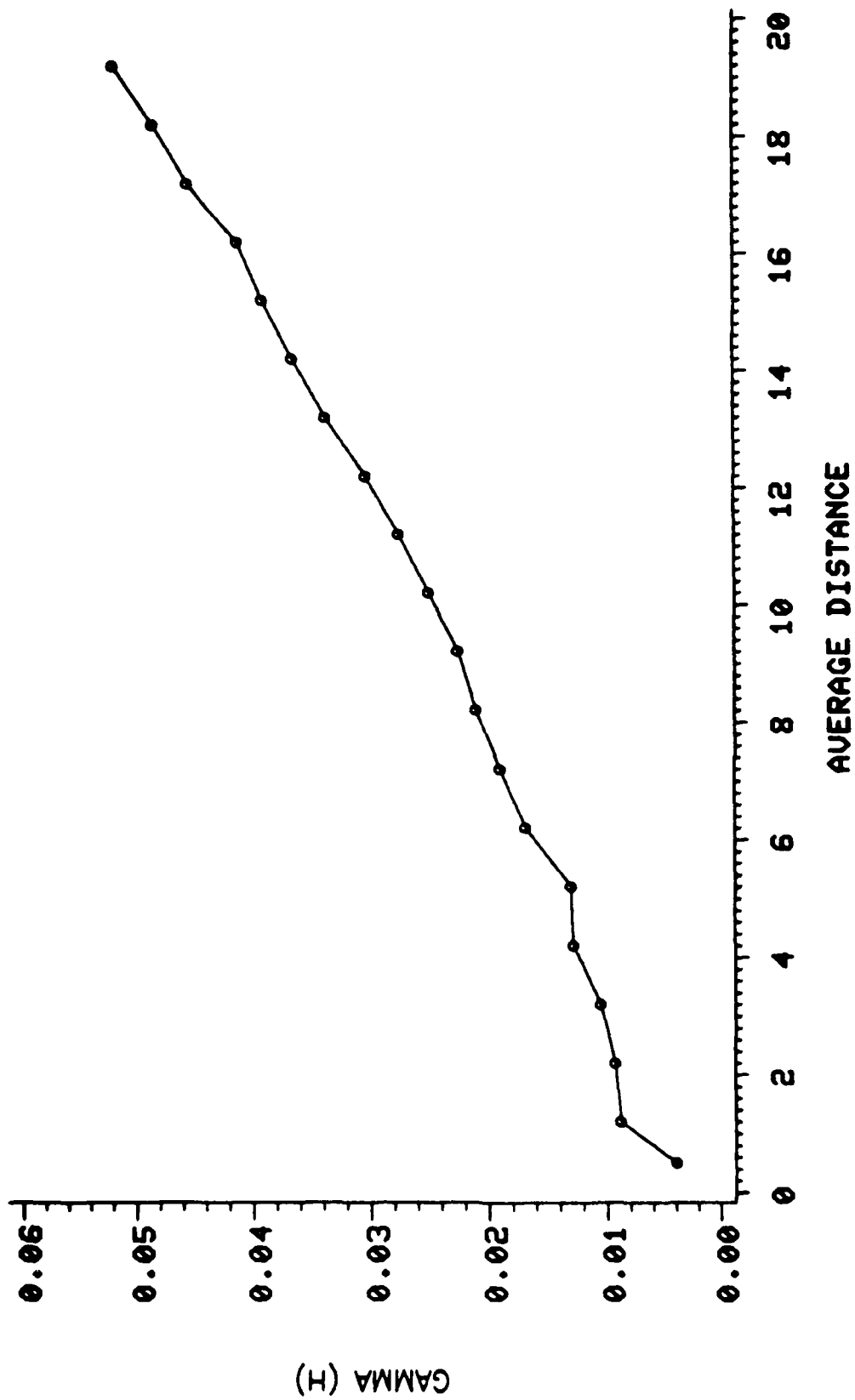


Figure F12. Variogram for the Wolf Creek Jct. joint surface

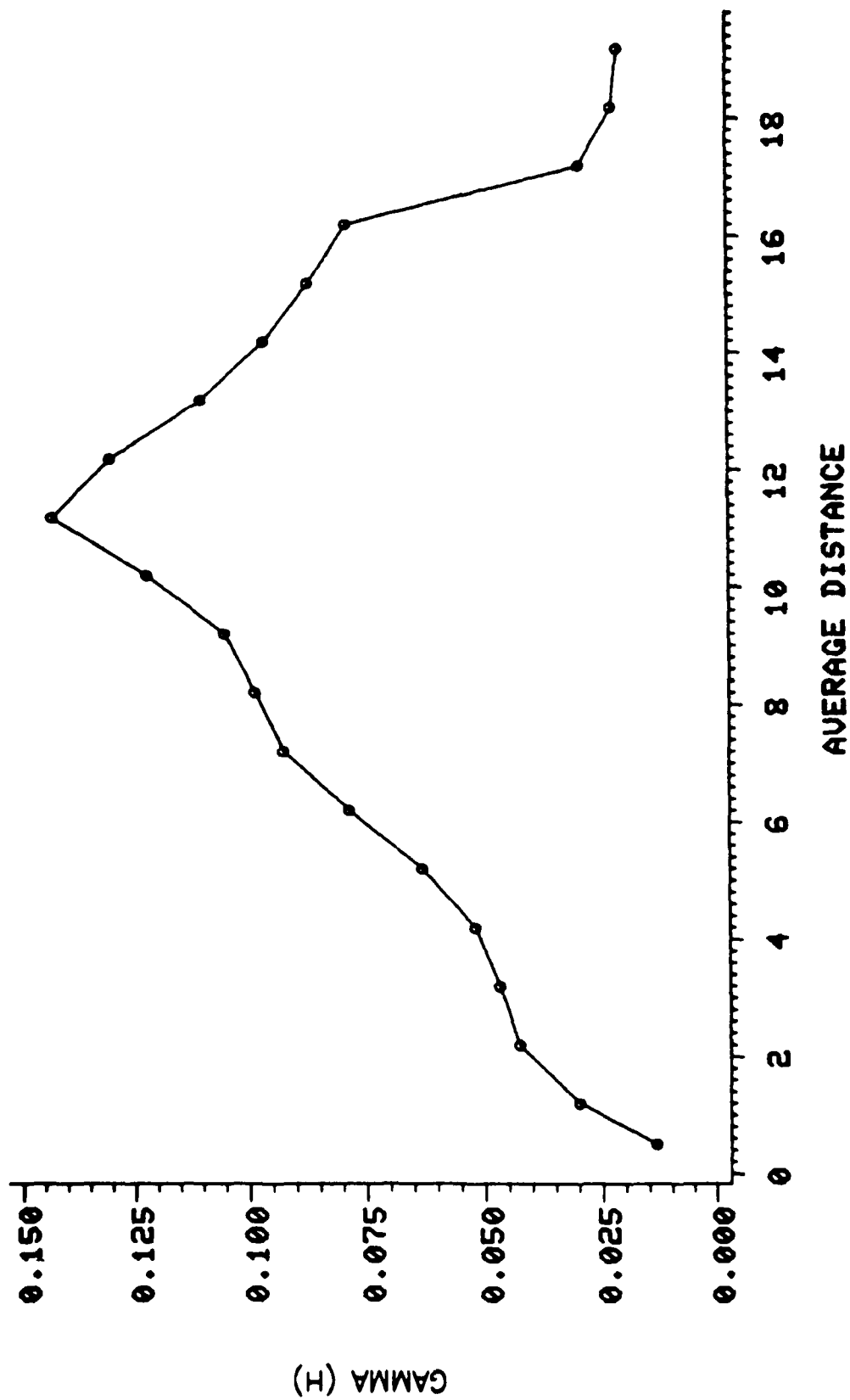


Figure F13. Variogram for the Dunn Creek Notch bedding surface

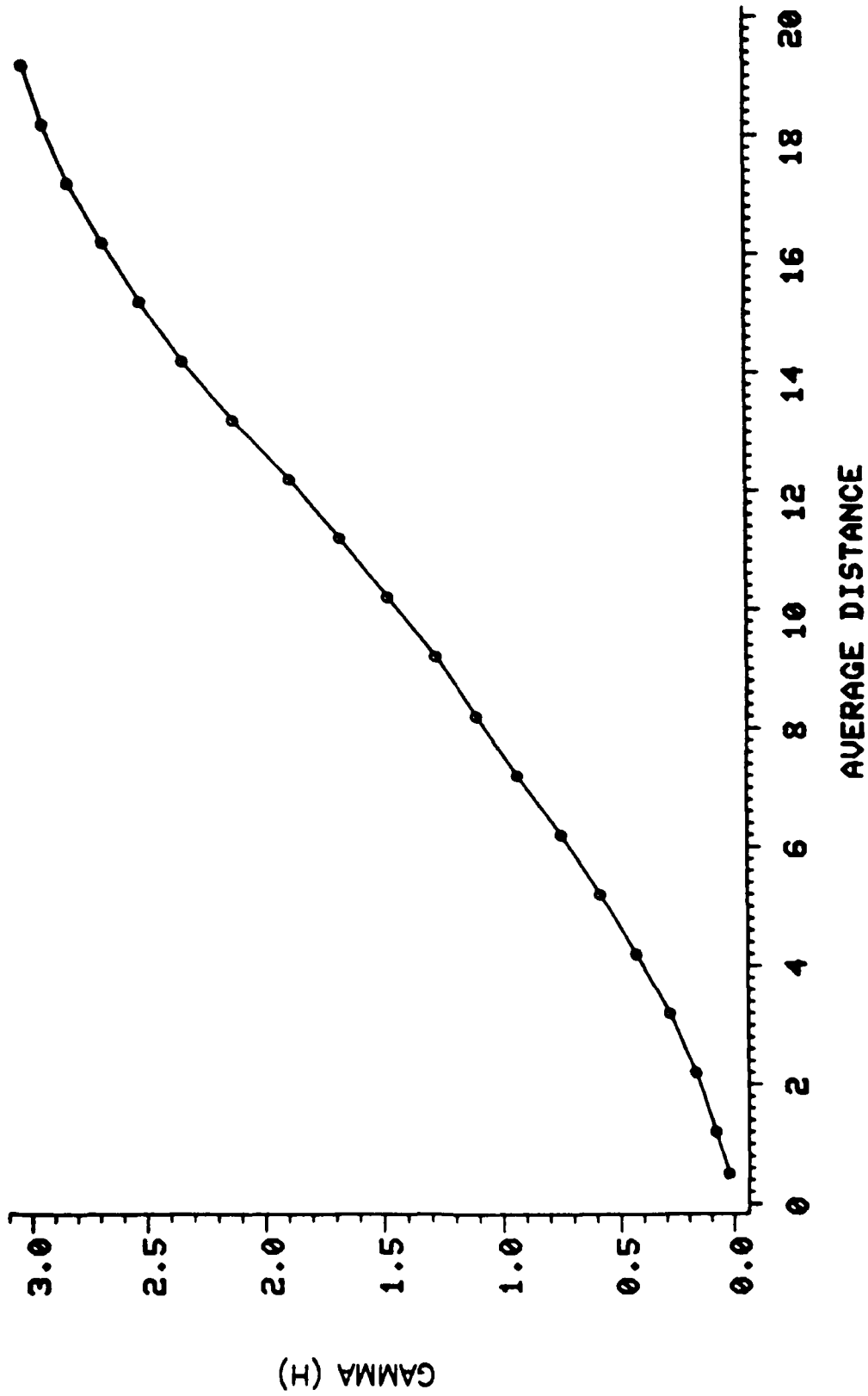


Figure F14. Variogram for the Old Notch No. 1 joint surface

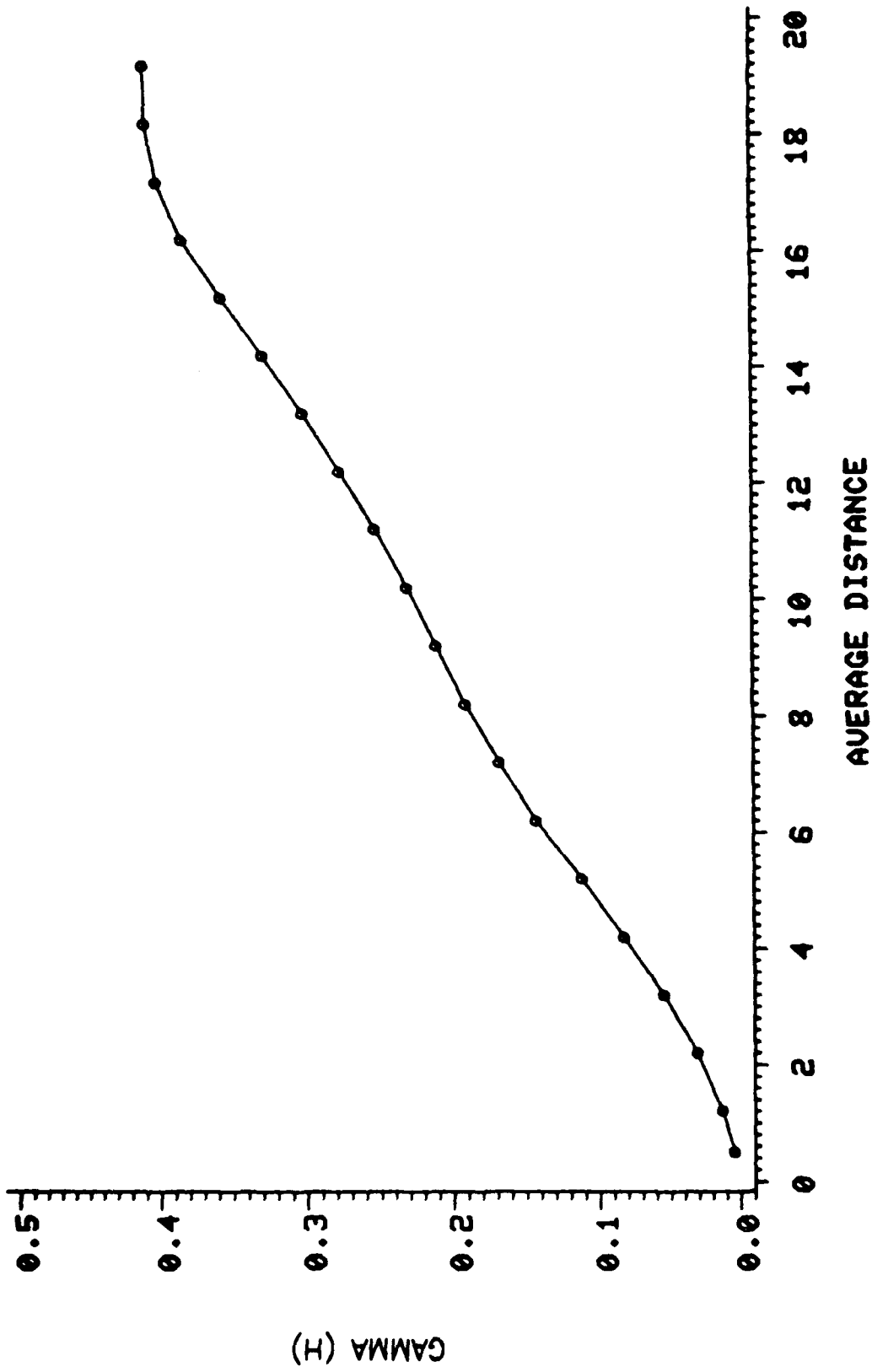


Figure F15. Variogram for the Backus Notch No. 1 joint surface